AF EOAR 63-58
June 1966

TECHNION, RESEARCH & DEVELOPMENT
FOUNDATION, HAIFA, ISRAEL

FINAL REPORT

EXPERIMENTAL AND THEORETICAL STUDIES ON BUCKLING OF CONICAL AND CYLINDRICAL SHELLS UNDER COMBINED LOADING

Josef Singer
Avraham Berkovits
Tanchum Weller
Ori Ishai
Menahem Baruch
Ovadia Harari

Technion - Israel Institute of Technology
Department of Aeronautical Engineering
Haifa, Israel

TAE REPORT 48.

AF EOAR 63 – 58
JUNE 1966

FINAL REPORT

EXPERIMENTAL AND THEORETICAL STUDIES ON BUCKLING OF CONICAL AND CYLINDRICAL SHELLS UNDER COMBINED LOADING

Josef Singer, Avraham Berkovits, Tanchum Weller,
Ori Ishai, Menahem Baruch and Ovadia Harari

Technion – Israel Institute of Technology
Department of Aeronautical Engineering
Haifa, Israel.

TAE REPORT No. 48

The research reported in this document has been sponsored by the AIR FORCE OFFICE OF SCIENTIFIC RESEARCH OAR under Grant AF EOAR 63 – 58 through the European Office of Aerospace Research, United States Air Force.

FOREWORD

This report covers the last phase of the work carried out under Grant EOAR 63-58. The earlier phases were reported in the following Scientific Reports and Publications:-

SR 1 (TAE 37) -"General Instability of Conical Shells with Non-Uniformly Spaced Stiffeners under Hydrostatic Pressure" - Published in the Proceedings of the 7th Israel Annual Conference on Aviation and Astronautics, February, 1965,Academic Press, Jerusalem, pp 62-71.

SR 2 (TAE 42)-"Further Remarks on the Effect of Eccentricity of Stiffeners on the General Instability of Stiffened Cylindrical Shells", (To be published in the Journal of Mechanical Engineering Science).

SR 3 (TAE 43)-"Effect of Eccentricity of Stiffeners on the General Instability of Stiffened Cylindrical Shells under Torsion" - Published in the Proceedings of the 8th Israel Annual Conference on Aviation and Astronautics, February, 1966, Academic Press, Jerusalem, pp 144-154.

SR 4 (TAE 44)-"On the Stability of Eccentrically Stiffened Cylindrical Shells Under Axial Compression".

"Buckling of Orthotropic Conical Shells under Combined Torsion and External or Internal Pressure" - Proceedings of the Sixth Israel Annual Conference on Aviation and Astronautics, February, 1964, Academic Press, Jerusalem, pp 179-189.

FOREWORD (Cont'd)

"Equilibrium and Stability Equations for Stiffened Shells" - Published In the Proceedings of the 6th Israel Annual Conference on Aviation and Astronautics, February, 1964, Academic Press, Jerusalem, pp.117-124.

"Buckling of Unstiffened Conical Shells under Combined Torsion and Axial Compression or Tension" - Published In the Proceedings of the 7th Israel Annual Conference on Aviation and Astronautics, February, 1965, pp.15-24.

"Buckling of Circular Conical Shells Under Uniform Axial Compression" - Published in AIAA Journal, Vol. 3, No. 5, May, 1965, pp.985-987.

"Equilibrium and Stability Equations for Discretely Stiffened Shells"- Published In the Proceedings of the 8th Israel Conference on Theoretical and Applied Mechanics, June, 1965, Israel Journal of Technology, Vol. 3, No. 2. pp.138-146.

"On the Buckling of Unstiffened Orthotropic and Stiffened Conical Shells" Presented at the VII Congres International Aeronautique, Paris,14-15 and 16 June 1965,pp. 1-22.

"Buckling of Clamped Conical Shells under External Pressure"- Published in AIAA Journal, Vol. 4, No. 2, February, 1966, pp.328-337.

III

SUMMARY

Results of an experimental program on the instability of unstiffened aluminum-alloy concial shells under combinations of 3 loadings, axial compression, torsion and external or internal pressure are presented and compared with linear theory. Improvements in experimental technique permitted many repeated buckling tests on the same metal specimen without noticeable damage and yielded reliable interaction curves.

Some tests on Mylar conical shells under similar combined loading, are then discussed. Tests of the mechanical properties of Mylar A sheets revealed considerable anisotropy that casts some doubt on the reliability of results obtained with Mylar specimens.

The general instability of stiffened cylindrical shells under combined axial compression and external or internal pressure is then discussed and design implications are considered.

The variation of stiffener spacing in stiffened conical shells yields an improvement in structural efficiency. Optimization studies that investigate this improvement for ring stiffened cones in detail are presented.

Results of a continuation of an experimental program on the general instability of ring-stiffened conical shells are presented. Tests on integrally machined steel specimens under torsion, axial compression and combined torsion and axial compression are discussed and compared with theory.

TABLE OF CONTENTS

LIST OF FIGURES

LIST OF FIGURES (Cont'd)

LIST OF FIGURES (Cont'd)

LIST OF FIGURES (Cont'd)

LIST OF FIGURES (Cont'd)

LIST OF SYMBOLS

a,b	distance between rings and stringers for a cylindrical shell.
a	in a truncated conical shell the distance of the top from the vertex, along a generator (see Fig. 1).
a_δ	$=(a_{o\delta}/x^\delta)$, distance between rings, for a conical shell (see Fig. 1).
$a_{o\delta}$	defined by Eq.(4.2) when $x = 1$.
a_n,b_n	defined by Eq.(16) of Ref. 20.
A_-,B_n,C_n,D_n	displacement coefficients.
A_1,A_2	cross-sectional area of stringers and rings.
c,d	in conical shells, the width and height of rings.
C	compression buckling coefficient.
D	$=Eh^3/12(1-\nu^2)$
E	Modulus of elasticity.
$g(\psi)$	function of the taper ratio of a cone $\psi = 1-(R_1/R_2)$, given in Ref. 35.
$G_1(n,m)$ etc.	algebraic expressions involving $x_2,\gamma \sin\alpha$, and number of circumferential waves.
h	thickness of shell.
$\bar{h}$	thickness of equivalent weight shell.
I_{o1},I_{o2}	moment of inertia of a stringer or ring cross-section about the middle line of the sheet respectively.
I_{11},I_{22}	moment of inertia of stiffener cross-section about its centroidal axis.
k_1,k_2,k_3,k_4	defined in Eqs.(4.4) to (4.9).

LIST OF SYMBOLS (Cont'd)

K	plate factor in plate buckling formula $N_{cr} = K(\pi^2 D/a^2)$.
K^4	$= 12(1-\nu^2)(a/h)^2$ in conical shell.
ℓ	$= a(x_2-1)$ (see Fig. 1).
L	length of shell between bulkheads.
m,n	integer.
n	number of half longitudinal waves in cylindrical shell.
N_x	critical axial load per unit circumference.
p	hydrostatic pressure.
p_{cr}	critical hydrostatic pressure in absence of torque and axial compressive force.
$\bar{p}_{cr}$	theoretical hydrostatic pressure.
p^{out}, p^{in}	critical pressure for outside and inside stiffeners.
P	axial force.
P_{cr}	critical axial compressive force in absence of torque and hydrostatic pressure.
$\bar{P}_{cr}$	critical axial compressive force determined by Eq.(1.7).
P^{out}, P^{in}	axial force for outside and inside stiffeners.
$Q(n,m)$, $R(n,m)$	algebraic expressions defined by Eqs.(1.2) and (1.3).
R, R_1, R_2	radius of cylindrical shell, and radii of small or large end of truncated cone, respectively.
t	number of circumferential waves.
T	torque.
T_{cr}	critical torque in absence of axial compression and hydrostatic pressure.

LIST OF SYMBOLS (Cont'd)

$\bar{T}_{cr}$	theoretical value of T_{cr}
u,v,w	non-dimensional displacements,in cylinder: $u=(u^*/R)$, $v=(v^*/R)$, $w=(w^*/R)$ in cone : $u=(u^*/a)$, $v=(v^*/a)$, $w=(w^*/a)$,(see Fig. 1).
x^*,z^*,ϕ	axial coordinate along a generator, radial and circumferential coordinates.
x	non-dimensional axial coordinate, $x = (x^*/a)$ for a conical shell, $x = (x^*/R)$ for a cylindrical shell.
x_2	ratio of the distance of the bottom of a truncated cone from the vertex, to that of the top.
$\bar{x}$	$=[(1+x_2)/2]$
Z	$=(1-\nu^2)^{1/2}(L/R)^2(R/h)$
$\bar{Z}$	$=Z/(I_{c2}/ah^3)$
α	cone angle.
β	$=(\pi R/L)$ for cylinder and $(\pi/\ell_g x_2)$ for cone
γ	$=(1-\nu)/2$
δ	defined by Eq.(4.2)
$\zeta_1,\eta_{o1},\eta_{t1},\mu_1,\chi_1$	changes in stiffnesses due to stringers and rings
$\zeta_2,\eta_{o2},\eta_{t2},\mu_2,\chi_2$	defined in Refs. 20,21 and 24.
$\eta_{2\delta}$	effective mean bending stiffness of the rings (Eq.4.17).
η	$=(P/E)(K^4/2\pi ha \sin\alpha\cos\alpha)$,axial compression parameter for conical shell.
λ	$= K^4(p/E)(a/h)\tan\alpha$,pressure parameter for conical shell.

LIST OF SYMBOLS (Cont'd)

λ_a	$=(PR/\pi D)$, axial compression parameter for cylindrical shell.
λ_p	$=(R^3/D)p$, pressure parameter for cylindrical shell.
μ	$=(K^4/E)(T/a^2h2\pi\sin^2\alpha)$, torque parameter for conical shell.
ν	Poisson's ratio.
ξ_n	defined by Eq.(4.20).
ρ_{av}	$=[(R_1+R_2)/2\cos\alpha]$, average radius of curvature for a truncated cone.
$\bar{\rho}_{av}$	average radius of curvature for a sub-shell.
$\sigma_{yp.}$	yield stress.
τ_{max}	maximum shear stress.
ψ	$=[1-(R_1/R_2)] = [1-(1/x_2)]$, taper ratio.

SECTION 1.

BUCKLING OF UNSTIFFENED CONICAL SHELLS UNDER COMBINED LOADING AND AXIAL COMPRESSION, TORSION AND EXTERNAL OR INTERNAL PRESSURE.

Avraham Berkovits, Josef Singer and Tanchum Weller.

1.1. INTRODUCTION

The buckling of cylindrical and conical shells under combined loading has been the subject of many investigations. At the Technion, the instability of conical shells has in recent years been studied theoretically and experimentally under combined torsion and external or internal pressure (Refs. 1 and 2) and under combined torsion and axial compression (Ref.3). Since only very little information has been published on triple-load interaction even for cylindrical shells (Ref. 4), the studies on conical shells have now been extended to combinations of three loadings: axial compression, torsion,and external or internal pressure. The theoretical work is a straightforward extension of the previous linear analysis and the emphasis in the present program was therefore on experimental techniques and experimental results. Improvements in experimental technique permitted many repeated tests on the same metal specimen with negligible damage, and yielded more reliable interaction curves.

The values for the theoretical interaction curves were calculated from two sets of linear equations

$$\sum_n \quad C_n Q(n,m) + D_n R(n,m) \quad = \quad 0$$

and

$$\sum_n \quad D_n Q(n,m) - C_n R(n,m) \quad = \quad 0 \qquad (1.1)$$

where

$$Q(n,m) = [(-1)^{m+n} x_2^{2\gamma-2} - 1]G_1(n,m)$$
$$+ K^4\cos^2\alpha[(-1)^{m+n} x_2^{2\gamma} - 1]G_2(n,m)$$
$$+ \eta[(-1)^{m+n} x_2^{2\gamma-1} - 1]G_5(n,m)$$
$$\pm \lambda[(-1)^{m+n} x_2^{2\gamma+1} - 1]G_3(n,m) \qquad (1.2)$$

$$R(n,m) = \mu[(-1)^{m+n} x_2^{2\gamma-2} - 1]G_4(n,m) \qquad (1.3)$$

η is an axial load parameter defined by

$$\eta = (P/E)(K^4/2\pi ha \sin\alpha \cos\alpha) \qquad (1.4)$$

λ is a pressure parameter defined by

$$\lambda = K^4(p/E)(a/h)\tan\alpha \qquad (1.5)$$

and μ is a torque parameter defined by

$$\mu = (K^4/E)(T/2\pi a^2 h \sin^2\alpha) = (K^4/E)\bar{\tau}_{max} \qquad (1.6)$$

Eqs. (1.1) and (1.2) are identical to Eqs.(59) and (60) of Ref. 1 except for the axial load term added in Q(n,m) or to Eqs.(9),(10),(11) and (13) of Ref. 3, except for the lateral pressure term added in Q(n,m). Hence the method of calculation is practically identical to that of Refs. 1 and 3.

1.2. TEST SPECIMENS

The conical shells tested during this program were from the same fabrication lot as shells used in an earlier investigation (Ref.3). These shells were of Alclad 2024-T3 aluminum-alloy sheet of 0.4 mm. nominal thickness, and had a cone angle of 40° and taper ratios of 0.500 and 0.678. The radius at the wide end of the conical shells was 140 mm.

1.3. TEST APPARATUS AND PROCEDURE

The load frame used to conduct the tests has been described in Refs.3 and 5. As shown schematically in Fig. 2a, the load frame, which was originally equipped for applying axial compression and torsion simultaneously, was modified to permit application of either internal or external pressure as well.

Internal pressure is applied to the specimen by allowing high-pressure air to pass from a control valve through a hole in the larger clamping fixture and into the vessel formed by the specimen and the clamping fixtures. External pressure is applied by partial evacuation of the vessel with a vacuum pump substituted in place of the high-pressure air system. In either case pressure on the specimen is measured by use of a mercury manometer, which is connected to the pressure vessel through a second opening in the large clamping fixture.

Improvement in the alignment of the test specimens in the load frame was achieved in the present program by use of the specially constructed aligning jig shown in Fig. 2b. Clamping the specimen to the smaller clamping fixture in the aligning jig ensured that the edges of the shell were parallel to each other

and to the surface of the clamping fixture. This procedure resulted in improvement in the measured out-of-roundness (see Tables 1.1, 1.2, and 1.3) and also in the test results.

Experimental technique was improved in the present program by use of strain gages to measure the onset of buckling. Up to 6 electric resistance strain-gages were attached around the midsection circumference of the aluminum shells. This permitted early detection of buckling and minimized inelastic effects at buckling. The buckling load could also be more accurately ascertained when external pressure was one of the loads applied during the tests.

1.4. EXPERIMENTAL RESULTS AND DISCUSSION

Results obtained from aluminum conical shells will be presented in the following order: axial compression, torsion, external pressure, combined loading with external or internal pressure. Experimental data will be compared with calculated results in each case.

Material constants for the Alclad 2024-T3 aluminum-alloy shells are:

Modulus of elasticity, $E = 10.6 \times 10^6$ psi (7540 kg/mm^2)

Poissons' ratio, $\nu = 0.33$

1.4.1. Axial Compression

Values of maximum load obtained during axial compression tests are presented in Table 1.1 and compared with calculated results. The calculated results were determined by use of the buckling equation

$$\bar{P}_{cr} = 2\pi C E h^2 \cos^2\alpha \qquad (1.7)$$

of Ref. [6], and an empirical value of the constant C = 0.23 obtained from Ref. 7, as was used in the previous reports, in place of the theoretical value. The average compression buckling load obtained from tests in the present series reached 95 percent of the load calculated from Eq.(1.7), 15 percent higher than results of the previous tests series. This improvement is due to improved test fixtures and clamping procedure.

1.4.2. Torsion

Results obtained in torsion buckling tests are presented in Table 1.2 and compared with linear theory (Refs. 1 and 8). The average buckling load obtained from initial tests in torsion was 81 percent of the theoretical load. As in the previous investigation, the torsion buckling load decreased with successive applications of torque, due to undetectable inelastic deformations at buckling. However, the use of strain gages during the present tests permitted earlier detection of buckling and thus greatly diminished the inelastic deformations.

1.4.3. External Pressure

Buckling pressures obtained in external pressure tests are presented in Table 1.3 and again compared with linear theory (Refs. 9 and 1). The average value of buckling pressure obtained in tests under external pressure was 89 percent of the theoretical value. As with torsion, only initial tests were considered in computing the average, since the buckling pressure was found to decrease somewhat with successive tests on the same specimen. Compensation was made for the decrease of buckling values in both external pressure and torsion during data reduction of combined-load tests.

TABLE 1.1

COMPRESSION BUCKLING OF ALCLAD 2024-T3 ALUMINUM-ALLOY CONICAL SHELLS OF CONE ANGLE 40°

SERIES A : $\psi = 0.678$; SERIES B : $\psi = 0.500$

Specimen No.	h (mm)	Test No.	Maximum Load P_{cr} (kg)	$P_{cr}/\bar{P}_{cr}$	Out-of-roundness (mm)
A24	.41	7	835	.827	.20
A28	.40	29	840	.832	.50
A29	.40	12	880	.871	.21
A30	.40	35	835	.827	.16
A31	.41	19	800	.792	.25
A32	.40	17	840	.832	.24
B21	.40	13	1020	1.063	.24
B23	.39	8	900	.938	.16
B26	.41	13	1012	1.054	.14
B27	.39	13	1080	1.125	.15
B28	.41	34	1110	1.156	.28
B29	.40	122	975	1.016	.34
		123	975	1.016	

TABLE 1.2

TORSION BUCKLING OF ALCLAD 2024-T3 ALUMINUM-ALLOY CONICAL SHELLS OF CONE ANGLE 40^{o}

SERIES A: $\psi = 0.678$; SERIES B: $\psi = 0.500$

Specimen No.	h (mm)	Test No.	Maximum torque T_{cr} (kg. m)	$T_{cr}/\bar{T}_{cr}$	Out-of-roundness (mm)
A24	.41	1	51.8	.770	.20
		2	52.9	.786	
		3	48.6	.722	
A25	.41	1	55.8	.829	.25
A26	.40	1	44.6	.663	.28
		10	42.9	.637	
A27	.40	7	36.3	.539	.29
A28	.40	1	55.8	.829	.50
		2	55.1	.819	
		10	50.2	.746	
		19	46.3	.688	
		27	38.3	.569	
A29	.40	2	49.0	.728	.21
		3	47.7	.709	
		11	36.5	.542	
A30	.40	2	51.8	.770	.16
		3	51.8	.770	
		29	41.5	.617	

TABLE 1.2 (Cont'd)

Specimen No.	h (mm)	Test No.	Maximum Torque T_{cr} (kg.m)	$T_{cr}/\bar{T}_{cr}$	Out-of-roundness (mm)
A31	.41	2	53.6	.796	.25
		3	54.0	.802	
		10	50.2	.746	
		13	45.9	.682	
A32	.40	2	50.6	.752	.24
		6	50.0	.743	
		10	45.9	.682	
		12	42.4	.630	
		16	41.8	.621	
B21	.40	4	84.4	.788	.24
		6	94.1	.879	
B23	.39	1	81.5	.761	.16
B24	.40	13	83.3	.778	.17
B25	.39	1	80.6	.753	.06
		12	64.8	.605	
B26	.41	2	91.5	.854	.14
B27	.39	2	83.3	.778	.15
		5	77.8	.726	
		11	77.4	.723	

TABLE 1.2 (Concl'd)

Specimen No.	h (mm)	Test No.	Maximum Torque T_{cr} (kg.m)	$T_{cr}/\bar{T}_{cr}$	Out-of-roundness (mm)
B28	.41	1	97.8	.913	.28
		9	87.3	.815	
		33	87.3	.815	
B29	.40	2	93.2	.870	.34
		139	84.3	.787	
		141	85.1	.795	
		143	86.8	.810	
B31	.40	1	91.8	.857	.12
		3	98.1	.916	
B32	.39	2	86.4	.807	.15
B33	.40	1	99.7	.931	.30
		4	89.5	.836	
B34	.40	1	83.3	.778	.13
		2	84.3	.787	

TABLE 1.3

BUCKLING UNDER EXTERNAL PRESSURE OF ALCLAD 2024-T3 ALUMINUM-ALLOY CONICAL SHELLS OF CONE ANGLE 40°

SERIES A: $\psi = 0.678$; SERIES B: $\psi = 0.500$

Specimen No.	h (mm)	Test No.	Buckling Pressure p_{cr} (mm.Hg)	$p_{cr}/\bar{p}_{cr}$	Out-of-roundness (mm)
A25	.41	2	253	.767	.25
A26	.40	2	258	.782	.28
		11	200	.667	
A27	.40	1	267	.809	.29
A28	.40	3	280	.848	.50
		11	247	.748	
		18	210	.636	
		28	160	.485	
A29	.40	1	254	.770	.21
A30	.40	1	272	.824	.16
		28	196	.594	
		30	193	.585	
A31	.41	1	264	.800	.25
A32	.40	1	260	.788	.24
A33	.40	1	267	.809	.25
		2	267	.809	
A34	.39	1	244	.740	.39
A35	.38	1	247	.748	.38
B21	.40	1	190	.611	.24
		2	190	.611	
B25	.39	2	233	.749	.06
		3	233	.749	
B26	.41	1	270	.868	.14
B27	.39	1	267	.859	.15
B28	.41	2	320	1.029	.28
		10	256	.823	
		32	280	.900	
B29	.40	1	307	.987	.34
		138	211	.678	
		140	222	.714	
		142	232	.746	
B30	.41	1	307	.987	.51
		2	293	.942	
		8	255	.820	

1.4.4. Combined Axial Compression, Torsion and External or Internal Pressure

Experimental results obtained from a large number of tests under combined axial compression, torsion and either external or internal pressure are tabulated in Table 1.4. Note that internal pressures are presented as negative external pressures in the table for convenience of comparison. Test data are compared with calculated results in Figs. 3 through 10.

Results of buckling tests under combined axial compression and torsion, as shown in Fig. 3, appear to follow the empirical curve defined by the relation

$$\left(\frac{T}{T_{cr}}\right)^2 + \frac{P}{P_{cr}} = 1 \qquad (1.8)$$

The present results are thus in agreement with experimental results obtained during the previous investigation (Ref. 3).

In Fig. 4 experimental results obtained under combined axial compression and external pressure are compared with the theoretically determined interaction curve. The test results are in reasonable agreement with theory for both taper ratios. Note however that the data points were plotted relative to the experimentally determined axial-compression buckling load (P_{cr}), which differs considerably from the theoretical value. The results presented in Fig. 4 are essentially similar to results reported on Mylar conical shells in Ref. 10.

TABLE 1.4

COMBINED LOAD BUCKLING OF ALCLAD 2024-T3 ALUMINUM-ALLOY CONICAL SHELLS OF CONE ANGLE 40°

SERIES A: $\psi = 0.678$; SERIES B: $\psi = 0.500$

Specimen No.	Test No.	P(kg)	T(kg.m)	p(mm.Hg.)
A24	4	-	55.3	- 100*
	5	670	25.2	- 100
	6	780	13.7	- 100
A25	3	183	49.5	-
	4	183	41.9	62
	5	183	32.9	114
	6	183	24.8	150
	7	183	18.0	187
	8	183	12.6	200
	9	183	8.1	200
	10	183	-	200
A26	3	345	33.4	-
	4	345	24.8	87
	5	345	18.0	120
	6	345	12.6	133
	7	345	8.1	133
	8	345	-	133
	9	345	-	133
	12	780	16.2	-
A27	2	508	28.8	85
	3	508	38.8	-
	4	508	18.0	100
	5	508	14.9	93
	6	508	8.1	117
A28	4	508	-	150
	5	508	31.1	53
	6	508	22.2	93
	7	508	-	133
	8	508	-	133
	9	508	34.7	-
	12	508	30.6	-
	13	508	28.8	27
	14	508	23.0	53
	15	508	16.2	80

TABLE 1.4 (Cont'd)

Specimen No.	Test No.	P(kg)	T(kg.m)	p(mm.Hg.)
A28 (cont'd)	16	508	-	113
	17	508	-	107
	20	508	-	107
	21	508	8.1	93
	22	508	18.0	73
	23	508	18.9	53
	24	508	21.9	33
	25	508	23.3	13
	26	508	23.3	-
A29	4	345	-	160
	5	345	-	157
	6	345	13.7	133
	7	345	19.4	100
	8	345	24.8	67
	9	345	27.0	33
	10	345	29.7	-
A30	4	183	-	223
	5	183	19.4	191
	6	183	26.3	153
	7	183	32.9	120
	8	183	37.4	87
	9	308	32.9	53
	10	508	33.8	27
	11	508	36.2	-
	12	508	27.4	53
	13	508	18.0	120
	14	508	-	153
	15	508	-	153
	16	508	-	153
	17	508	16.2	120
	18	508	21.9	87
	19	508	27.0	60
	20	508	30.6	33
	21	508	33.8	-
	22	508	30.6	33
	23	508	25.9	60
	24	508	23.0	87
	25	508	14.9	120
	26	508	-	147
	27	508	-	147
	31	75	-	187
	32	183	-	153
	33	290	-	123
	34	395	-	100

TABLE 1.4 (Cont'd)

Specimen No.	Test No.	P(kg.)	T(kg.m.)	p(mm.Hg.)
A31	4	-	21.4	227
	5	-	29.0	187
	6	-	36.0	147
	7	-	42.9	107
	8	-	45.3	67
	9	-	49.1	33
	11	-	52.0	- 50
	12	-	54.5	-100
	14	75	41.6	-
	15	183	36.5	-
	16	290	30.6	-
	17	398	24.4	-
	18	508	18.7	-
A32	3	103	46.3	- 50
	4	183	51.3	-100
	5	183	43.2	-
	7	345	38.9	-
	8	345	39.2	- 50
	9	345	41.5	-100
	11	508	27.0	-100
	13	615	16.4	-
	14	615	18.0	- 50
	15	615	19.4	-100
A33	3	1105	-	-267
A34	2	915	-	-106
A35	2	885	-	- 50
B21	3	-	32.5	160
	5	-	33.5	163
	7	110	84.4	-
	8	295	73.4	-
	9	450	64.8	-
	10	120	63.8	60
	11	330	54.0	60
	12	470	43.3	61
B22	1	240	60.3	60
	2	430	45.2	60
	3	600	27.8	60
	4	660	15.4	60
	5	610	23.0	60

TABLE 1.4 (Cont'd)

Specimen No.	Test No.	P(kg.)	T(kg.m)	p(mm.Hg.)
B23	2	130	68.8	-
	3	230	63.8	-
	4	400	52.6	-
	5	360	38.7	-
	6	400	50.0	-
	7	220	61.0	-
B24	1	-	68.9	114
	2	-	65.0	114
	3	75	62.0	115
	4	153	57.5	114
	5	153	58.5	114
	6	237	55.0	115
	7	156	58.0	115
	8	75	61.8	114
	9	315	45.7	114
	10	315	47.8	114
	11	400	42.0	114
	12	472	26.0	114
	14	540	25.0	115
	15	615	9.0	115
	16	568	-	114
B25	4	-	32.5	183
	5	-	39.0	155
	6	-	43.0	135
	7	-	47.5	111
	8	-	49.5	88
	9	-	55.0	69
	10	-	59.0	44
	11	-	60.0	21
	13	-	23.0	200
	14	-	16.0	220
B26	3	-	75.0	87
	4	-	37.4	293
	5	-	27.0	300
	6	-	18.0	327
	7	-	59.5	187
	8	130	-	250
	9	238	-	213
	10	348	-	183
	11	755	-	153
	12	510	-	133

TABLE 1.4 (Cont'd)

Specimen No.	Test No.	P(kg.)	T(kg.m)	p(mm.Hg.)
B27	3	183	64.0	67
	4	183	39.0	173
	6	183	30.6	186
	7	183	23.0	200
	8	183	17.0	213
	9	183	8.1	233
	10	183	-	233
	12	390	56.3	27
B28	3	390	47.7	133
	4	390	39.2	173
	5	390	30.6	187
	6	390	23.0	213
	7	390	16.2	213
	8	390	8.1	208
	11	508	39.2	107
	12	508	23.0	147
	13	508	16.2	173
	14	508	8.1	187
	15	508	-	191
	16	670	27.0	111
	17	670	23.0	97
	18	670	18.9	87
	19	670	16.2	96
	20	670	10.8	101
	21	690	8.1	98
	22	670	18.9	93
	23	670	10.8	107
	24	670	-	124
	25	780	18.9	80
	26	780	16.2	80
	27	780	12.6	87
	28	780	9.4	90
	29	780	5.8	87
	30	780	16.2	87
	31	800	-	80

TABLE 1.4 (Cont'd)

Specimen No.	Test No.	P(kg.)	T(kg.m.)	p(mm.Hg.)
B29	3	345	76.9	-
	4	345	54.0	101
	5	345	27.0	177
	6	345	-	199
	7	345	27.0	178
	8	345	54.0	107
	9	345	76.2	-
	10	345	54.0	103
	11	345	27.0	178
	12	345	-	193
	13	345	54.0	107
	14	345	27.0	176
	15	345	-	194
	16	345	27.0	175
	17	345	54.0	107
	18	345	76.2	-
	19	345	54.0	93
	20	345	27.0	174
	21	345	-	193
	22	345	27.0	173
	23	345	54.0	106
	24	345	74.7	-
	25	345	54.0	93
	26	345	27.0	171
	27	345	-	191
	28	345	27.4	170
	29	345	54.0	93
	30	345	73.3	-
	31	345	54.0	93
	32	345	27.0	172
	33	345	-	191
	34	345	27.0	170
	35	345	54.0	97
	36	345	74.0	-
	37	345	54.0	99
	38	345	27.0	171
	39	345	-	192
	40	345	27.0	171
	41	345	54.0	93
	42	345	75.5	-
	43	345	54.0	95

TABLE 1.4 (Cont'd).

Specimen No.	Test No.	P(kg.)	T(kg.m.)	p(mm.Hg.)
B29 (Cont'd)	44	345	27.0	168
	45	345	-	190
	46	345	27.0	168
	47	345	54.0	104
	48	345	75.6	-
	49	345	54.0	97
	50	345	27.0	168
	51	345	-	187
	52	345	27.0	167
	53	345	54.0	87
	54	345	72.9	-
	55	345	54.0	93
	56	345	27.0	169
	57	345	-	187
	58	345	27.0	167
	59	345	53.1	93
	60	345	74.7	-
	61	345	54.0	99
	62	345	27.0	169
	63	345	-	187
	64	345	27.0	168
	65	345	54.0	98
	66	345	75.0	-
	67	345	54.0	97
	68	345	27.0	167
	69	345	-	185
	70	345	27.0	165
	71	345	54.0	107
	72	345	75.6	-
	73	345	56.2	97
	74	345	24.3	167
	75	345	-	185
	76	345	26.6	167
	77	345	52.2	97
	78	345	76.0	-
	79	345	54.0	97
	80	345	24.8	167
	81	345	-	183
	82	345	23.2	167
	83	345	54.9	97
	84	345	75.0	-

TABLE 1.4 (Cont'd)

Specimen No.	Test No.	P(kg.)	T(kg.m)	p(mm.Hg.)
B29 (cont'd)	85	345	49.0	97
	86	345	19.4	167
	87	345	-	177
	88	675	-	103
	89	675	16.2	90
	90	675	26.6	73
	91	675	49.7	-
	92	675	26.6	77
	93	675	16.2	90
	94	675	-	100
	95	675	16.2	90
	96	675	26.6	80
	97	675	48.7	-
	98	675	26.6	78
	99	675	16.2	93
	100	675	-	100
	101	675	16.2	92
	102	675	26.6	78
	103	675	48.7	-
	104	675	26.6	80
	105	675	16.2	91
	106	675	-	103
	107	675	16.2	93
	108	675	26.6	78
	109	675	48.0	-
	110	675	26.6	73
	111	675	16.2	91
	112	675	-	97
	113	675	16.2	93
	114	675	26.6	70
	115	675	47.5	-
	116	675	26.6	78
	117	675	16.2	89
	118	675	-	99
	119	675	16.2	95
	120	675	26.6	77
	121	675	43.4	-
	124	345	-	171
	125	345	27.0	149
	126	345	54.0	74
	127	345	66.8	-
	128	345	54.0	71

TABLE 1.4 (Cont'd)

Specimen No.	Test No.	P(kg.)	T(kg.m.)	p(mm.Hg.)
B29 (Cont'd)	129	345	27.0	153
	130	345	-	172
	131	675	-	95
	132	675	16.2	83
	133	675	26.6	72
	134	675	47.6	-
	135	675	26.6	72
	136	675	16.2	79
	137	675	-	100
	144	777	37.4	-
	145	777	30.6	16
	146	777	24.8	22
	147	777	18.9	42
	148	777	-	59
	149	670	45.9	-
	150	670	39.2	30
	151	670	30.6	55
	152	670	-	82
	153	517	57.2	-
	154	517	47.7	47
	155	517	47.7	47
	156	517	-	127
	157	410	63.5	-
	158	410	60.3	27
	159	410	60.3	20
	160	410	60.3	17
	161	410	-	153
	162	410	52.0	50
B30	3	183	-	260
	4	345	-	237
	5	505	-	197
	6	670	-	153
	7	780	-	133
	9	1745	-	-200
B31	2	-	96.3	-304
	4	-	106.5	-304
	5	-	108.5	-304
	6	-	111.6	-304
	7	-	125.3	-304
	8	345	109.4	-304
	9	183	109.4	-304
	10	506	90.7	-304

TABLE 1.4 (Concluded)

Specimen No.	Test No.	P(kg.)	T(kg.m.)	p(mm.Hg.)
B31	11	670	81.9	-304
(Cont'd)	12	780	68.8	-304
	13	1202	-	-304
B32	1	-	104.9	-100
	3	185	97.2	-100
	4	345	80.0	-100
	5	508	74.6	-100
	6	670	68.3	-100
	7	780	59.4	-100
	8	508	79.2	-100
	9	185	93.0	-100
	10	1235	-	-100
	11	1275	-	-100
B33	2	-	106.5	-200
	3	-	108.1	-200
	5	-	119.0	-200
	6	-	114.3	-200
	7	183	105.3	-200
	8	505	85.5	-200
	9	670	62.1	-200
	10	780	80.5	-200
	11	505	74.0	-200
	12	505	75.0	-200
	13	1255	-	-200
B34	3	-	108.0	-200
	4	183	105.0	-200
	5	345	93.1	-200
	6	505	83.7	-200
	7	670	69.5	-200
	8	670	72.9	-200
	9	780	61.2	-200
	10	1128	-	-200

* Minus sign indicates internal pressure.

Buckling data obtained under axial compression, torsion and external pressure combined are compared in Figs. 5 and 6 with theoretical results. The theoretical interaction curves are presented as torsion against external pressure, with axial compression as a parameter. For $(P/P_{cr}) = 0$ (that is, zero axial compression) the experimental results are in good agreement with the theoretical interaction curve, in accordance with results reported in Ref. 2.

For finite values of axial compression the interaction curves were modified to accommodate for the marked difference of shape between theoretical and experimental interaction curves for combined torsion and axial compression. This difference has been observed in both cylindrical (Ref. 11) and conical shells (Refs. 3 and 6). The theoretical interaction curve obtained by use of Eqs.(11) for each value of (P/P_{cr}) was modified by multiplying the ordinates of the curve by a constant of proportionality. For each (P/P_{cr}) an appropriate constant was chosen so that the modified interaction curve was made to intersect the ordinate axis $(p/p_{cr} = 0)$ in accordance with the empirical relation Eq.(1.8). This empirical modification is generally satisfactory as may be seen from the reasonable agreement of test results with the modified curves in Figs. 5 and 6. For load combinations with dominant axial compression, test data appear to fall somewhat below the calculated curves in some cases. Analysis of data obtained showed a mean deviation from calculated curves of 5 percent of the buckling load, with a standard deviation of 9 percent.

The interaction curves of Fig. 5 and 6 were plotted with axial load (P/P_{cr}) as parameter, for convenience of comparison with experimental data. Cross-plotting of the interaction curves with (T/T_{cr}) and (P/P_{cr}) as coordinates and external pressure (p/p_{cr}) as the parameter leads to a most significant result. The cross-plotted curves are parabolic in form, and are almost identical to curves constructed independently of linear theory by use of the empirical relation Eq.(1.8), with experimental values of T_{cr} and P_{cr} corresponding to the given external pressure ratio (p/p_{cr}) substituted into the equation. Thus it appears that the experimentally determined interaction curve at any given external pressure bears the same relation to the corresponding theoretical interaction curve as in the case of zero external pressure. It is therefore concluded that the interaction curve for combined axial compression and torsion, at any external pressure, may be constructed by use of the theoretical results of Fig. 4 ($T/T_{cr} = 0$) and Figs. 5 and 6 (for $P/P_{cr} = 0$) in conjunction with the empirical relation Eq. (1.8).

It is worthy of note that the order of load application did not effect the buckling loads significantly. The difference in results obtained from tests conducted under similar load conditions, but in which the loading order was changed, was generally in the neighborhood of 2 percent, and never greater than 5 percent of loads at buckling. The variation was therefore well within the normal scatter band, which indicates that the buckling behavior was essentially linear. However, the type of loading that was being varied when buckling occurred generally determined the buckling mode. Thus

if axial load and external pressure were held constant as torque was increased, asymmetrical buckling occurred. If either axial load or external pressure was increasing when buckling occurred, a symmetrical buckling mode was obtained. In tests near the torsion (ordinate) axis in Figs. 5 and 6, external pressure buckling occurred gradually, while at relatively high external pressures buckling was instantaneous, causing an audible pop. Typical buckle patterns obtained during the combined load tests are shown in the photographs of Fig. 7.

Results of buckling tests under combined axial compression, torsion and internal pressure are presented together with theoretical interaction curves calculated from Eq.(1.1) in Figs. 8, 9 and 10. In the figures internal pressure appears nondimensionally as (p/p_{cr}), where p_{cr} is the external buckling pressure. Tests were conducted at increasing internal pressure until the trend of results obtained was well established. Internal pressures used were thus limited to the order of magnitude of the external buckling pressure or less.

In Fig. 8 experimental data obtained under torsion and internal pressure are compared with theoretical results. Agreement between theory and experiment appears to be reasonable, and the results are generally similar to results obtained on Mylar conical shells of Ref. 11. Data obtained under axial compression and internal pressure are shown in Fig. 9. The experimental results indicate an increase in stability due to pressurization of the shell comparable to the increase of axial buckling load at relatively low internal pressures reported for conical shells in Ref. 12 and for cylindrical shells in Ref. 13.

Data obtained from triple-load tests including axial compression, torsion and internal pressure are shown as symbols in Fig. 10. The buckling behavior was essentially linear as evident from the fact that order of loading had negligible effect on the buckling loads. The discrepancy between experimental results and the theoretical (solid) curves is immediately apparent in the figures, as is the case whenever axial load is involved. The dashed curves, however, are in good agreement with the experimental data. The dashed curves were obtained from the empirical relation Eq. (1.8), after substitution of the appropriate experimentally obtained values of T_{cr} and P_{cr}, corresponding to the given value of internal pressure (p/p_{cr}). Thus, in the region investigated, with internal pressure on the order of magnitude of the external buckling pressure or less, the interaction curve for combined axial compression and torsion is determined by use of the results of Figs. 8 and 9 together with the empirical relation Eq. (1.8), as in the case of external pressure.

In general it may be concluded that the empirical interaction curve for axial compression, torsion, and either external or internal pressure is defined by the empirical interaction curve for axial compression - pressure (T = 0), the theoretical curve for torsion-pressure (P=0), and the empirical relation for axial compression - torsion (p=0). For a given pressure ratio (p/p_{cr}) the appropriate buckling values of P_{cr} and T_{cr} are obtained respectively from the two former curves, and are then substituted into the empirical compression-torsion relation.

Such a procedure is possible because of the essentially linear buckling behavior observed in the region of pressures investigated. Results presented

in Ref. 12 indicate that a similar procedure may be suitable for higher internal pressures, in the region where experimental data correspond with the linear theory. The present method would also be expected to yield satisfactory results for cylindrical shells, due to the similarity of interaction curves for conical shells to those for cylinders (Ref. 14).

1.4.5. Repeated Buckling.

Earlier work (Ref. 3 and 40) has shown that the scatter of results obtained from repeated buckling of a single specimen is generally less than scatter resulting from initial differences between distinct specimens. As already mentioned in Section 1.3, a considerable number of combined-load buckling tests could be carried out on each specimen in the present series, because the use of many strain-gages permitted detection of buckling before any noticeable plastic deformation occurred. The average number of tests conducted on each specimen was 15, as compared with a maximum of 9 tests reported in Ref. 3, where strain-gages were not used. In several cases the condition of the specimen before the concluding test would have permitted many further tests on the specimen. In the concluding test, however, a combination of axial compression and internal pressure was applied, which always resulted in severe damage to the specimen.

Localized plastic deformation, as reflected in the decrease of buckling torque and buckling pressure, was much less in the present program than in Ref. 3. The average rates of decrease of buckling torque and buckling pressure in the present study were found to be 0.8 and 1.2 percent per test respectively, The decrease was roughly proportional to the number of tests, and did not show

the large drop during early tests on a given specimen, that was observed in Ref. 3.

Results obtained from specimen No. B29 have not been included in the above average values. On this specimen 162 successful tests were carried out. Without doubt further tests could have been conducted on the specimen, had test No.163 not been the first test with internal pressure, in which a bursting failure unexpectedly occurred.. Rates of decrease of buckling torque and buckling pressure for specimen No.B29 were 0.05 and 0.2 percent per test respectively, an order of magnitude lower than the average for other specimens.

The causes of the exceptional behavior of specimen No. B29 are not entirely clear. Out-of-roundness was similar to that of other specimens and the general finish and quality of the specimen was also not different to that of the others. Perhaps the success of this test series was due to its occurance at the end of the external pressure test program, when considerable experimental experience has been developed.

1.5. CONCLUSION

Theoretical interaction curves for buckling under combined axial compression, torsion, and external or internal pressure loading of unstiffened conical shells have been obtained by extension of the linear theory solutions of two-load problems.

The significant conclusion to be drawn from the experimental program is that for the range of pressures investigated, the interaction curve for compression-torsion-pressure loading is defined by direct superposition of

compression-pressure, torsion-pressure and compression-torsion behavior. This is due to the linear buckling behavior observed in the conical shells. A similar relationship would be expected to hold in the case of cylindrical shells.

The use of strain-gages to detect buckling of the conical shells in the present program permitted a large number of tests on each specimen, with only small decrease in buckling loads. Fewer specimens were therefore required, and the scatter of results obtained was reduced considerably.

SECTION 2

MECHANICAL PROPERTIES OF MYLAR POLYESTER AND THE BUCKLING OF MYLAR CONICAL SHELLS.

O. Ishai, T. Weller and J. Singer.

2.1. INTRODUCTION

In many recent experimental studies of the stability of thin shells the specimens were made of Mylar polyester sheets (see for example Refs. 15,10,16, 17). Mylar was introduced for buckling tests mainly because it was commercially available in very thin sheets of uniform thickness that made tests in the high (R/h) range representative of large boosters possible with small test specimens. Mylar has a low modulus of elasticity and a relatively high proportional limit and yield point. Hence pure elastic buckling is usually assured and large deflections can take place entirely in the elastic range of the material, permitting repeated tests on the same specimen. Some of the earlier investigators had some doubts about the uniformity and isotropy of the material (see for example Ref. 15), but after a few tests they concluded that nonuniformity and anisotropy are only slight and need not be considered (for example Refs. 17,18), provided E is measured separately for each specimen.

Though Mylar specimens are not very suitable if one wishes to obtain empirical data to be applied later to metal shells, they are inherently suited for verification tests of elastic stability theory and especially of theoretical interaction curves. Hence a test program with Mylar conical shells was planned to supplement the combined loading tests of Section 1.

Examination of the available date on the mechanical properties of Mylar A, however, immediately cast some doubts on the optimistic appraisal of the likely non-uniformity made by earlier investigators. The specifications of the manufacturer (Du-Pont) give a tensile Young's modulus of about 550000 psi for Maylar A (Ref. 18), whereas Ref. 15 gives a value of approximately 700000 psi

and Ref. 17 a value of 711000 psi (500 kg/mm^2).

Hence it was decided to preceed the buckling tests of Mylar cones by careful tests of the mechanical properties. The results of these tests, described below, are not very encouraging, and indicate that tests results with Mylar specimens have to be interpreted with more caution than one would expect at first sight.

2.2. MECHANICAL PROPERTIES OF MYLAR A

a. Dimensional Uniformity

A simple device was prepared for measuring and mapping the exact thickness of a whole Mylar sheet (Fig. 11). The sheets were mounted on a very flat and rigid plate above which a dial gage was fixed on a movable arm. The dial gage is calibrated in 0.01 mm. divisions. Coordinates of 50 x 50 mm. apart were plotted on the sheet, and the measurements were drawn as a respective topographic map.

Results have shown that the thickness variations of the four sheet gages measured did not exceed 3% of the average, with the exception of Mylar A-1400 which was characterized by a slight increase in thickness in a narrow strip along the sheet edges. The average thickness obtained in each case is given in Table 2.1:

TABLE 2.1

AVERAGE THICKNESS OF MYLAR A SHEETS.

Sheet	Average Thickness
MYLAR A	
1400	0.35 mm
1000	0.26 mm
750	0.20 mm
500	0.13 mm

b. Young's Modulus

Two series of tests were carried out on specimens of 20mm width and 100 mm gage length.

Static Tests: The samples were clamped at the uppe edge of a special device (Fig. 12) and static weights were loaded at ..e lower edge, through a similar clamp. Deflections at two sides of the lower clamp were measured by means of dial gages calibrated in 0.01 mm. divisions. Load was applied by increments of 2 kg. up to 20kg. in the case of Mylar A-1400. (Maximum tensile stress of about 3 kg/mm^2) followed by similar unloading procedure. Deflections were measured simultaneously. Two groups of 6 samples each, which were taken along two perpendicular directions in the Mylar A-1400 sheet, were tested. Results obtained show that, while scatter within the

group is reasonable, considerable variation of the average Young's modulus occurs between two perpendicular directions. (Table 2.2.).

TABLE 2.2.

TENSILE YOUNG'S MODULUS OF MYLAR A-1400 SHEET

Sample No.	E[kg/mm^2]	
	Direction X	Direction Y
1	396	355
2	383	354
3	400	333
4	414	336
5	408	326
6	415	360

The results in Table 2.1 are avidence of apparent anisotropy in the elastic properties of the sheet material. In order to investigate these characteristics more thoroughly the following series of tests were carried out by means of an Instron Universal Testing Machine.

Tests on Instron Testing Machine: In the Instron Universal Testing Machine a constant rate of deformation, can be maintained, and this rate was held at 0.01 min^{-1} in the present tests. One of the drawbacks of the machine, however, is that it measures the total displacement of the overall

length between the two moving heads, including strains and displacements produced within the clamped regions. As the use of strain gages is ruled out in the case of very flexible thin samples because of the local stiffening effects of the gage, the following procedure was developed: each sample tested had its length cut down successively during the test to yield at least 4 specimens of similar properties but different length. After each loading cycle, the sample was released, cut shorter by 20 mm. and tested again. In most cases this procedure was begun at 100 mm. and continued until a gage length of 40 mm. was reached. Curves of total deformation (under the same load) versus initial gage length yielded straight lines in most cases, from which average values of Young's modulus could be obtained without inclusion of edge effects (Fig. 13). The intersection of the straight lines (Fig.13) on the deflection axes give the part of the deformation contributed by the clamped regions (zero gage length). Four groups of 5-6 samples each,were cut from each sheet along 4 directions (45^{o} between each direction). 3 Mylar sheets were represented, namely A-1400, A-1000, A-500 and 68 samples were tested. The results showed little scatter within any group (of uniform direction), and significant variations between different directions (exceeding 25% in extreme cases). Tables 2.3, 2.4 and 2.5 and Fig. 14 demonstrate this anisotropy of the Mylar sheets tested. In the case of Mylar A-1400, for example, the highest value of Young's modulus was found to be 483 kg/mm^2 and the lowest 370 kg/mm^2 in fair agreement with the static test results. As expected, values of E increased with decrease in sheet thickness (Fig.14). A similar trend was found in Ref. 19 (there, however, samples were taken in in one direction only).

TABLE 2.3.

TENSILE YOUNG'S MODULUS OF MYLAR A-1400 SHEET ALONG 4 DIRECTIONS

t = 0,35 mm

Sample No.	E (kg/mm^2)			
	Direction A	Direction B	Direction C	Direction D
1	416	475		480
2	435	495	378	465
3	410	475	369	476
4	420	475	369	458
5	410	495	378	440
AVERACE	418	483	370	464

Mean value E_m = 434 kg/mm^2

TABLE 2.4.

TENSILE YOUNG'S MODULUS OF MYLAR A-1000 SHEET ALONG 4 DIRECTIONS

t = 0.26 mm

Sample No.	E (kg/mm^2)			
	Direction A	Direction B	Direction C	Direction D
1	494	583	449	605
2	458	575	481	575
3	467	583	464	527
4	475	575	445	542
5	447	601	453	531
6	463	631	432	530
AVERAGE	467	591	454	552

Mean value E_m = 516 kg/mm^2

TABLE 2.5.

TENSILE YOUNG'S MODULUS OF MYLAR A-500 SHEET ALONG 4 DIRECTION

t = 0.13 mm

Sample No.	E kg/mm^2			
	Direction A	Direction B	Direction C	Direction D
1	521	591	503	514
2	578	603	505	523
3	578	612	503	527
4	586	603	501	530
5	567	584	499	514
6	571		514	521
AVERAGE	566	598	504	520

Mean value E_m = 547 kg/mm^2

c. Yield and Ultimate Tensile Strength

After the tensile modulus tests, the same samples were loaded up to fracture in the Instron testing machine at a constant mean strain rate of 0.01 min^{-1}. Load deflection curves (Fig. 15) reveal four distinct regions: a linear portion at low stresses, a curved section above the proportional

limit which terminates with a clear yield point, a drop of stress after yielding, and a fourth region that exhibits a steady increase in stress ("strain hardening") up to the ultimate value. In this last region the sample is subjected to significant dimensional changes characterized by a considerable extension, accompanied by a uniform lateral contraction. The specimens failed in a ductile type of fracture. Typical values of proportional limit stress, yield stress and ultimate stress samples from the different sheets and directions are given in Tables 2.6,2.7, and 2.8. The scatter in this case is larger and the influence of anisotropy is less pronounced but follows the same trend as in the case of Young's modulus (Fig.16). One may note that whereas the anisotropy hardly influences the yield stress, the ultimate stress is noticeably affected.

TABLE 2.6.

PROPORTIONAL LIMIT,YIELD,AND ULTIMATE STRESSES FOR MYLAR A-1400 SHEET ALONG 4 DIRECTIONS .

t = 0.35 mm

σ kg/mm^2											
σ Proportional Direction				σ Yield Direction				Nominal σ Ultimate Direction			
A	B	C	D	A	B	C	D	A	B	C	D
4.3	3.6	4.3	3.6	9.9	9.9	9.0	9.9	12.1	13.8	10.0	12.8
	3.6	4.3	4.3	9.6	10.1	9.0	9.7	13.3	13.3	11.0	13.1
3.6	3.6	3.6	4.3	9.4	10.0	9.0	9.6	12.6	12.1	10.9	13.1
3.6	3.6	3.6	3.6		9.9	9.3	9.4		14.9	11.4	12.8
	2.9				10.0				14.3		
Average											
3.83	3.46	3.95	3.95	9.63	9.98	9.08	9.65	12.7	13.68	10.8	13.0

TABLE 2.7

YIELD AND ULTIMATE STRESSES FOR MYLAR A-1000 SHEET ALONG 4 DIRECTIONS

t = 0.26

σ kg/mm^2

σ_{yield} (kg/mm^2) Direction				Nominal $\sigma_{ultimate}$ (kg/mm^2) Direction			
A	B	C	D	A	B	C	D
9.6	10.9	9.8	10.6	17.0	21.5	19.9	24.0
10.2	10.1	9.4	10.8	17.6	19.7	16.6	24.1
10.0	10.8	9.6	10.8	16.2	19.0	19.8	23.5
10.0	10.9	9.4	10.8	15.5	15.2	18.3	23.5
10.2	10.7	9.6	9.6	14.4	21.9	18.2	16.8
10.0	10.9		10.0	12.0	20.7		17.9
Average							
10.0	10.8	9.6	10.4	15.5	19.7	18.6	21.8

TABLE 2.8

YIELD AND ULTIMATE STRESSES FOR MYLAR A-500 SHEET ALONG 4 DIRECTIONS

t = 0.13 mm

σ_{yield} (kg/mm^2)				Nominal $\sigma_{ultimate}$ (kg/mm^2)			
Direction				Direction			
A	B	C	D	A	B	C	D
10.6	10.2	10.1	10.2	15.4	23.2	18.4	16.5
10.6	10.6	10.1	10.2	17.6	25.6	18.0	17.8
10.6	10.6	10.1	10.2	20.9	24.3	21.8	23.3
10.6	10.5	10.1	10.1	18.8	31.6	23.7	26.3
10.5	10.2	10.1	10.1	21.2	28.6	24.8	24.7
10.5			10.1	18.5			18.9
Average							
10.6	10.4	10.1	10.1	18.7	26.7	21.3	21.2

The true ultimate stress for Mylar A-1400 Sheet is given in Table 2.9.

TABLE 2.9

TRUE ULTIMATE STRESS FOR MYLAR A-1400 SHEETS ALONG 4 DIRECTIONS

$A_o = 7.0\ mm^2$

$A_{ultimate}$ (mm^2)				True $\sigma_{ultimate}$ kg/mm^2			
Direction				Direction			
A	B	C	D	A	B	C	D
3.84	3.2	3.46	3.94	22.1	30.3	20.2	22.8
3.04	3.52	3.2	3.78	30.6	26.4	24.0	24.4
3.04	3.87	3.2	3.65	29.0	22.0	23.7	25.2
	2.58	3.2	3.81		34.9	25.0	23.6
	3.20				31.3		
			Average	27.2	28.9	23.2	24.0

2.3. INFLUENCE OF STRAIN RATE

Tests with different strain rates in the Instron machine, ranging from 0.1 mm/min up to 10 mm/min reveal almost no influence of strain rate on the tensile Young's modulus. However, after yield, an increase in loading speed

resulted in higher stresses in the strain hardening region, which did not exceed 10% of the average yield value.

2.4 SHEAR STRENGTH

Circular samples of Mylar A-1400 sheet were tested by means of special device (Fig.17) which was loaded on the Instron testing machine up to ultimate values. Results (Table 2.10) reveal the high shear strength and the low scatter which indicates fair uniformity of shear resistance.

TABLE 2.10

ULTIMATE SHEAR STRENGTH FOR SAMPLES OF MYLAR A-1400 SHEET

	1	2	3	4	5	6	7	8	Average
kg/mm^2	11.4	11.2	11.5	11.3	11.4	10.7	10.9	10.8	11.1 kg/mm^2

2.5 TIME-DEPENDENT PROPERTIES

a) Creep Samples taken from Mylar A-1400 sheet (0.35 x 20 x 100 mm) were clamped in the device used for static loading (Fig. 12) and loaded overnight with a static load of 10kg.(a stress of approximately 0.14 kg/mm^2) at room temperature (approx. 23° C). Creep appears to become stabilized after a few hours, and does not exceed 2% of the instantaneous elastic deformation (Fig.18).

b)Relaxation Tensile specimens of Mylar A-1400 sheet were loaded in the Instron testing machine up to about 0.3 of their yield value and were fixed

at constant deformation. Stress relaxation was recorded for 10 minutes. Almost no relaxation was observed during this period. It may be concluded that Mylar sheet show negligible sensitivity to time effects.

2.6. BUCKLING TESTS ON MYLAR SHELLS

a. Purpose of Tests

The anisotropy of Mylar A sheets found in series of tests described above casts serious doubts on the suitability of Mylar specimens for buckling tests. Since Mylar specimens were, however, used in several other studies, it was decided to test conical shells made of Mylar A under combined loading of axial compression, pressure and torsion in order to complement the experiments on aluminum cones reported in Section 1, and by comparison of results to examine the influence of anisotropy of the buckling behavior.

b. Fabrication of Specimens

Mylar A-1400 sheets were cut and glued to form three types of conical shells, with taper ratios $\psi = 0.50$, 0.68 and 0.80 (Fig.19). After extensive tests with different glues, the joints were glued with Mylar adhesive No. 46950 (90%) and R.C. 805 (10%) as a hardner. This type of adhesive was preferred to epoxy types, as it has superior peeling strength, and a reasonable shearing strength. The lap-joint was cold cured under pressure for 48 hours. Each specimen was tested at least 7 days after fabrication. Ten Mylar conical shells were tested altogether, at least three of each taper ratio.

c. Test Apparatus and Procedure

The specimens were mounted in the test ring (Fig.20), which had earlier been used for similar buckling tests on aluminum shells described in Section 1.

For the tests on Mylar shells, the lower part of the test fixture that received the small end of the cone, was made of aluminum. Axial compression was applied by a hand-operated jack, and the force was measured by means of a proof-ring of 0.5%. Air pressure and vacuum were measured with an alcohol manometer with an accuracy of ± 3mm of alcohol. Torsion was applied by means of deadweight loading transmitted through a string and pulleys to a horizontal arm 50cm long, which apply a couple to the lower part of the shell. Two additional dial gages were used to detect axial displacement and angle of twist.

d. Test Procedure

Each shell was first loaded to buckling under a single load, torsion, axial compression and external pressure, in order to determine the critical reference values T_{cr}, P_{cr} and p_{cr}. The critical load was determined visually as the load at which all buckling waves had appeared. Since this point of complete buckling was not always clearly defined, the sudden change in the axial displacement, which was found to occur simultaneously, was taken as the criterion of complete buckling. No significant change in the buckling strength of the shell was noticed after more than 100 buckling cycles. After the critical values were established, each shell was subject to the following loading cycles:

First, torque was kept constant. Five levels of torque were maintained, namely, 0, 0.2, 0.4, 0.6 and 0.8 of the critical torque. At each level the axial force was varied while the corresponding critical external pressures were determined. In tests with internal pressure, the pressure was varied and the necessary axial force to cause buckling was found. At the end of such a series of tests, the direction of the applied torque was reversed and the same shell was subjected to a similar series of tests in the opposite direction.

e. Order of Loading

In several series of tests, the order of loading was changed in order to examine the linearity of the buckling behavior under combined load. The order of axial and pressure loading was changed, and instead of the regular order the external pressure was varied and the respective critical axial load was found. Results (see Fig. 21) show that the critical values and the interaction curves are not influenced by the order of loading, and hence non-linear coupling of load effects can be neglected.

2.7. TESTS RESULTS

The general behavior of the loaded shells up to buckling is characterized by a gradual development of isolated waves, producing "prebuckling flats" in the load displacement curves. Complete buckling occurred when all waves (usually 9~10) appeared (see Fig. 22). The interaction curves for the three taper ratios tested (Figs. 23,24,25) exhibit the following characteristics:

The plots of (P/P_{cr}) versus (p/p_{cr}) are curved at small values of T/T_{cr} and tend to straighten out at larger (T/T_{cr}). At small T/T_{cr} values and under small axial compression the interaction curves are very close and coincided or even intersected in many cases. At larger (T/T_{cr}) the increase in torque has a considerable influence on the interaction curves. With internal pressure complete " linear behavior" was observed in most cases contrary to the negligible effect of the change in the order of loading, the reversal of the direction of torque influenced both the critical torsion and the shape of interaction curves in many cases (see Fig. 24). Even where the critical torque did not change significantly, the interaction curves show a definite change in shape (Figs. 23,25). It should be noted that the interaction behavior of the same shell when retested, following removal from and reinstallation in the test apparatus.

The elastic modulus of specimens cut from the tested shells shows the same high scatter and anisotropy observed on specimens taken from the corresponding Mylar Sheets.

2.8. DISCUSSION.

Tests results on Mylar conical shells confirm the conclusions on material properties arrived at the beginning of this Section. While the negligible effect of change in order of loading indicates " linear behavior" up to buckling, the change in shape of the interaction curve, as well as the significant influence of the direction of torque indicate anisotropic behavior of the shell. Comparison with the interaction curves obtained with aluminum shells of the same taper ratios shells (Figs. 26,27), demonstrates the peculiar buckling behavior of Mylar Shells. The detailed comparison in Figs. 26 and 27 shows more pronounced discrepancies between

aluminum and regular shells at zero or small torques than at large torques when torsion dominates buckling. It may be pointed out that the comparison was for torque acting in the same direction for both types of specimens. Due to the appreciable change in buckling behavior of the regular shells when the direction of torque is reversed, even more pronounced discrepancies would be observed if the comparison were for torques acting in opposite directions. Comparison with linear theory (Fig. 28) shows that same basic behavior as observed in Section 1, fairly good agreement for all cases where torsion or external pressure is dominant and poor agreement when axial compression dominates. This is in accordance with the usual low experimental values obtained under axial compression. Since no tests were carried out on similar aluminum shells, no comparison could be made but discrepancies similar to those appearing in Figs. 26 and 27 may be expected. The empirical interaction curves for Mylar cones of taper ratio 0.80 shown in Fig. 28, should therefore, be taken as approximations only, on account of the anisotropy of the Mylar, and cannot be applied with certainty to metal shells of the same taper ratio.

2.9. CONCLUSIONS

Mylar A Sheets are characterized by considerable anisotropy, especially in Young's modulus. Hence some doubt is cast on the reliability of results obtained with Mylar specimens. This is also evident from the strong influence of the direction of torque on interaction curves for Mylar cones and from the discrepancies observed between the interaction curves for aluminum and Mylar specimens.

SECTION 3

GENERAL INSTABILITY OF STIFFENED CYLINDRICAL SHELLS UNDER COMBINED AXIAL COMPRESSION AND EXTERNAL OR INTERNAL PRESSURE.

J. Singer, M. Baruch and O. Harari.

During the mission of a launch vehicle or missile it is subject to combinations of axial and pressure loads. The general instability behavior of stiffened cylindrical shells under combined loads is therefore studied. The analysis employs linear Donnell type equations and is an extension of that given in Refs. 20 and 21. For classical simple supports, the third stability equation, Eq.(18) of [20], becomes for axial compression and external or internal pressure,

$$\zeta_1(-n^3\beta^3 a_n) + \zeta_2(-2t^2 - b_n t^3)$$
$$+ (1 + \eta_{o1})n^4 t^4 + (2 + \eta_{t1} + \eta_{t2})n^2\beta^2 t^2 \quad (1 + \eta_{o2})t^4$$
$$+ 12(R/h)^2[(1 + \mu_2)(1 + b_n t) + \nu n\beta a_n]$$
$$-\lambda_a(n^2\beta^2/2) - \lambda_p[(n^2\beta^2/2) + t^2] = 0 \qquad (3.1)$$

where

$$\lambda_a = (PR/\pi D) \quad \text{and} \quad \lambda_p = (R^3/D)p \qquad (3.2)$$

n are the number of axial half waves, t the number of circumferential waves, μ_1, μ_2, η_{o1}, η_{o2}, η_{t1} and η_{t2} are the changes in stiffnesses due to stringers and rings χ_1, χ_2, ζ_1, and ζ_2 are the changes in stiffnesses caused by the eccentricity of the stringers and rings, as in [20], and a_n and b_n are given by Eqs.(16) of [20]. When one of the load parameters, say λ_a is given, the second, say λ, is calculated from Eq. (3.1). Note that in Eq. (3.2) positive p represents external pressure and negative p internal pressure.

Computations have been carried out for many typical shell covering a wide range of shell and stiffener geometries. The relative efficiency of stringers and rings

and their position is investigated for five typical shells, with (R/h) = 250, 1000 and 5000, (L/R) = 0.5, 2.0 and 4.0, and a stiffeners weight ratio (ratio of total weight of the stiffened shell to that of the unstiffened shell) $(\bar{h}/h)$ = 1.5 and 2.0 where $\bar{h}$ is the equivalent thickness of the stiffened shell and h is the wall thickness of the unstiffened shell

$$(\bar{h}/h) = [1 + (A_1/bh) + (A_2/ah)] \qquad (3.3.)$$

The interaction curves for combined axial compression and external or internal hydrostatic pressure consist essentially of two straight lines that represent two different buckling modes, one with one longitudinal half wave n = 1, and one with many logitudinal waves n ≠ 1. Unstiffened cylindrical shells under the same combined load exhibit a similar behavior. There the transition from the n = 1 mode to the n ≠ 1 mode occurs very near the zero pressure axis (it is sometimes assumed that this transition occurs exactly at the zero pressure axis, whereas actually it occurs at a small positive pressure - see Ref.22 - but still very near the zero pressure axis). In stiffened cylindrical shells, on the other hand, the transition appears at different places along the pressure axis depending on the stiffener geometry (see Figs.29, and 31 to 35). Hence the interaction curves for stiffened and unstiffened shells differ considerably in shape and nature, and one cannot assume that the same interaction applies to both types of shells, as for example in Ref.23 .

In Fig.29 for example the weight ratio $(\bar{h}/h)$ = 1.5 is kept constant and interaction curves are shown with different fractions of the stiffener area allocated to rings and stringers. The most effective distribution of stiffener material for uniformly spaced and constant area rings and stringers can be found from Fig.29 for any combination of axial load and pressure. There is an interplay between the

stiffening contribution of stringers and rings. The longitudinal stiffening of stringers postpone the $n \neq 1$ buckling mode. Since higher critical axial loads correspond to the $n = 1$ mode than to the $n \neq 1$ mode, the interaction curve is raised, or in other words for a certain pressure a higher axial buckling load is attained. On the other hand, since increase in stringer area decreases that of the rings, and therefore the resistance to lateral pressure is reduced, the interaction curve shifts to the left. Along the pressure axis, the conclusions of Ref.24 that rings are the most effective stiffeners under hydrostatic pressure is reconfirmed, and along the axial compression axis a combination of about half the stiffener area allocated to rings and half to stringers is found to be most effective. (A similar conclusion is arrived at in Ref. 25).

It should be recalled here that the superiority of rings alone for stiffening against hydrostatic pressure does not always hold. Since hydrostatic pressure is actually a combination of axial compression and lateral pressure, the same two modes appear in buckling under hydrostatic pressure (see also Ref.24). Hence for certain values of Z, for which the $n \neq 1$ buckling mode would appear with rings only, the addition of stringers of very small area may suffice to cause transition to the $n = 1$ mode and result in considerable increase in buckling pressure. For example, in Fig.35, allocation of 2.5% of the total weight to stringers(inside rings and outside stringers) raises the buckling pressure by 47%, and in Fig. 33 allocation of 1.3% of the total weight to stringers(rings inside and stringers outside) raises the critical pressure by 42%. It may be recommended therefore, that, when the modified stiffened shell parameter $\bar{Z} < 65$, stringers be added to a ring stiffened cylinder under hydrostatic pressure even at the expense of the ring area.

If the shell is stabilized by internal pressure, stringers are found to be the most efficient stiffeners. This is clearly seen at the left hand side of Figs. 29,33 and 35, where the interaction curves for stringers only rise very rapidly with internal pressure and exceed those for stringers and rings. This is not surprising, since the internal pressure stabilises the shell mainly in the circumferential direction, and hence additional longitudinal stiffening is more important.

The influence of the position of the stiffener on the interaction curves is shown in Figs. 30 and 33. The curves shown are envelopes of the interaction curves for different weight distributions between stringers and rings for a constant stiffener weight ratio $(\bar{h}/h) = 1.5$. These envelopes represent the maximum axial buckling load that can be attained with a given weight of stiffened shell for any hydrostatic pressure below the critical. The most efficient configuration for most of the range of combined loads is that with both stringers and rings on the outside. This could be expected from the behavior of stiffened shell under separate loads (Refs. 21 and 24). Stringers are the main stiffeners against the axial load component, and outside stringers are more effective than inside ones over the entire practical geometry range. For rings, on the other hand, which are the main stiffeness against the lateral load component outside rings are more effective only in shell with small Z, and the eccentricity effect inverts as Z increases. Hence the conclusion that both outside rings and stringers are most efficient holds for the entire range of combined loads only in short shells (see for example Fig.33 , where $\bar{Z} = 13.6$), whereas for long shells inside rings and outside stringers are more efficient at the pressure end of the interaction curves.

Figs. 31 and 32 represent shells with the same (L/R) and ($\bar{h}$/h) as Fig.29 but with different values of (R/h). The interaction curves are very similar, except that with internal pressure stringers are more effective for thicker shells, and for external pressure only rings are more efficient the thinner the shell. Figs. 29, 33 and 34 study the influence of length of shell. The interaction curves are again very similar and stringers are more effective in short shells. Heavier stiffeners (Fig. 35) also yield very similar interaction curves.

It should be pointed out that the eccentricity effects for combined stiffening or combined loads are smaller than those corresponding to one type of stiffeners only and separate loads. For example, in Fig. 33, at the axial compression axis, (p^{out}/p^{in}) for stringers only is about 1.88 whereas for combined stringers and rings of equal area (p^{out}/p^{in}) is 1.28. Or at about the middle of the interaction curve, at (p/E) = 0.8 x 10^{-6}, (p^{out}/p^{in}) is 1.55 for (A_2/ah) = 0.4 and (A_1/bh) = 0.1. This reduction in eccentricity effect is due to the presence of both rings and stringers, wheres only either rings or stringer - depending on the dominant load - are directly influenced by the eccentricity effect.

The structural efficiency of stiffening is indicated in Figs.30 and 33, by a comparison with equivalently thickned shells. The very large increase in buckling load attained by stiffening, reemphasize the relative inefficiency of monocoque shells. The fact, that buckling loads for monocoque shells often fall much below the prediction of the linear theory considered here, whereas stiffened shells usually carry the "linear" loads, discredits the monocoque shell even further.

SECTION 4

OPTIMIZATION OF CONICAL SHELLS WITH NON-UNIFORMLY SPACED RINGS

M. Baruch, J. Singer and O. Harari.

In ring-stiffened conical shells under hydrostatic pressure the local conditions of the sub-shells differ, and hence unequal stiffener spacing may be more efficient. The optimum configurations of conical shells with uniformly and non-uniformly spaced rings of rectangular cross-section are therefore studied and compared.

Before one embarks on an optimization study one should scrutinize the assumptions to be employed. One of the commonly used assumptions in the analysis of the local instability in a ring stiffened cylindrical or conical shell subjected to hydrostatic pressure appears then to be unjustified and hence warrants a detailed discussion.

In a stringer-stiffened cylindrical shell subjected to axial compression, the load is shared by stringers and skin, and the axial stress is the load divided by the total cross-sectional area of skin and stringers. When this stress reaches the critical stress of the curved panel between two stringers, usually considered simply supported, local instability has occured. The local buckling in the corresponding case of a ring-stiffened cylindrical shell under lateral or hydrostatic pressure does not represent an obvious extension of that in the axially loaded stringer-stiffened shell, due to the different manner of load application.

Consider first lateral pressure loading. If the rings are very stiff relative to the subshells they will practically not distort and the sub-shell behaves like a simply supported cylindrical shell. The applied circumferential membrane stress is then $\sigma_\phi = (pR/h)$, where h is the thickness of the skin, and the shell prebuckling stress is not noticeably relieved by the stiffeners, as it was in the case of the axially loaded stringer-stiffened shell. The difference

between the two cases becomes immediately obvious if one imagines perfectly rigid stiffeners. No buckling is then possible in the axially compressed stringer-stiffened shell, provided rigid end rings transmit the load, whereas in the ring-stiffened shell under lateral pressure the buckling of the sub-shells is hardly affected, except for slight changes in the boundary conditions. These boundary effects, caused by increase in ring stiffness consist of an effect on the pre-buckling deformation already investigated in 1932 (Ref. 26) and reconsidered recently in a more precise manner (Refs.27,28), and of a rotational restraint effect during buckling (Ref. 27). The prebuckling deformation effect increases the buckling pressure noticeably only in extremely short shells, whereas the rotational restraint during buckling may be appreciable even for sub-shells with Z up to 10.

Minimum-weight analyses (Refs.29 and 30) yield configurations with many closely spaced rings. The buckling behavior of the resulting very short sub-shells approaches that of a long flat plate (See Ref. 31). For lateral pressure the limiting case is a plate loaded by σ_ϕ and the corresponding plate factor $K = 4$. Though the very small length of the sub-shells will augment the boundary effects, this increase will not be directly proportional to the area of the rings. Hence the assumption (employed for example in Ref. 32) that the applied stress for local buckling is $\sigma_\phi = (pR/\bar{h})$ where $\bar{h}$ is the equivalent thickness of the stiffened cylindrical shell, $\bar{h} = h\,[1 + (A_2/ah)]$, does not appear justified for ring-stiffened cylindrical shells under lateral pressure. This assumption is even less justified for hydrostatic pressure loading. The buckling behavior of very short sub-shells under hydrostatic pressure again approaches that of long flat plate (Ref. 31). Now, however, the limiting case is a plate loaded in two perpendicular directions by σ_ϕ and $\sigma_x = (pR/2h)$. An analysis of such a plate shows that for a long plate the

axial stress component becomes dominant. As the plate lengthens, a buckling pattern of a plate free at the short ends is approached, with the plate factor K = 1. The conclusion reached in Ref. [27], that very short shells with Z<1.89 buckle axisymmetrically under hydrostatic pressure has essentially the same meaning. Only σ_x affects axisymmetric buckling (or Euler type buckling in the case of the long plate). Hence the rings cannot affect local buckling, except for some rotational boundary restraint, which again can only be very small with the rings of small torsional stiffness considered here. The assumption, that the applied stress depends on the equivalent thickness for hydrostatic pressure loading, employed in Refs. 29,30,32 and 33, is therefore not justified.

In conical shells under hydrostatic pressure, as in cylindrical shells, rings are the most efficient stiffeners, except in very short shells. A minimum-weight analysis and optimization analysis (for fixed number of rings) is given in Ref. [29] for uniformly spaced rings. Similar analyses for non-uniformly spaced rings are now derived.

For the very closely spaced rings demanded by minimum-weight designs, the sub-shell behaves as a simply supported long plate and local buckling is determined by

$$(\sigma_x/E) = (paxtan\alpha/2h) = [\pi^2h^2/12(1-\nu^2)a_\delta^2] \qquad (4.1)$$

where a_δ is the length of a sub-shell. The ring spacing law that determined a_δ is

$$a_\delta = a_{o\delta}/x^\delta \qquad (4.2)$$

It should be pointed out that $a_{o\delta}$, defined as the ring spacing when x = 1, is only a mathematical parameter devoid of physical meaning, since there exists no sub-shell whose midpoint is x = 1. Substituting for a_δ in terms of $a_{o\delta}$ Eq. 4.1 yields

$$(p/E) = [\pi^2 h^3 x^{(2\delta-1)}/6(1-\nu^2)\ a \tan\alpha\ a_{o\delta}^2] \tag{4.3}$$

where x may take any value between 1 and x_2 that minimizes (p/E). The appropriate choice of x then yields

$$a_{o\delta} = \{\pi^2 h^3 k_1^{2\delta-1}/[6(1-\nu^2)\ a \tan\alpha\ (p/E)]\}^{1/2} \tag{4.4}$$

where for $\delta > 0.5$, $k_1 = 1$ and for $\delta < 0.5$, $k_1 = x_2$.

Since the minimum-weight designs require many more rings than feasable in practice, more realistic optimal configurations can be obtained if the number of rings is specified as a practical restraint. The ring-spacing is then no longer small enough to ensure "plate behavior" and the sub-shells are short conical shells, considered simply supported, whose buckling is determined (Ref.34) by

$$(p/E) = 0.92(\bar{\rho}_{av}/a_\delta)(h/\bar{\rho}_{av})^{2.5} g(\psi) \tag{4.5}$$

and due to shortness of the sub-shells $g(\psi) \approx 1$. Note that $\bar{\rho}_{av}$ is the average radius of curvature for any sub-shell

$$\bar{\rho}_{av} = x a \tan\alpha \tag{4.6}$$

where again x may take any value between 1 and x_2 that minimizes (p/E). Hence, with the appropriate choice of x, one obtains here

$$a_{o\delta} = \{0.92\ h^{2.5} k_2^{(\delta-1.5)}/[(a \tan\alpha)^{1.5}(p/E)]\} \tag{4.7}$$

where for $\delta > 1.5$, $k_2 = 1$ and for $\delta < 1.5$, $k_2 = x_2$.

For estimation of their local instability, the rings are represented by an infinite narrow plate simply supported on one long side and free of the other, as in Refs. 29 and 30, or, alternatively, clamped on one long side and free on the other. The stress applied to the ring is computed with the assumption that rings and shell share the external load according to their cross sectional area. For ring buckling to occur, first, the shell must still be unbuckled and the skin will hence carry at least the part of the load proportional to its cross-sectional area. If the membrane stress distribution is unequal due to wider ring spacing, the skin will carry a larger portion of the load and the rings a smaller load. The assumption of area-proportional load sharing is therefore at most conservative here.

Hence

$$(\sigma_\phi/E)_R = [k_3\pi^2/12(1-\nu^2)](c/d)^2 = \{pax \tan\alpha/[Eh(1 + dcx^\delta/a_{o\delta}h)]\} \quad (4.8)$$

and then for $\nu = 0.3$

$$(p/E)_R = 0.904k_3(c/d)^2(h/a)[1 + (dck_4^\delta/a_{o\delta}h](1/k_4 \tan\alpha) \quad (4.9)$$

where $k_3 = 0.5$ for simple supports at one side, and $k_3 = 1.33$ for one side clamped. k_4 can take any value between 1 and x_2. The correct value for k_4 is that minimizes $(p/E)_R$ in Eq.(4.9).

For $\delta \leq 1$, the minimum value of $(p/E)_R$, occurs at the upper boundary of the given region and hence

$$k_4 = x_2 \qquad \text{for} \qquad \delta \leq 1 \quad (4.10)$$

For $\delta > 1$, k_4 may be between 1 and x_2. k_{4m} which minimizes $(p/E)_R$ mathematically is found to be

$$k_{4m} = [a_{c\delta}h/cd(\delta-1)]^{1/\delta} \tag{4.11}$$

In the calculations one must check, however, if k_{4m} is inside the given region. Hence the appropriate value for k_4 when $\delta > 1$ is given by

$$\begin{aligned} k_4 &= 1 && \text{if} && k_{4m} < 1 \\ k_4 &= x_2 && \text{if} && k_{4m} > x_2 \\ k_4 &= k_{4m} && \text{if} && 1 < k_{4m} < x_2 \end{aligned} \tag{4.12}$$

Substitution of Eq.(4.10) or Eq.(4.12) into Eq. (4.9) and solution for d then yields

$$d = (F_1/2) + \sqrt{(F_1/2)^2 + F_2} \tag{4.13}$$

for

$$k_4 = 1 \quad \text{or} \quad k_4 = x_2$$

where

$$F_1 = (ck_4^{\delta}/a_{o\delta}h)F_2$$

$$F_2 = (0.904k_3c^2h)/[(p/E)k_4 \, a \tan\alpha] \tag{4.14}$$

or

$$d = \left\{[(0.904k_3c^2h)/[(p/E)a \tan\alpha]][\delta/(\delta-1)][(\delta-1)c/a_{o\delta}h]^{(1/\delta)}\right\}^{1/[2-(1/\delta)]}$$

$$\text{for} \quad 1 < k_{4m} < x_2 \tag{4.15}$$

The general instability is computed with the approximate formula of Ref. 35

$$(p/E)_G = 0.92(\rho_{av}/\ell)(h/\rho_{av})^{2.5}[(1+\eta_{2\delta}\,\bar{x}^{\delta})^{0.75} - (\rho_{av}/\ell)(h/\rho_{av})^{0.25}\eta_{2\delta}\,\bar{x}^{\delta}]g^{(1-0.3\delta)} \tag{4.16}$$

which neglects the eccentricity of the rings. Since the main aim of the present study is a comparison of the structural efficiency of non-uniformly spaced rings with that of uniformly spaced rings, and the eccentricity effect is approximately the same for both types of stiffening, the neglect of the eccentricity is not detrimental here.

The effective mean bending stiffness of the rings is represented by

$$\eta_{2\delta} = 0.91(c/a_{o\delta})(d/h)^3 + \{3[(d/h) + 1]^2/[\bar{x}^{\delta} + (c/1.1\, a_{o\delta}h/dc)]\} \tag{4.17}$$

and the equivalent thickness of the stiffened shell $\bar{h}$ (the thickness of an unstiffened conical shell of identical weight) is given by

$$\bar{h} = h\{1 + (cd/a_{o\delta}h)[2(x_2^{(2+\delta)} - 1)/(2+\delta)(x_2^2 - 1)]\} \tag{4.18}$$

The investigation includes a minimum weight analysis as well as several optimization studies with specified numbers of rings for uniform spacing. The calculations were performed in the following manner: A value for h, the shell wall thickness, is chosen and with Eqs.(4.4) or (4.7) the required basic spacing $a_{o\delta}$ is computed for various ring-distribution factors δ. Then $\eta_{2\delta}$ is computed from Eq. (4.17) and the width of the ring c and its height b are found from Eqs. (4.13) or (4.15), and Eq.(4.17). Finally, the equivalent thicknesses of the stiffened shell is computed from Eq.(4.18).

The number of rings for non-uniform spacing can be found from the ring spacing law Eq.(4.2). For hydrostatic pressure loading comparison with uniformly spaced stiffening is based on the sub-shell with the largest mean radius of

curvature. When the ring spacing varies according to Eq.(4.2), the length of this sub-shell is

$$(a_\delta)_m = a_{o\delta}/\{x_2 - [(a_\delta)_m/2]\}^\delta \tag{4.19}$$

Eq.(4.2) can be expressed as a difference equation (see also Fig.1)

$$a_\delta = a(\xi_{n+1} - \xi_n) = a_{o\delta}/[(1/2)(\xi_n + \xi_{n+1})]^\delta\} \tag{4.20}$$

where $a\xi_n$ is the distance along the generator from the vortex to the n^{th} ring, the boundary values of ξ are

$$\xi_o = 1, \quad \text{and} \quad \xi_{N+1} = x_2 \tag{4.21}$$

and N is the total number of rings.

The number of rings for non-uniform spacing, or $a_{o\delta}$ for given N, can be alternatively also calculated from a formula, obtained with a simple kinematic analogue. The analogue is that of a body moving along the generator of the cone with a varying velocity.

$$v = (a_\delta/t_o) = (adx/dt) \tag{4.22}$$

The velocity varies in such a manner that the body traverses the distance between the two rings, a_δ, in a constant time, t_o . By substitution of Eq. (4.2) into Eq. (4.22) one can calculate the total time necessary for the moving body to traverse the distance between the bulkheads

$$T = \int_o^T dt = (at_o/a_{o\delta}) \int_1^{x_2} x^\delta dx = (at_o/a_{o\delta})[(x_2^{\delta+1} - 1)/(\delta+1)] \tag{4.23}$$

The total time T, divided by the constant time t_o in which a_δ is traversed, gives the number of bays (or number of rings plus one).

$$N = [a(x_2^{\delta+1} - 1)a_{o\delta}(\delta+1)] - 1 \qquad (4.24)$$

where N has to be rounded off to the nearest higher integer.

In Figs. 36-46 results are presented for various geometries and loads.

The equivalent thickness of the stiffened shell which represents the total weight is plotted versus the number of rings N. A discontinuity in slope appears in all the curves of Figs. 36-46. This discontinuity is caused by transition from "plate behavior" of sub-shells to "shell behavior". For very small ring-spacing (large number of rings) at the right of Figs. 36-46 "plate behavior" is appropriate and Eq.(4.4) applies. As the ring-spacing increases towards the left of figures, the sub-shells have to be considered as conical shells and Eq. (4.5) applies. With increasing number of rings, or diminishing ring-spacing, the discontinuity is the point where the curves computed from Eqs.(4.5) and (4.4) intersect, and to the right of which the approximate shell buckling formula Eq. (4.5) is more conservative than the "plate behavior" approximation, which in itself is slightly conservative. If the actual curve for the critical pressure of the sub-shells were used, no discontinuities would appear in Figs. 36-46.

One may note that for $\delta = 1.5$ the transition occurs in all the graphs, except for short shells, Figs. 40 and 46, at an N beyond the minimum-weight and is hence of no interest. Also in the short shells, Figs. 40 and 46, the transition for $\delta = 1.5$ occurs at a considerably larger N than that for $\delta = 0$ and $\delta = 0.5$. The computations were carried out in all the figures with rings taken as a simply supported-free plate ($k_3 = 0.5$). For one case, however, Fig. 38, the computations were also carried out for $\delta = 0$ and $\delta = 1.5$ with rings

taken as a clamped - free plate ($k_3 = 1.33$). Obviously the non-conservative clamped-free assumption yields smaller weights, but the differences are seen to be small, particularly in practical range of N. All the graphs, except those for short shells, Figs. 40 and 46, indicate that for minimum-weight design, $\delta = 0.5$ results in the most efficient structure. This is not surprising since the minimum-weight configuration has very small ring-spacings with corresponding "plate behavior". In the "plate regime" sub-shells of equal local stiffness are obtained with $\delta = 0.5$, and hence this ring distribution is most efficient. The minimum weight configuration, however, are not practical due to the very large number of rings required, as already mentioned earlier. In the optimal design region with a reasonable predetermined number of rings, $\delta = 1.5$ results in a more efficient structure, since in the "shell regime" $\delta = 1.5$ yields sub-shells of equal local stiffness.

Whereas in the minimum-weight design region only small weight-savings are possible with unequal ring-spacing, considerable savings may be obtained in more practical configurations. For example, in Fig. 38 only about 5% saving is possible in the minimum-weight design region, but with N = 11 the shell considered in is 27% lighter with non-uniform ring, spacing ($\delta = 1.5$) than with uniform spacing ($\delta = 0$). Or, if one aims at a reduction of manufacturing costs rather than weight saving, less rings are needed with varying ring-spacing. As for example for $\bar{h} = 0.106$ inches in Fig. 38, 11 rings are needed with $\delta = 1.5$, whereas with $\delta = 0$ 21 rings would be required.

In order to investigate the effect of various parameters, optimization of stiffened conical shells of different dimensions and at different levels of external pressure is shown in Figs. 36-46. A decrease in x_2 Figs. 38, 40 and 46

shifts the minimum-weight configuration to a smaller number of rings, N. The ratio of (N/x_2) corresponding to minimum-weight appears to be roughly constant, and hence the optimal number of rings is approximately a linear function of the length. For a predetermined non-optimal ratio of (N/x_2) the weight saving with $\delta = 1.5$, compared to uniform spacing $\delta = 0$, increases with x_2, as could be expected since the non-uniform ring-spacing law yields noticeable differences in ring-spacing only in long shells. For example, for $(n/x_2) = 2.5$ the increase is from 11 percent at $x_2 = 1.3$, Fig.46, to 20 percent at $x_2 = 4$, Fig. 38.

Loading variation does not effect the relative efficiency of non-uniform to uniform spacing. For example, with a predetermined $N \sim 10$ the gain with $\delta = 1.5$ compared to $\delta = 0$ remains at approximately 25% when (p/E) varies from 0.3 to 4.8. Figs. 36-39.

If on the other hand the overall efficiency of stiffening compared to thickening of the shell (though not directly related to the discussion here) is considered, it is found to decrease with increase in pressure. If one compares the optimal $\bar{h}$ in Figs. 36-39 with the equivalent thickness of the monocoque shell, $\bar{h}_{monocoque}$, one finds that the relative weight of the stiffened shell $(\bar{h}/\bar{h}_{monocoque})$ increases roughly linearly with log (p/E). Again this could be expected since stiffening becomes more efficient the thinner the basic shell.

Variation of the cone angle (see Figs. 36,41,42,43) does not produce large changes in the relative efficiency of non-uniform ring-spacing. For example, with a predetermined number of rings N = 10, the weight saving at

first rises slightly from 21% at $\alpha = 15^{\circ}$ to 22% at $\alpha = 30^{\circ}$ and 45°, and then at $\alpha = 60^{\circ}$ it falls to 11%. There appears therefore a v[illegible] flat maximum at medium cone angles. Consideration of the limiting cases of a cylindrical shell for $\alpha = 0$ and a circular plate $\alpha = \pi/2$ for which uniform spacing is most efficient, explains the observed maximum. A further minor "cone angle effect" is a shift of the intersection of the $\delta = 1.5$ curves to smaller N with increasing α .

In figures 44 and 45 the effect of a change in "a" is studied, and no noticeable influence on the relative efficiency of non-uniform stiffening is found.

An additional general conclusion emerges from these studies with varying parameters" a decrease in the overall stiffness of the structure (larger x_2, "a" and α), shifts the minimum-weight design point to a smaller number of rings N. This is of considerable importance, since the nearer the optimal N is to practical values, the larger the weight savings that can actually be realized in practice.

Since the general instability pressure is calculated in this section with an approximate formula Eq.(4.16) that neglects the eccentricity of the rings, the general instability pressure of some points in Fig. 38 has been recalculated with the more exact method of Ref. 38. The differences are found to be very small for inside rings, less than 6% in all cases (corresponding to a weight difference of about 2%), and only slightly larger for outside rings, 3 - 12% (corresponding to a weight difference of about 1 - 4.5%).

SECTION 5.

EXPERIMENTAL STUDIES ON BUCKLING OF STIFFENED CONICAL SHELLS UNDER TORSION AND AXIAL COMPRESSION

J. Singer and T. Weller.

5.1. INTRODUCTION

A method of analysis of the general instability of stiffened cylindrical and conical shells was developed in Refs. 20 and 36. In the analysis the stiffeners are "distributed" or "smeared" over the entire shell and hence it applies only to closely spaced stiffeners which, however, need not necessarily be evenly spaced and equal. The effect of the eccentricity of the stiffeners is considered in this theory, which is applied to uniformly stiffened cylindrical shells under external pressure in Refs. 20 and 24 and under axial compression and torsion in Refs. 21 and 37, to uniformly stiffened conical shells in Ref. 36 and to conical shells with nonuniformly spaced stiffeners in Ref. 35.

The results of an experimental investigation on the buckling of ring-stiffened conical shells under uniform hydrostatic pressure carried out at the Technion, that verify the theoretical results of Ref. 36 are reported in Ref. 5. In Ref. 38 some preliminary results for buckling under torsion and axial compression are presented. Agreement between experimental and approximate theory is found to be fairly good in the case of torsion, but poor in the case of axial compression (only slightly better than for unstiffened cones).

The work on stiffened shells has been preceded by and is related to earlier studies on the buckling of unstiffened conical shells under torsion, axial compression and combined torsion and axial compression (Refs. 3,6, and 42).

The main purpose of the present test program is to study the general instability of integrally ring-stiffened conical shells under torsion, axial compression and combined torsion and axial compression. The specimens used are integrally machined ring-stiffened shells of high strength steel alloy. The specimens have different uniform stiffener spacing, and the dimensions of skin thickness of the shell and the eccentricity of the stiffeners were varied accordingly to ensure completely elastic buckling. Some shells were made with very close stiffener spacing in order to raise the axial buckling load to the linear classical value.

In the experiments, the onset of buckling (the appearance of the first buckling wave) and the complete buckling of the whole shell were recorded. The experimental results are compared with a linear theory which is an extension of Ref. 36, and with approximate theories discussed in Ref. 39.

5.2. TEST APPARATUS AND PROCEDURE

The load frame employed in the experimental work for the investigation of buckling under combined torsion and axial compression is the same one as used in the tests of Section 1 of the present report and is shown in Fig. 2a. The complete test set-up is shown in Fig. 47. The load capacity of this frame load was found to be too small to study the buckling under axial compression. The axial compression tests were therefore carried out on a 30 ton "Amsler" universal test machine.

Resistance strain gages bonded to the specimens were used to measure

strains on the surface of the shell during loading and detect buckling. Furthermore, the symmetry of loading was checked with the aid of strain gages located on the same circle and oriented in the same direction.

Strain gages were located circumferentially at various stations around and along the shell as well as longitudinally and at angles of about 45° in order to measure buckling modes of either torsion or axial compression. More gages were attached near the smaller radius of the shell, where the buckling waves are expected in torsion, in order to detect and "arrest" the buckling load in time to ensure completely elastic behavior. Sufficient care will then permit repetition of tests with different loading combinations. As discussed in Ref. 40 and Section 1 of this report, such a test procedure yields interaction curves with less scatter. Strain measurements were recorded on a B & F-24-channel strain plotter Fig. 47 and load-strain curves were obtained during tests. The points on these curves where the strain gage plots cease to be linear are a direct indication of onset of buckling.

In the present tests, the specimens were approximately clamped at the ends. The end fittings have a conical shape (see Fig. 48), and there is almost no rotation of the generators at the ends of the shell.

The out-of-roundness was measured prior to each test. It was mapped in each case to obtain a clear picture of the imperfection of shell and to find A_o by Holt's method (Ref. 41).

5.3. TEST SPECIMENS

Seven integrally ring-stiffened conical shells were machined from Ph 17-7 steel alloy. The mechanical properties of the plates used for fabrication of the conical shells were as follows (before hydro-spinning and stress relief):

$$E = 27.5 \times 10^6 \text{psi}$$

$$\nu = 0.278$$

Thick conical shells were first formed by shear-spinning. This process yields uniform shells with no seams or welds. Another advantage of the spinning process here comes from the fact that in order to get higher strength properties of Ph 17-7 steel alloy, its structure has to be transformed from the austenitic state into the martensitic state and then undergo an aging process by heat treatment. Trasformation from austenitic into martensitic state can be obtained by a cold drawing process and the spinning process serves this purpose here. The "raw" shells were therefore highly pre-stressed and had to undergo a thermal stress-relief process and "aging". Specimens were cut out from typical shells and were tested for optimal heat-treatment, aging time and temperature, the optimum here being most efficient stress relief with reasonable strength. The heat-treatment and "aging" that was finally chosen achieved about 80% stress relief and a yield strength of 122 kg/cm^2 (173.5×10^3 psi) of shell material.

Though the conical shells were formed on a very accurate and precise mandrel, the inner surface of the shell was not found to be as smooth as expected. The inner surfaces of the shells were therefore ground, and then the shells were mounted on another conical madrel of exactly the same cone angle as the shell for machining of the required stiffened shell profile. The machining mandrel was fitted separately for each shell.

As the purpose of the present work was to achieve elastic buckling of the shells, the possibility of early yielding had to be kept remote. Hence the shells had to have a very thin skin, the thickness of which had to be very accurate and uniform. At first, it was thought that grinding would answer these exacting requirements better than turning. Later it was found, however, that because of the high thermal stresses that occur during grinding, the shape of the skin between stiffeners distorted and this resulted in a less precise skin than expected, Turning, was, therefore, found preferable, if care was taken to avoid high local pressures during machining.

Shells with different stiffeners spacing were made, but the distances between stiffeners were always chosen in such a manner as to ensure that general instability of the shell preceeded local buckling of shell skin between stiffeners. The present test program included 3 shells, with almost identical dimensions, which were investigated under torsion and combined loading of torsion and axial compression, and another 4 shells with very close stiffening which were tested under axial compression. Two of these were heavily stiffened while the other two had weaker rings. Distances between rings were nearly the same in all the 4 shells of the axial compression series and the geometry of the shells was similar, except for length and taper ratio. All the dimensions were carefully measured prior to test and after it. The thickness was measured at many circumferential points along as many generators as possible, and the measurements were repeated on specimens cut out from the shell after buckling. The measured dimensions of the shells tested, defined in Fig. 1 are presented in Table 5.1.

TABLE 5.1.

DIMENSIONS OF RING-STIFFENED SPECIMENS

Specimen No.	DIMENSIONS OF SHELL									DIMENSIONS OF STIFFENERS					
	Thickness h (mm)	Small Radius R_1 (mm)	Large Radius R_2 (mm)	a (mm)	x_2	Cone Angle α (deg)	Taper Ratio $\psi = 1-R_1/R_2$	ρ_{av}/h	ℓ/ρ_{av}	d (mm)	c (mm)	a_o (mm)	e_2/h	$A_2/a_o h$	$I_{22}/a_o h^3$
M 3-1	.32	45	140	131.6	3.111	20	.678	308	2.82	.41	2.2	20.5	-1.14	.140	.0190
3-2	.32	45	140	131.6	3.111	20	.678	308	2.82	.48	2.2	20.0	-1.25	.150	.0281
3-3	.31	45	140	131.6	3.111	20	.678	316	2.84	.40	4.0	11.0	-1.13	.459	.0650
3-3A	.31	70	140	204.7	2.0	20	.500	358	1.84	.40	4.0	11.0	-1.13	.459	.0650
3-4	.31	45	140	131.6	3.111	20	.678	318	2.82	.39	2.0	20.0	-1.13	.126	.0166
3-5	.30	45	140	131.6	3.111	20	.678	329	2.81	.50	1.5	10.0	-1.33	.249	.0574
3-5A	.31	70	140	204.7	2.0	20	.500	362	1.83	.49	1.5	10.0	-1.29	.237	.0477

5.4. EXPERIMENTAL RESULTS AND DISCUSSION

Specimens M3-1; M3-2; and M3-4 were tested in torsion and under combined torsion and axial compression. The results obtained are presented in Table 5.2, in which the results of earlier tests on similar shells (Ref. 38) are also included. The theoretical torque T_{th} is obtained by an extension of the method of Ref. 36, and the approximate value $T_{th\cdot B\text{-}G\text{-}S}$ is obtained by consideration of an equivalent orthotropic cylindrical shell, as in Refs. 38 and 39, for which the critical torque is computed with formulae proposed by Becker and Gerard (Ref. 43). The agreement between experiment and linear theory of the 3 shells of the present program is fairly good. The partial clamping of the ends in the tests can be expected to raise the critical torque considerably, and hence the good agreement with the theoretical values for simple supports is classified as only fairly good. Since the 3 shells M3-1, M3-2 and M3-3 differed only slightly, similar experimental torques were expected, and the experimental scatter was very small indeed for buckling tests. The experimental values of the buckling torques for the 3 shells were within less than 4 percent. The small scatter can in part be attributed to the lower imperfection sensitivity of closely stiffened shells compared to unstiffened ones.

The critical torques for local instability at the small and large ends of the cones, computed from an approximate formula due to Seide (Ref.8), are also given in Table 5.2, but are well above the critical torque for general instability. The maximum shear stress at buckling, shown in Table 5.2, is much below the yield stress, and hence plasticity effects should be practically negligible.

In Table 5.3. the buckling loads under axial compression obtained with specimens

TABLE 5.2.

BUCKLING OF RING-STIFFENED CONICAL SHELLS UNDER TORSION - RESULTS OF TESTS AND COMPARISON WITH THEORY

Specimen	Taper Ratio	Out-of-roundness [mm]	T_{ex} [Kg.m]	T_{th} [Kg.m]	T^*_{th} [Kg.m]	$T_{th\text{-}B.G.S.}$ [Kg.m]	$T_{Local\ buckle\ near\ R_1}$ [Kg.m]	$T_{local\ buckle\ near\ R_2}$ [Kg.m]	$\frac{T_{ex}}{T^*_{th}}$	$\frac{T_{L.B.R_1}}{T_{ex}}$	$\frac{T_{L.B.R_2}}{T_{ex}}$	$\frac{\tau_{max}}{[Kg/mm^2]}$
M3-1	.678	.106	146	158	158	156	182	666	.926	1.25	4.56	35.6
M3-2	.678	.096	152		178	176	182		.854	1.20		37.3
M3-4	.678	.083	148		142	140	170		1.04	1.15		36.4
Sul-1A-Ref.38	.725		125			125						
Sul-1B-Ref.38	.554		254			198						

Special Notation - T_{ex} = experimental buckling torque

T_{th} = theoretical torque calculated by extension of method of Ref. 36.

T^*_{th} = T_{th} of M3-1 corrected by ratio of $T_{th\ B\text{-}G\text{-}S}$ to that corresponding to M3-1.

$T_{th.B\text{-}G\text{-}S}$ = approximate theoretical torque computed for an equivalent orthotropic shell as in Ref. 39.

$T_{L.B.R_1}$ = T for local buckling near small end.

$T_{L.B.R_2}$ = T for local buckling near large end.

TABLE 5.3.

BUCKLING OF RING STIFFENED SHELLS UNDER AXIAL FORCE - RESULTS OF TESTS AND COMPARISON WITH THEORY

Specimen No.	$\tilde{h}$ [mm]	h_{min} [mm]	Taper Ratio ψ	Out-of-Roundness [mm]	P_{ex} [kg]	P_{cr} Eq.5.1 [for $\tilde{h}$] [kg] (I)	P_{cr} Eq.5.2 [for $\tilde{h}$] [kg] (II)	P_{cr} Eq.5.1 [for h_{min}] [kg] (III)	P_{cr} Eq.5.2 [for h_{min}] [kg] (IV)	$\frac{P_{ex}}{P}$ I	$\frac{P_{ex}}{P}$ II	$\frac{P_{ex}}{P}$ III	$\frac{P_{ex}}{P}$ IV	$(\sigma_x)_{max}$ [kg/mm^2]
M														
3-3	.31	.30	.678	.068	5800	6210	7510	5820	7100	.934	.773	.997	.825	70.0
3-3A	.31	.31	.500	.044	6000	6210	7510	6210	7510	.966	.800	.966	.800	70.0
3-5	.30	.25	.678	.011	3750	5820	6500	3640	4190	.645	.577	1.03	.923	47.2
3-5A	.31	.29	.500	.014	3000	6210	6910	5220	5870	.805	.724	.95	.861	39.4
SUL-2A (Ref.38)	.33				4550	7660	8200			.595	.555			

M3-3; M3-3A; M3-5; and M3-5A are presented. The experimental critical axial loads obtained are compared in Table 5.3 with linear theory. The critical loads are first computed from an approximate formula.

$$P_{cr} = 2\pi c E h^2 \cos^2\alpha \qquad (5.1)$$

proposed by Seide for unstiffened conical shells (Ref. 6) where C = 0.605 as in cylindrical shells. Then the stiffening effect of the rings was taken into account in an approximate manner as for cylindrical shells (Ref. 21) and a modified approximate formula results

$$P_{cr} = 2\pi c E h^2 \cos^2\alpha [1 + A_2/a_o h]^{1/2} \qquad (5.2)$$

The theoretical values were computed for the mean thickness of the shell $\bar{h}$ and for the minimum measured thickness h_{min} .

Except for specimen M3-5, where edge buckling occurred, the experimental buckling loads approach the value predicted by classical linear theory. The closer the rings and the heavier, the better the agreement with linear theory. In shell SUL-2A in Table 5.3 (result obtained in Ref. 38) the rings were not very closely spaced and therefore not very effective. Hence only less than 60% of the classical buckling load of the unstiffened shell, or 56% of the stiffened shell was obtained. For the very closely and heavily stiffened shells M3-3 and M3-3A, on the other hand, 93%-97% of the classical load of the unstiffened shell and 77%-80% of the stiffened shell was obtained. These comparisons are for the mean thickness of the shell $\bar{h}$ and even higher values are obtained with calculations based on h_{min} .

The prediction of Ref. 38 that closer ring spacing will raise the experimental buckling loads to the vicinity of the classical value is hence verified by the present tests, as could be expected in view of similar results for cylindrical shells (Refs. 43 and 44). The stresses at buckling are also given in Table 5.3, and again they are much below the yield stress. Hence probably no appreciable plasticity effects occurred.

The buckle pattern of a heavily stiffened shell (M3-3A) under axial compression is shown in Fig. 49.

Table 5.4 gives the critical loads for shells M3-1; M3-2 and M3-4 under combined loading of torsion and axial compression. An empirical theoretical curve based on these results is plotted in Fig. 50.

There was a significant difference in the critical axial load for the shells tested, since the 3 shells tested under combined loading did not have very closely spaced rings and were therefore still imperfection-sensitive under axial compression. A common interaction curve could, however, be fitted to all the results (which were related to the single load critical values of each shell) with fairly small scatter. The two points that deviate considerably (shell M3-2) were accompanied by visible plastic deformation and can therefore be disregarded and are, therefore, of doubtful validity.

It may be noted that the load-strain plots, obtained on the B & F recorder during the tests nearly always exhibited linearity up to buckling. This verifies the general conclusion that the buckling behavior of closely stiffened shells is better described by linear theory than that of unstiffened shells.

TABLE 5.4.

COMBINED TORSION-COMPRESSION BUCKLING DATA OBTAINED FROM PH17-7 STEEL ALLOY RING-STIFFENED CONICAL SHELLS OF CONE ANGLE 20°

M3-1		M3-2		M3-4	
P(kg)	T(kg.m)	P(kg)	T(kg.m)	P(kg)	T(kg.m)
0	146	0	152	0	148
220	146	550	133	550	133
720	141	1080	79	1080	114
1200	135	1350	47	1640	81
1640	121	1780	27	1900	57
2080	95	1860	18	2180	0
2620	67				

5.5. CONCLUSIONS

Bucklings tests of ring stiffened conical shells under torsion yielded fairly good agreement with linear theory. Under axial compression, good agreement with linear theory was found for shells with closely spaced heavy rings, while for shells with weaker stiffening the agreement was poor. An empirical interaction curve for ring stiffened conical shells under torsion and axial compression was obtained.

Further tests appear desirable and a continuation of the present experimental program has been initiated.

REFERENCES

1) Singer, J. and Baruch, M., Buckling of Circular Conical Shells under Combined Torsion and External or Internal Pressure, Topics in Applied Mechanics, Elsevier Publishing Co., Amsterdam 1963, p. 65. Also Chapter 1, TAE Report 19, Technion Research and Development Foundation Haifa, Israel, September 1962.

2) Singer, J. and Eckstein, A., Recent Experimental Studies of Buckling of Conical Shells Under Torsion and External Pressure, Proceedings of 5th Israel Annual Conference on Aviation and Astronautics, Jerusalem Academic Press, February 1963, p. 1935.

3) Berkovits, A. and Singer, J., Buckling of Unstiffened Conical Shells Under Combined Torsion and Axial Compression or Tension, Proceedings of 7th Israel Annual Conference on Aviation and Astronautics, Jerusalem Academic Press, February 1965, p. 15.

4) Terebushko, O.I., Stability of Cylindrical Shell under Twisting, External Pressure and Compression, ARS Journal, Vol. 31, March 1961, p. 378.

5) Singer, J., Eckstein, A., Fersht-Scher, R. and Berkovits, A., Buckling of Isotropic, Orthotropic and Ring-Stiffened Conical Shells, TAE Report 30, Technion Research and Development Foundation, Haifa, Israel, 1963.

6) Seide, P., Axisymmetrical Buckling of Circular Cones Under Axial Compression, Journal of Applied Mechanics, Vol. 23. No. 4, December 1956, p. 625.

REFERENCES (Cont'd)

7) Lackman, L. and Penzien, J., Buckling of Circular Cones Under Axial Compression, Journal of Applied Mechanics, Vol. 27, No. 3, September 1960, p. 458.

8) Seide, P., On the Buckling of Truncated Conical Shells in Torsion. Journal of Applied Mechanics, Vol.29, No.2,June 1962, p. 321.

9) Singer, J., Buckling of Conical Shells under Axisymmetrical External Pressure, Journal of Mechanical Engineering Science, Vol.3, No.4, December 1961, p.330.

10) Weingarten, V.I., and Seide, P., Elastic Stability of Thin-Walled Cylindrical and Conical Shells under Combined External Pressure and Axial Compression, AIAA Journal, Vol.3, No.5, May 1965, p.913.

11) Weingarten, V.I., Stability of Internally Pressurized Conical Shells under Torsion, AIAA Journal,Vol.2, No.8, 1964, p. 1782.

12) Weingarten, V.I., Morgan, E.J., and Seide, P., Elastic Stability of Thin-Walled Cylindrical and Conical Shells under Combined Internal Pressure and Axial Compression, AIAA Journal, Vol.3, No.6, June 1965, p. 1118.

13) Thielemann, W.F., New Developments in the Nonlinear Theories of the Buckling of Thin Cylindrical Shells, Aeronautics and Astronautics, Proceedings of the Durand Centennial Conference, August 1959, Pergamon Press, Oxford, 1960, p. 76.

REFERENCES (Cont'd)

14) Batdorf, S.B., Stein, M. and Schildcrout, M., Critical Combinations of Torsion and Direct Axial Stress for Thin-Walled Cylinders, NACA TN 1345, June 1947.

15) Weingarten, V.I., Morgan, E.J. and Seide, P., Elastic Stability of Thin-Walled Cylindrical and Conical Shells under Axial Compression, AIAA Journal, Vol. 3, No. 3, March 1965, p. 50.

16) Thielemann, W.F., On the Postbuckling Behavior of Thin Cylindrical Shells, Collected Papers on Instability of Shell Structures - 1962, NASA TN D-1510, December 1962.

17) Schnell, W. and Schiffner, K., Experimentelle Untersuchungen des stabilitätsverhaltens von dünnwandigen Kegelschalen unter Axiallast und Innendruck, Deutsche Versuchanstalt für Luft-und Raumfahrt, Bericht Nr. 243., November 1962.

18) Du Pont Mylar Polyester Film, Technical Information Bulleting M-1A, Summary of Properties, E.I. Du Pont De Memours & Co. (Inc.) Wilmington 98, Delaware.

19) Becker, H. Elastic Modulus of Mylar Sheet, Journal of Applied Polymer Science, Vol. 9, No.3, March 1965, p. 911.

20) Baruch, M. and Singer, J., Effect of Eccentricity of Stiffeners on the General Instability of Stiffened Cylindrical Shells Under Hydrostatic Pressure, Journal of Mechanical Engineering Sciences, Vol. 5, No. 1, March 1963, p. 23.

REFERENCES (Cont'd)

21) Singer, J., Baruch, M. and Harari, O., On the Stability of Eccentrically Stiffened Cylindrical Shells Under Axial Compression, TAE Report 44, Technion Research and Development Foundation, Haifa, Israel, December, 1965.

22) Singer, J., Comment on a Theoretical Interaction Equation for the Buckling of Circular Shells Under Axial Compression and External Pressure, AIAA Journal, Vol. 2, No. 2, February 1964, p. 410.

23) Burns, A.B. and Skogh, J., Combined Loads Minimum Weight Analysis of Stiffened Plates and Shells, Journal of Spacecraft and Rockets, Vol. 3, No. 2, February 1966, p. 235.

24) Singer, J., Baruch, M. and Harari, O., Further Remarks on the Effect of Eccentricity of Stiffeners on the General Instability of Stiffened Cylindrical Shells, TAE Report 42, (revised), Technion Research and Development Foundation, Haifa, Israel, August 1965, (to be published in the Journal of Mechanical Engineering Science).

25) Burns, A.B. and Almroth, B.O., Structural Optimization of Axially Compressed Ring-Stringer Stiffened Cylinders, Journal of Spacecraft and Rockets, Vol. 3, No. 1, January, 1966, p. 19.

26) Von Sanden, K. and Tolke, F., Über Stabilitatsprobleme dünner Kreiszylindrischer Schalen, Ingenieur Archiv, Vol. 3, 1932, p. 24.

27) Reynolds, T.E., Elastic Lobar Buckling of Ring-Supported Cylindrical Shells Under Hydrostatic Pressure", David Taylor Model Basin Report 1614, September 1962.

REFERENCES (Cont'd)

28) Stein, M., The Effect on the Buckling of Perfect Cylinders of Prebuckling Deformations and Stresses Induced by Edge Support, Collected Papers on Instability of Shell Structures, - 1962, NASA TN D-1510, December 1962, p. 217.

29) Burns, A.B., Minimum-Weight, Hydrostatically Compressed Ring-Stiffened Cones, Journal of Spacecraft and Rockets, Vol. 3, No. 3, March 1966, p. 387. Also LMSC-2-60-64-30, Lockheed Missile and Space Company, Sunnyvale, California, July 1964.

30) Nickell,E.H. and Crawford, R.F., Optimum Ring-Stiffened Cylinders Subjected to a Uniform Hydrostatic Pressure, Society of Automotive Engineers, Preprint 578F, 1962. Also LMSC-6-90-62-57, Lockheed Missiles and Space Company, Sunnyvale, California, 1962.

31) Batdorf, S.R., A Simplified Method of Elastic Stability Analysis for Thin Cylindrical Shells, NACA Report 874, 1947.

32) Gerard, G., Minimum Weight Design of Ring Stiffened Cylinders Under External Pressure, Journal of Ship Research Vol. 5, 1961, p. 44.

33) Crawford, R.F. and Burns, A.B., Minimum Weight Potentials for Stiffened Plates and Shells, AIAA Journal, Vol. 1, No. 4, April 1963,p.879.

34) Seide, Paul, On the Buckling of Truncated Conical Shells Under Uniform Hydrostatic Pressure, Proceedings of the IUTAM Symposium on the Theory of Thin Elastic Shells, Delft, 1959, North-Holland Publishing Company, Amsterdam, 1960, p. 363.

REFERENCES (Cont'd)

35) Baruch, M., Singer, J. and Harari, O., General Instability of Conical Shells with Non-Uniformly Spaced Stiffeners Under Hydrostatic Pressure, Proceedings of the 7th Israel Annual Conference on Aviation and Astronautics, Israel Journal of Technology, Vol. 3, No. 1, February 1965, p. 62.

36) Baruch, M. and Singer, J., General Instability of Stiffened Circular Conical Shells under Hydrostatic Pressure, The Aeronautical Quarterly, Vol. 26, Part 2, May 1965, p. 187, Also, TAE Report 28, Technion Research and Development Foundation Haifa, Israel, June 1963.

37) Baruch, M., Singer, J. and Weller, T., Effect of Eccentricity of Stiffeners on the General Instability of Cylindrical Shells Under Torsion, Proceedings of the 8th Israel Annual Conference on Aviation and Astronautics, Israel Journal of Technology, Vol. 4, No. 1, February 1966, p. 144. Also TAE Report 43, Technion Research and Development Foundation, Haifa, Israel, August 1965.

38) Singer, J., On the Buckling of Unstiffened, Orthotropic and Stiffened Conical Shells, Presented at the 7th Congres International Aeronautique, Paris, June 1965.

39) Singer, J., Fersht-Scher, R. and Betser, A., Buckling of Orthotropic Conical Shells Under Combined Torsion and External or Internal Pressure, Proceedings of the 6th Israel Annual Conference on Aviation and Astronautics, Israel Journal of Technology, Vol. 2, No. 1, February 1964, p. 179.

REFERENCES (Cont'd)

40) Singer, J., On Experimental Technique for Interaction Curves for Buckling of Shells, Experimental Mechanics, Vol. 4, No. 9, September, 1964, p. 279.

41) Holt, M., A Procedure for Determining the Allowable Out-of-Roundness for Vessels Under External Pressure, Transactions ASME, Vol. 74, 1952, p. 1225.

42) Singer, J., Buckling of Circular Conical Shells Under Uniform Axial Compression, AIAA Journal, Vol. 3, No.5, May 1965, p.985.

43) Becker, H. and Gerard, G., Elastic Stability of Orthotropic Shells, Journal of the Aerospace Sciences, Vol. 29, No. 5, May 1962, p. 505.

44) Milligan, R., Gerard, G., Lakshmikantham, C., and Becker, H., General Instability of Orthotropically Stiffened Cylinders, Report AFFDL-TR-65-161, Air Force Flight Dynamics Laboratory, USAF, Wright Patterson Air Force Base, Ohio, July 1965.

ACKNOWLEDGEMENT

The authors would like to thank Messrs. J. Frum, A. Klausner, A. Greenwald, Y. Porath and S. Nachmani for their assistance during the course of the tests, to Miss A. Adler and Miss M. Rosiano for assistance with the computations and the staff of the Technion Computing Center for their valuable help.

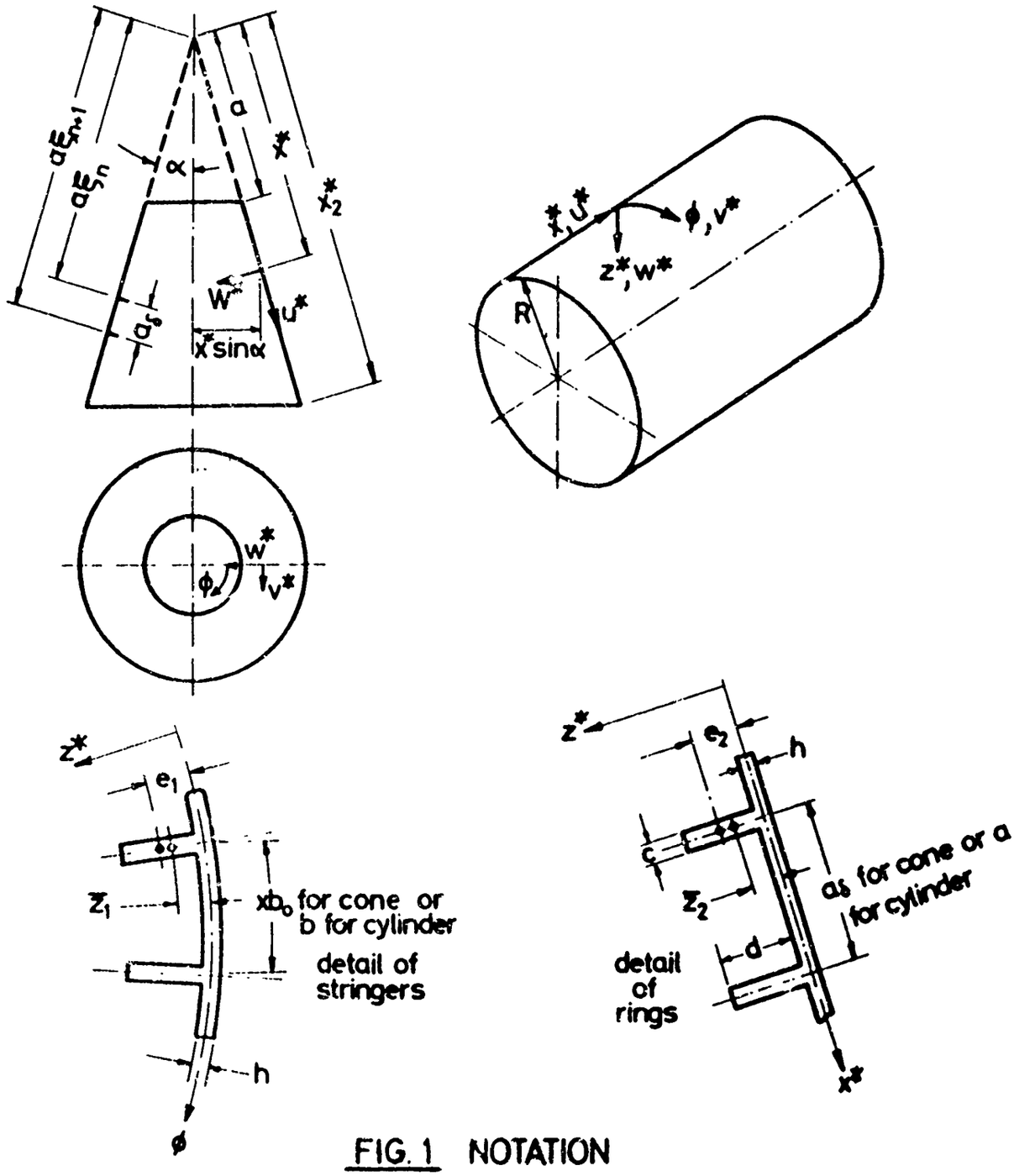

FIG. 1 NOTATION

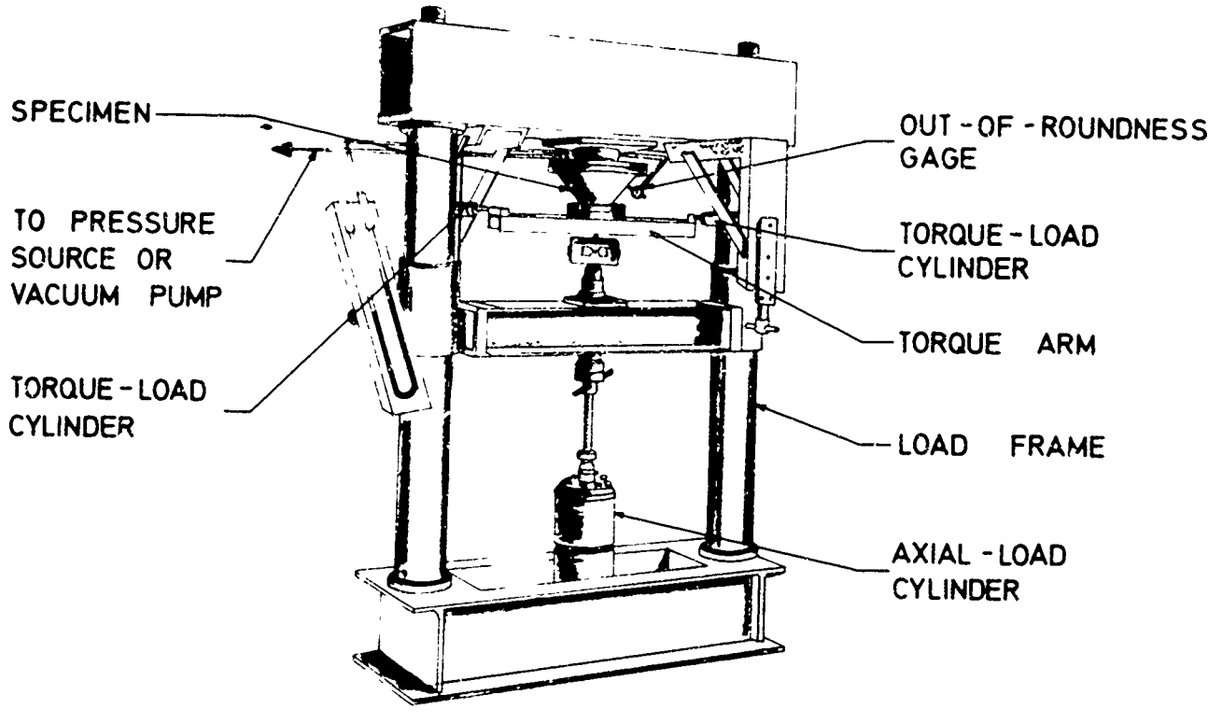

FIG. 2a SCHEMATIC REPRESENTATION OF LOAD FRAME FOR TESTS OF CONICAL SHELLS UNDER COMBINED LOADS.

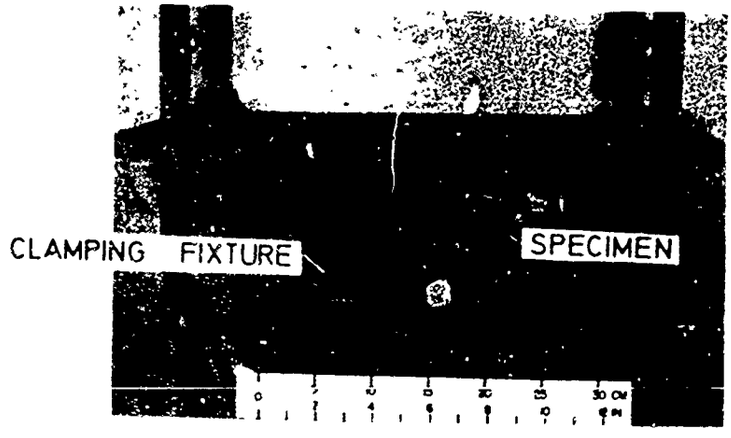

FIG. 2b ALIGNING JIG FOR CLAMPING OF CONICAL SHELLS.

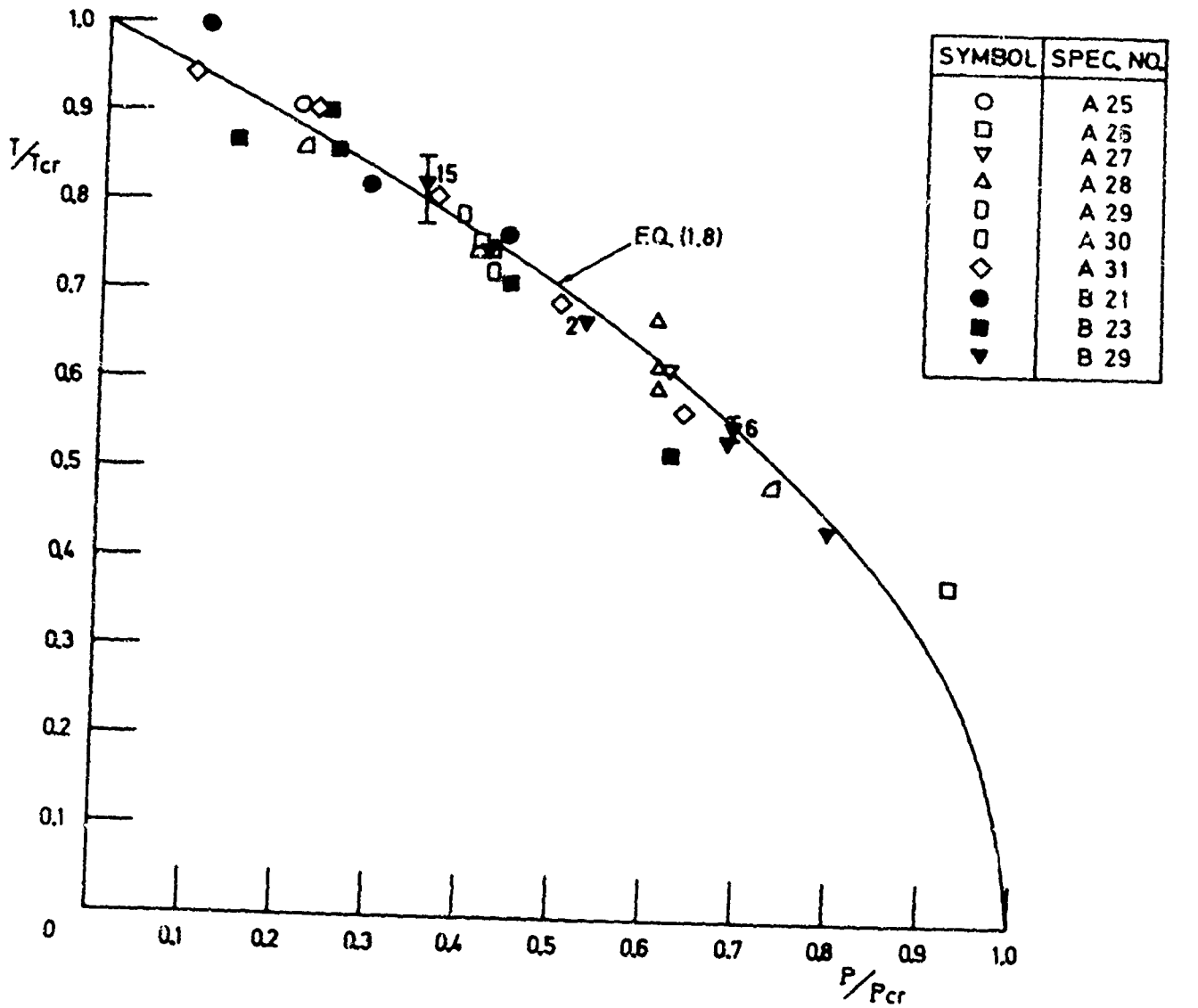

FIG. 3 BUCKLING OF ALCLAD 2024-T3 ALUMINUM-ALLOY UNSTIFFENED CONICAL SHELLS UNDER COMBINED TORSION AND AXIAL COMPRESSION ; $\alpha = 40°$; SERIES A : $\psi = 0.678$, SERIES B : $\psi = 0.500$.

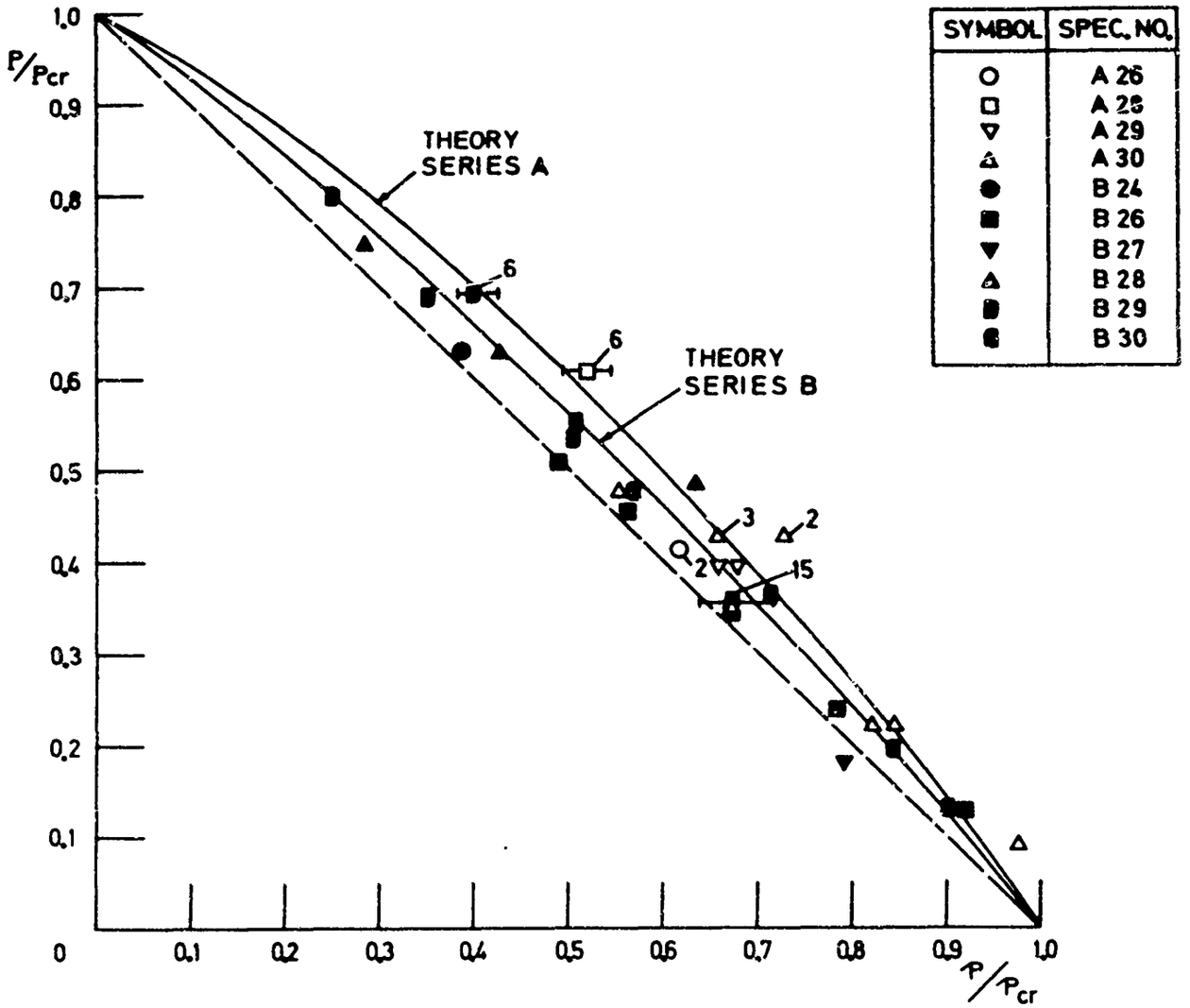

FIG. 4 BUCKLING OF ALCLAD 2024-T3 ALUMINUM-ALLOY UNSTIFFENED CONICAL SHELLS UNDER COMBINED AXIAL COMPRESSION AND EXTERNAL PRESSURE ; $\alpha = 40°$; SERIES A: $\psi = 0.678$, SERIES B: $\psi = 0.500$.

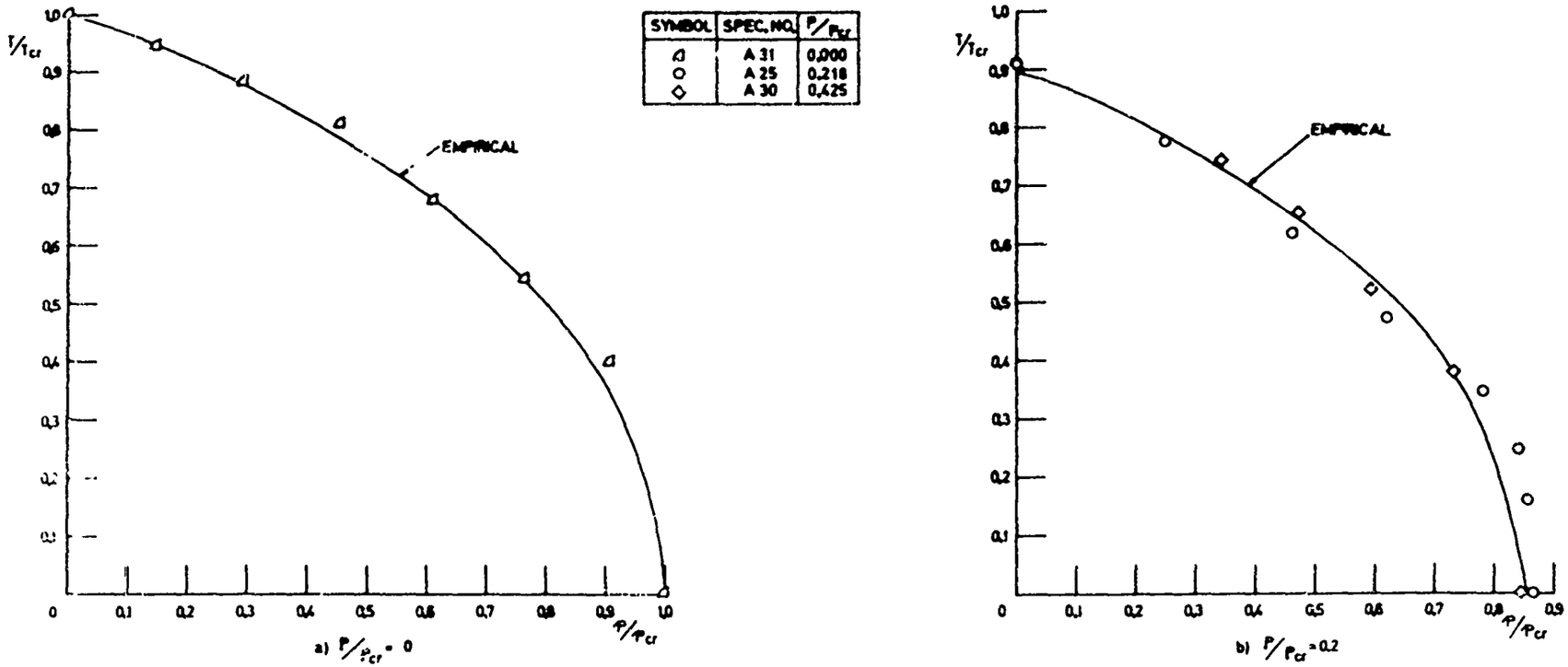

FIG. 5 BUCKLING OF ALCLAD 2024-T3 ALUMINUM-ALLOY UNSTIFFENED CONICAL SHELLS UNDER COMBINED AXIAL COMPRESSION, TORSION AND EXTERNAL PRESSURE; $\alpha = 40°$; $\psi = 0.678$.

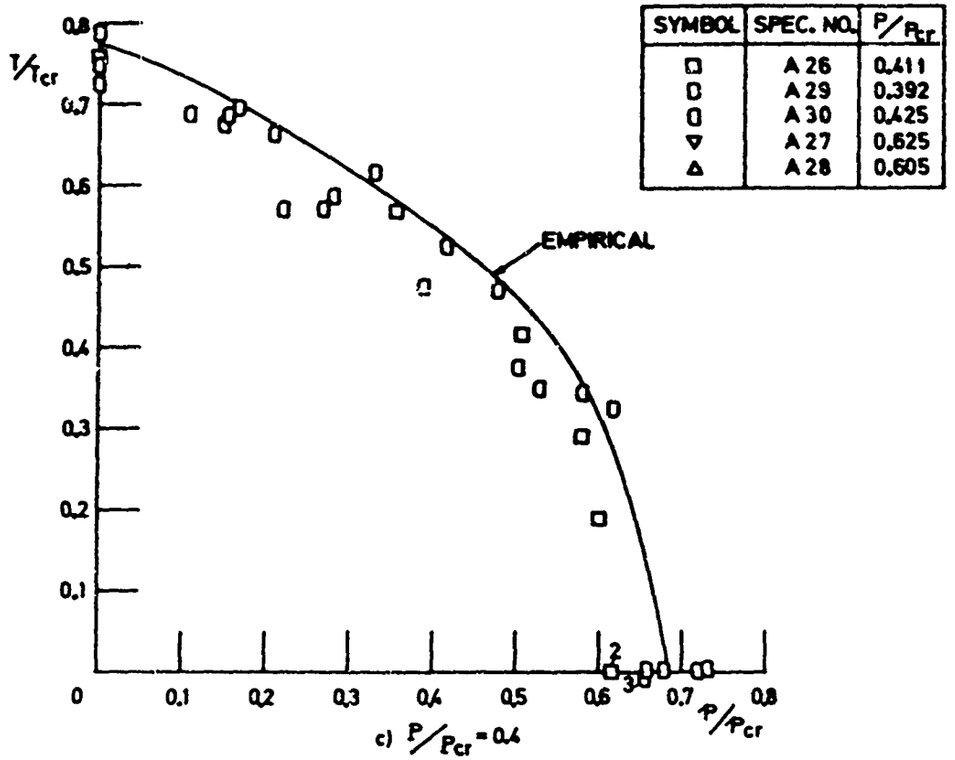
SYMBOL
SPEC. NO.
P/Pcr
A 26
0.411
A 29
0.392
A 30
0.425
A 27
0.625
A 28
0.605
T/Tcr
EMPIRICAL
P/Pcr
c) P/Pcr = 0.4

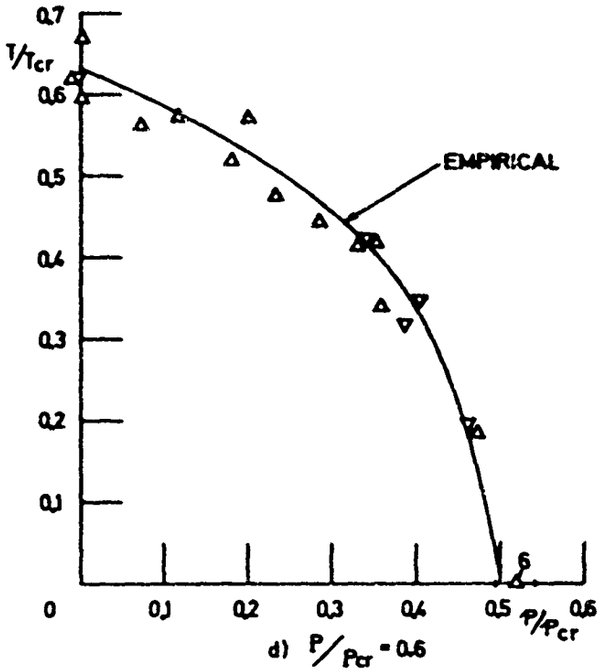
T/Tcr
EMPIRICAL
P/Pcr
d) P/Pcr = 0.6

FIG. 5 (CONCL'D)

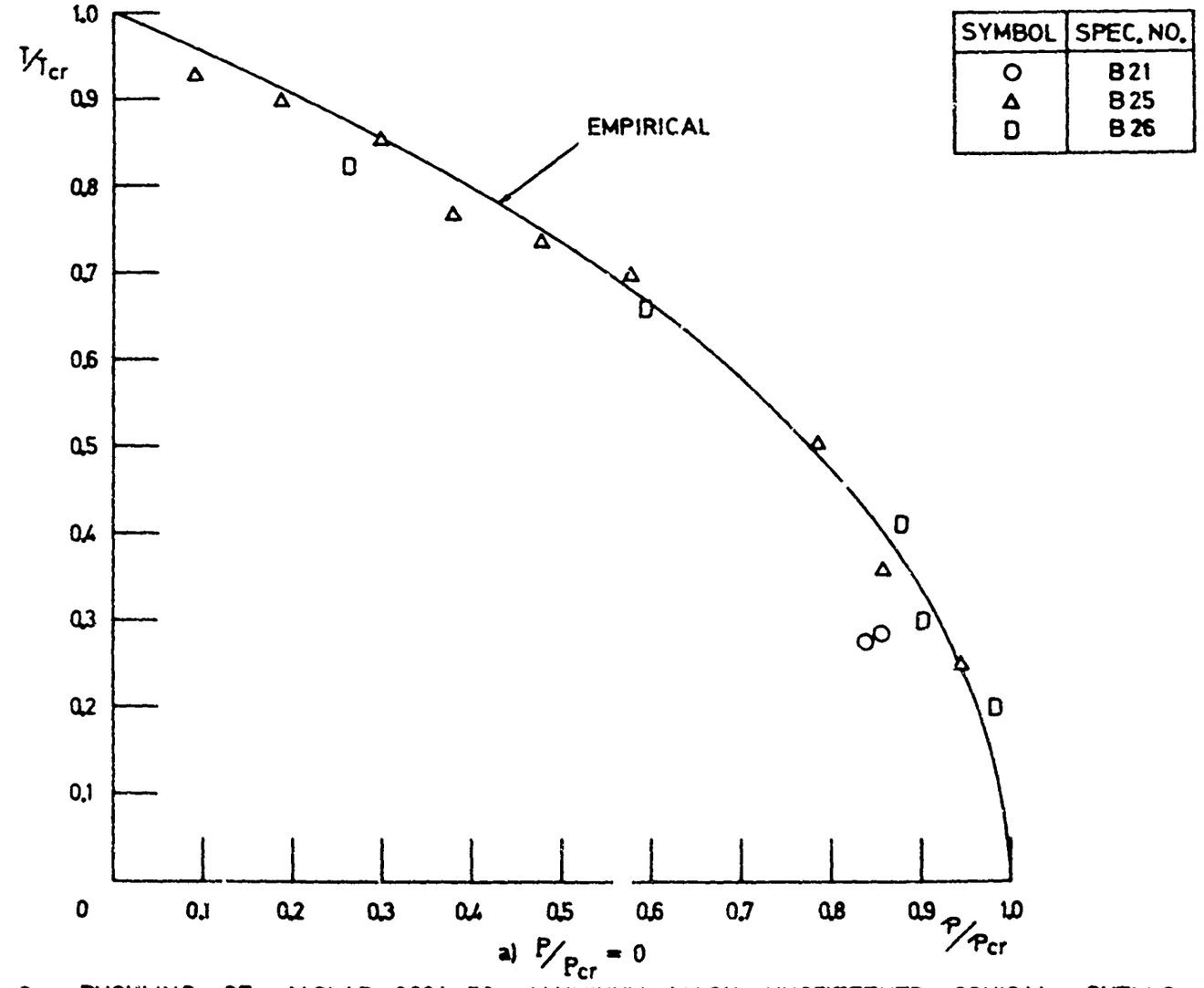

FIG. 6 BUCKLING OF ALCLAD 2024-T3 ALUMINUM-ALLOY UNSTIFFENED CONICAL SHELLS UNDER COMBINED AXIAL COMPRESSION, TORSION AND EXTERNAL PRESSURE; $\alpha = 40°$, $\psi = 0.500$.

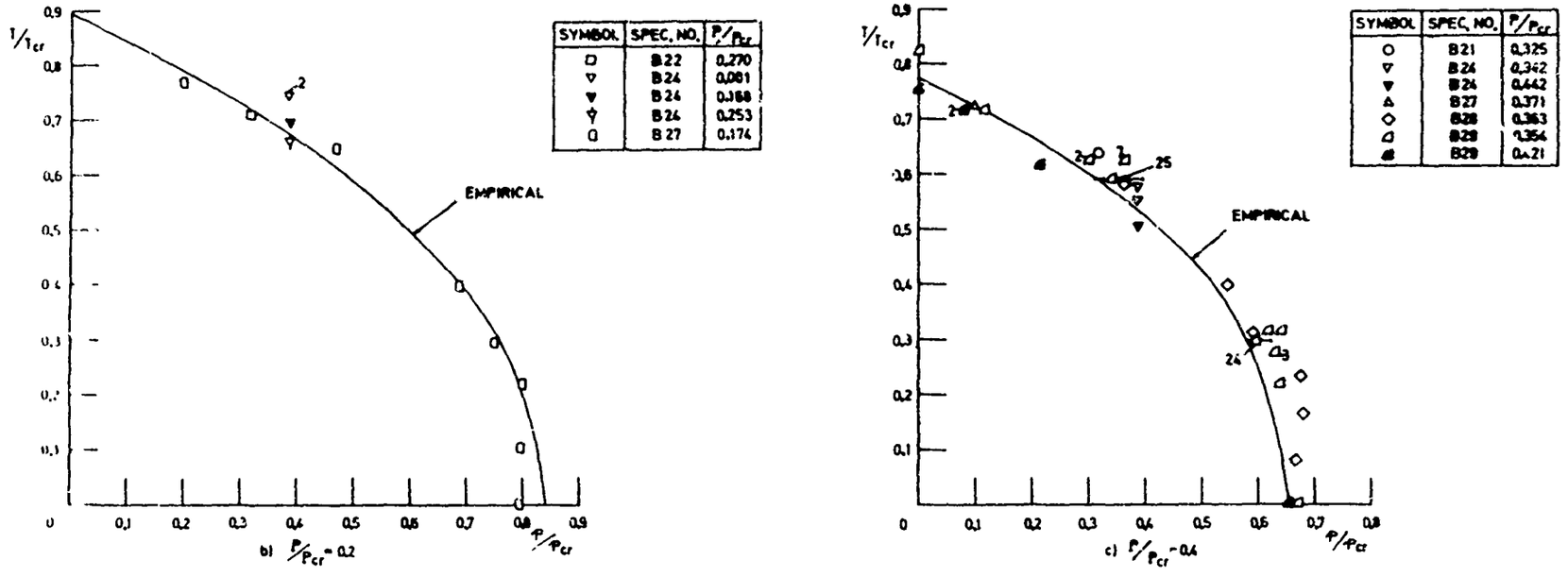
SYMBOL
SPEC. NO.
P/Pcr
B22 0.270
B24 0.081
B24 0.188
B24 0.253
B27 0.174
EMPIRICAL
T/Tcr
P/Pcr
b) P/Pcr = 0.2
SYMBOL
SPEC. NO.
P/Pcr
B21 0.325
B24 0.342
B24 0.442
B27 0.371
B28 0.363
B28 0.354
B29 0.421
EMPIRICAL
T/Tcr
P/Pcr
c) P/Pcr = 0.4

FIG. 6 (CONT'D)

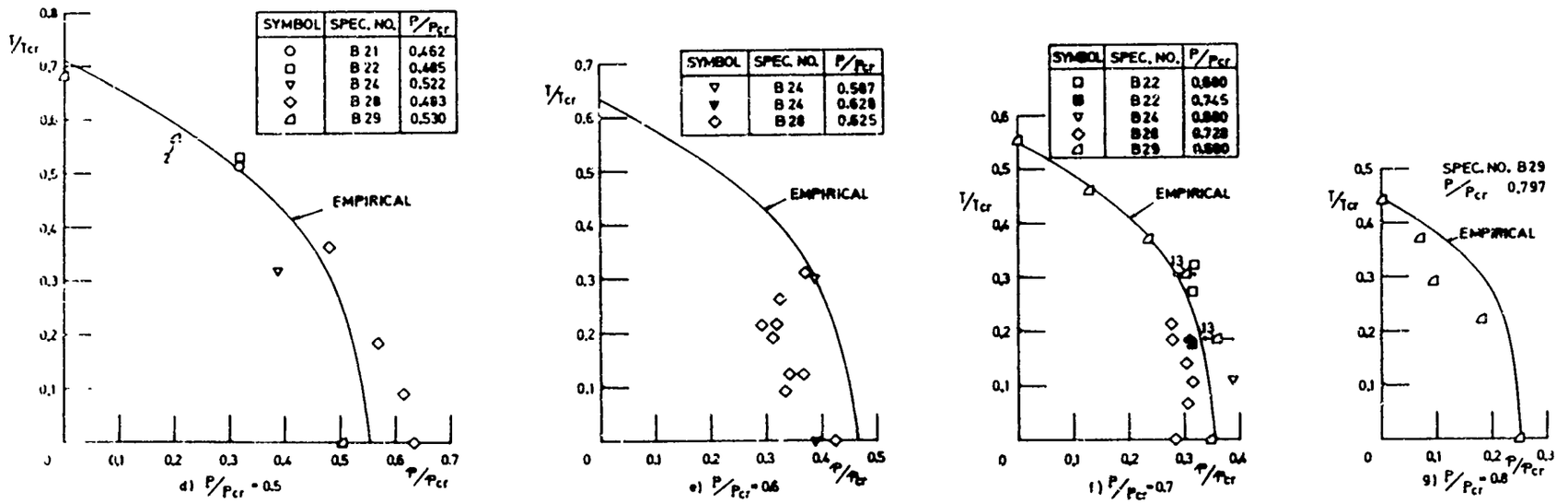
SYMBOL | SPEC. NO. | P/Pcr
B 21 | 0.462
B 22 | 0.485
B 24 | 0.522
B 28 | 0.483
B 29 | 0.530
EMPIRICAL
T/Tcr
P/Pcr
d) P/Pcr = 0.5
SYMBOL | SPEC. NO. | P/Pcr
B 24 | 0.587
B 24 | 0.628
B 28 | 0.625
EMPIRICAL
T/Tcr
P/Pcr
e) P/Pcr = 0.6
SYMBOL | SPEC. NO. | P/Pcr
B 22 | 0.880
B 22 | 0.745
B 24 | 0.880
B 28 | 0.728
B 29 | 0.880
EMPIRICAL
T/Tcr
P/Pcr
f) P/Pcr = 0.7
SPEC. NO. B 29
P/Pcr 0.797
EMPIRICAL
T/Tcr
P/Pcr
g) P/Pcr = 0.8

FIG. 6 (CONCL'D)

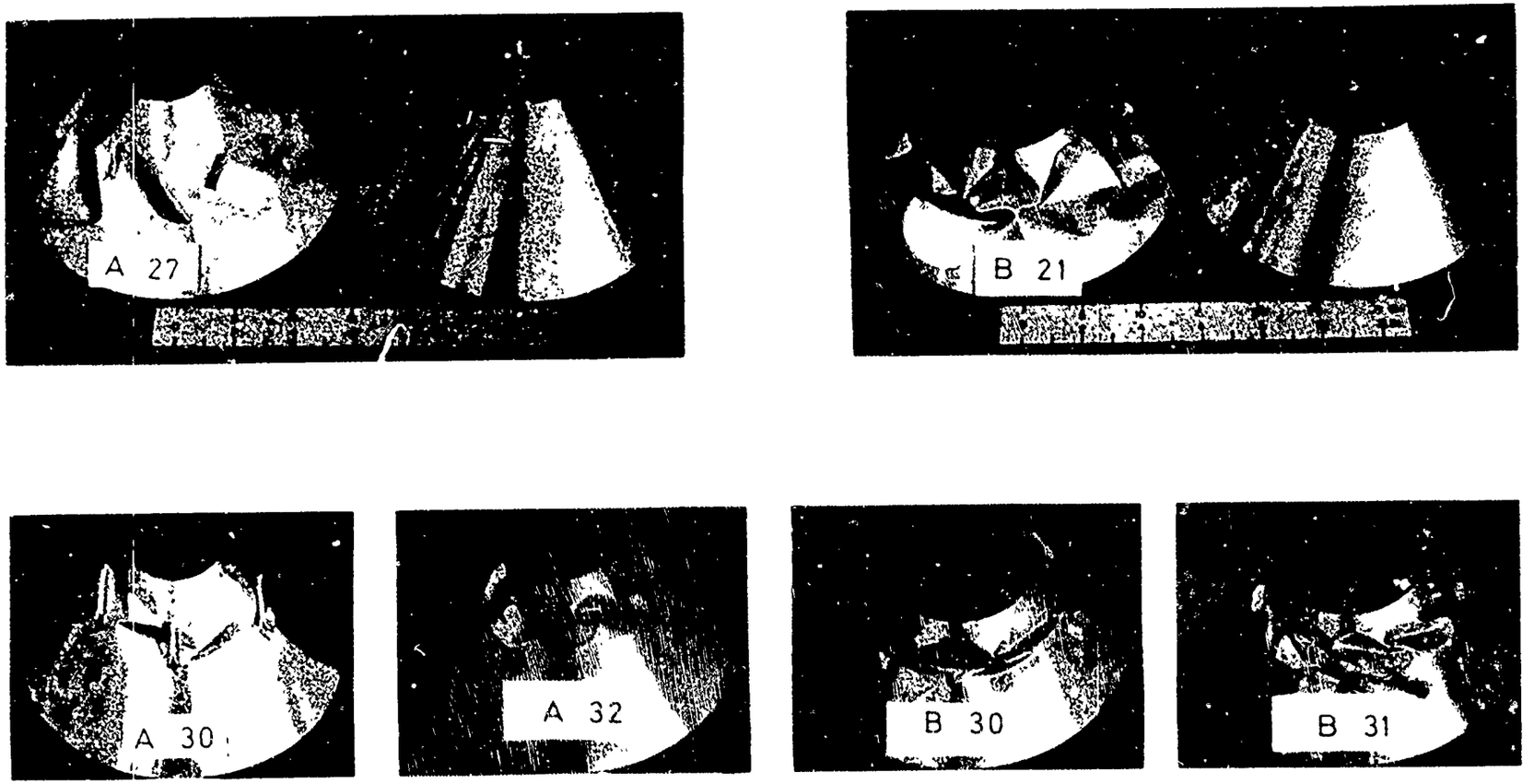

FIG. 7 TYPICAL FINAL BUCKLE PATTERNS OBTAINED IN COMBINED LOAD TESTS OF ALUMINUM-ALLOY UNSTIFFENED CONICAL SHELLS.

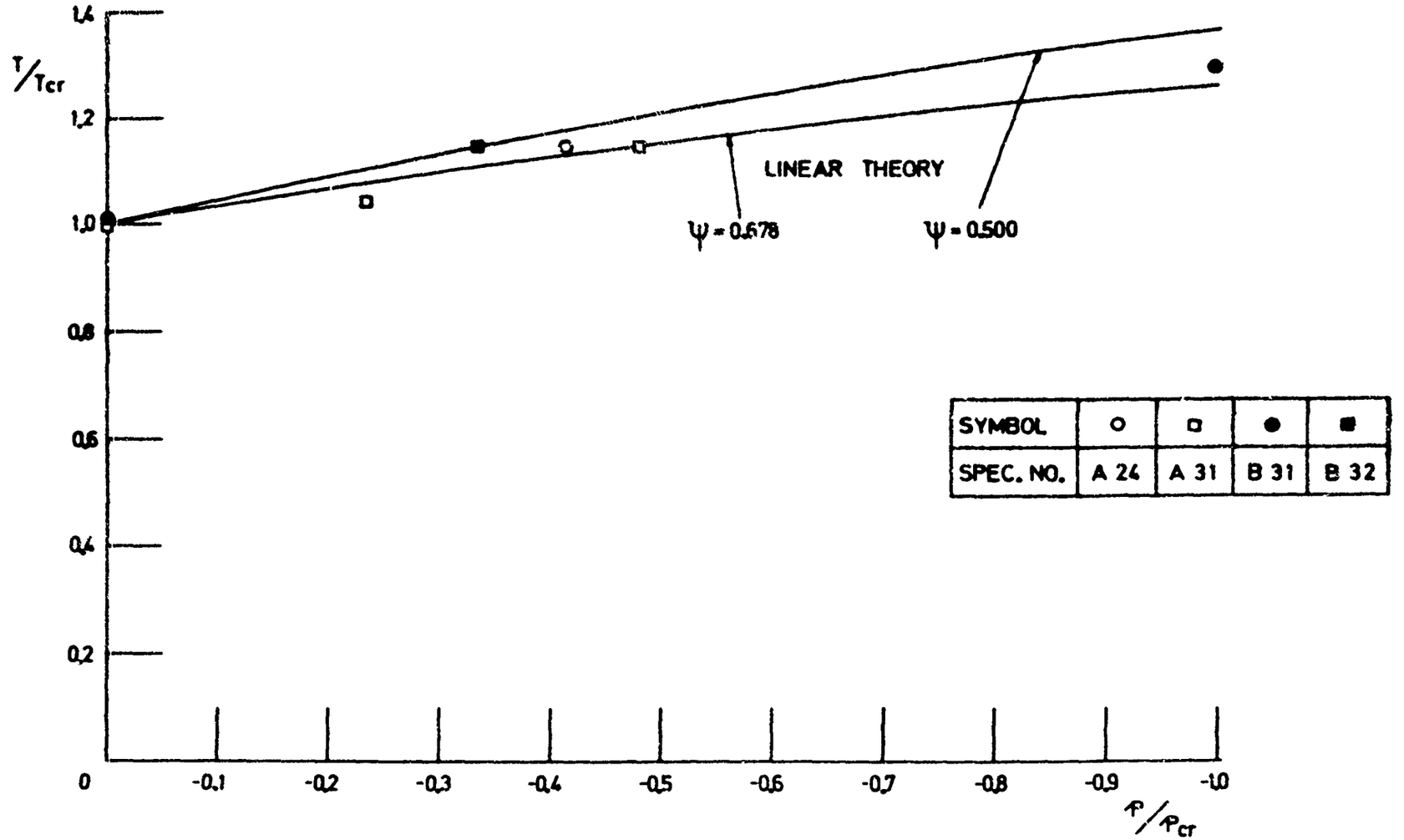

FIG. 8 BUCKLING OF ALCLAD 2024-T3 ALUMINUM-ALLOY UNSTIFFENED CONICAL SHELLS UNDER COMBINED TORSION AND INTERNAL PRESSURE ; $\alpha < 40°$; SERIES A : $\psi = 0.678$, SERIES B : $\psi = 0.500$.

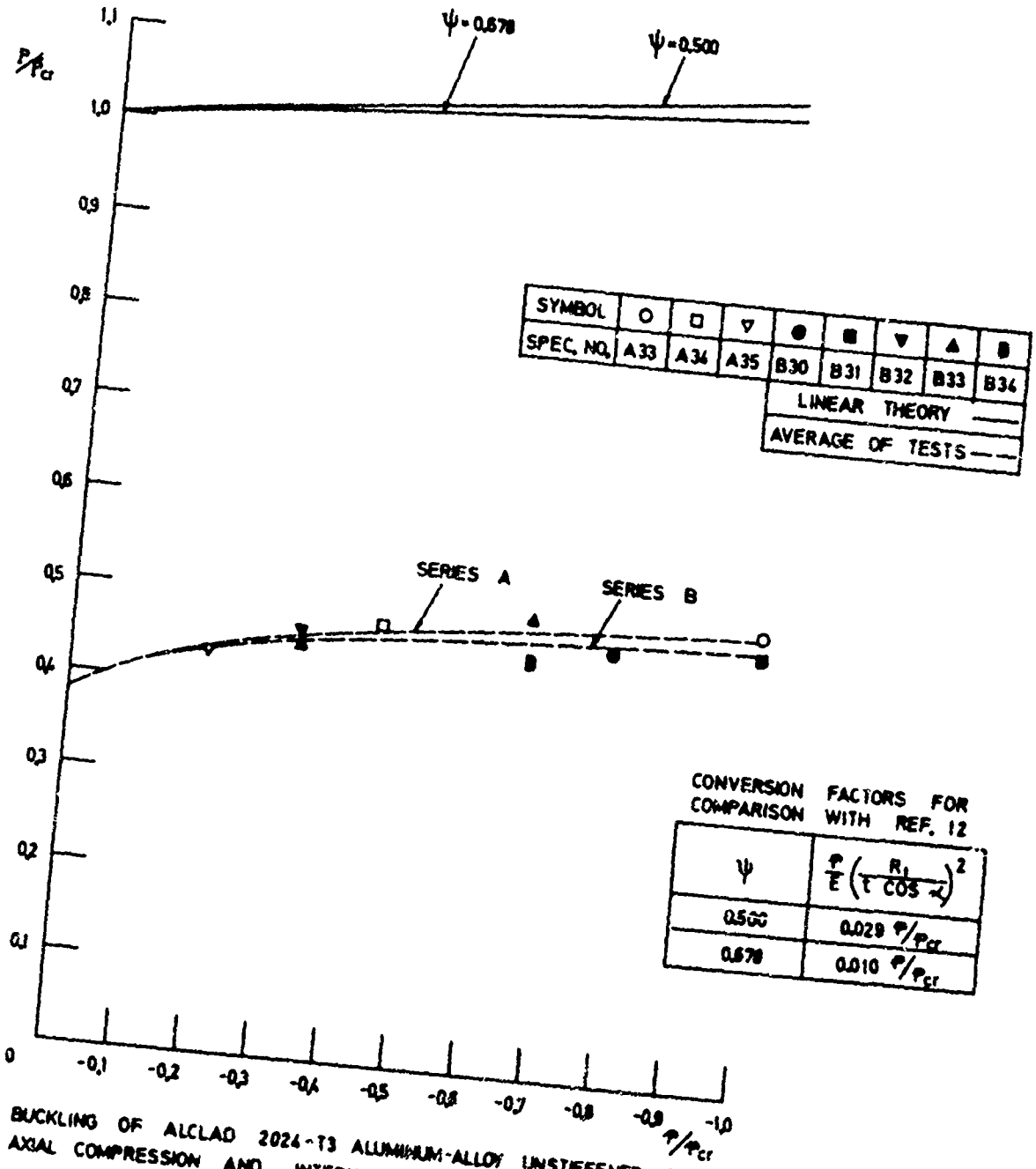

CONVERSION FACTORS FOR COMPARISON WITH REF. 12

ψ	$\frac{P}{E}\left(\frac{R_1}{t\ \cos\alpha}\right)^2$
0.500	$0.029\ P/P_{cr}$
0.678	$0.010\ P/P_{cr}$

FIG. 9 BUCKLING OF ALCLAD 2024-T3 ALUMINUM-ALLOY UNSTIFFENED CONICAL SHELLS UNDER COMBINED AXIAL COMPRESSION AND INTERNAL PRESSURE; $\alpha = 40°$; SERIES A: $\psi = 0.678$, SERIES B: $\psi = 0.500$.

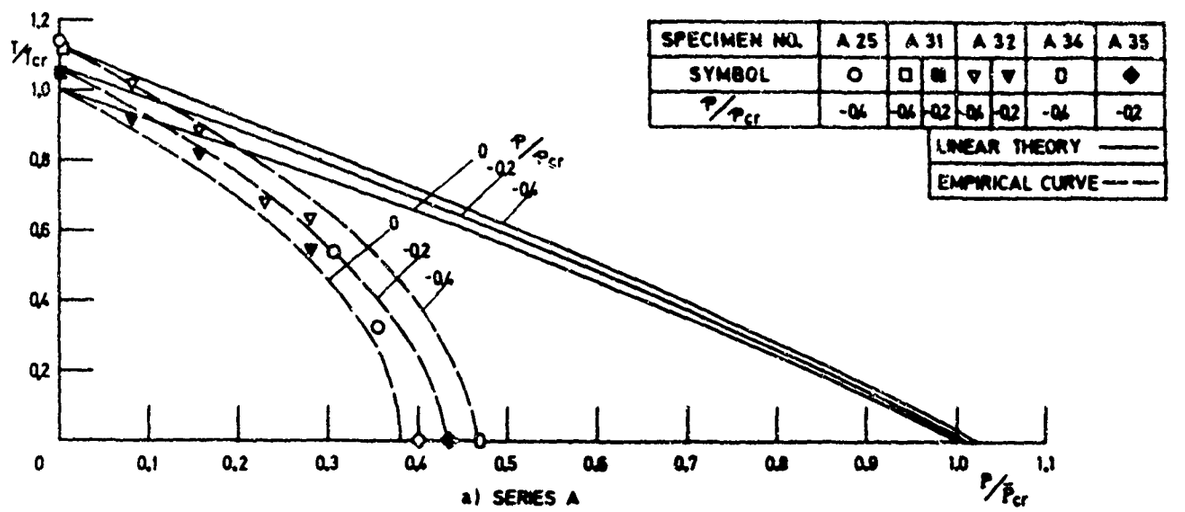

a) SERIES A

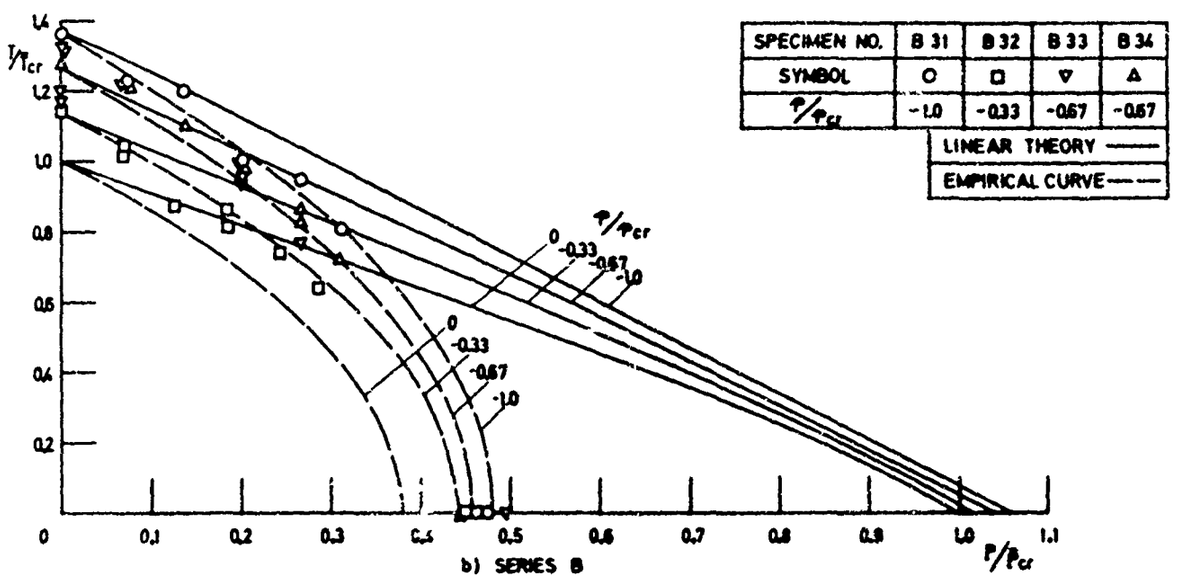

b) SERIES B

FIG. 10 BUCKLING OF ALCLAD 2024-T3 ALUMINUM-ALLOY UNSTIFFENED CONICAL SHELLS UNDER COMBINED AXIAL COMPRESSION, TORSION AND INTERNAL PRESSURE; $\alpha = 40°$.

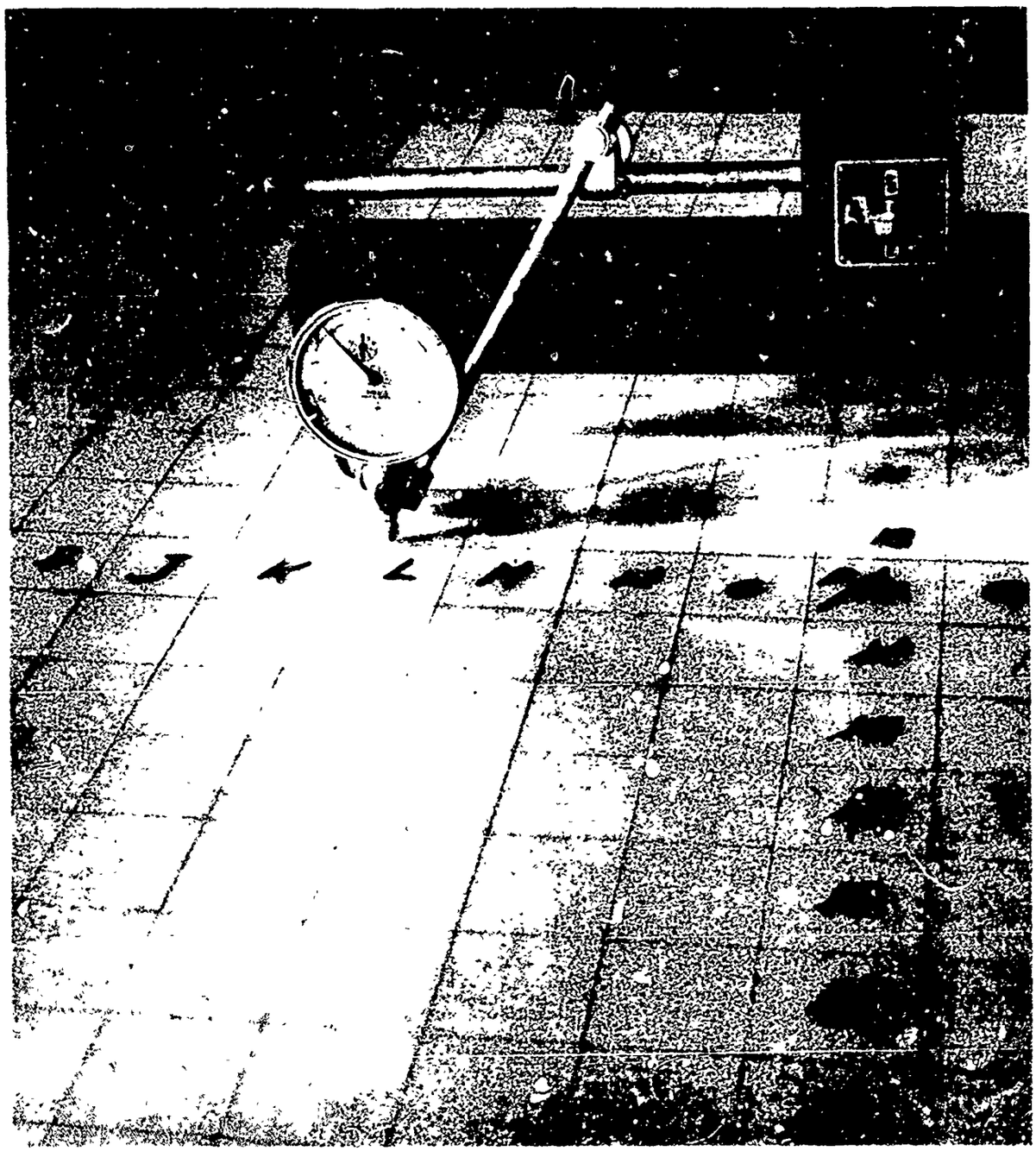

FIG. 11 MEASUREMENT OF THICKNESS VARIATION OF MYLAR SHEETS

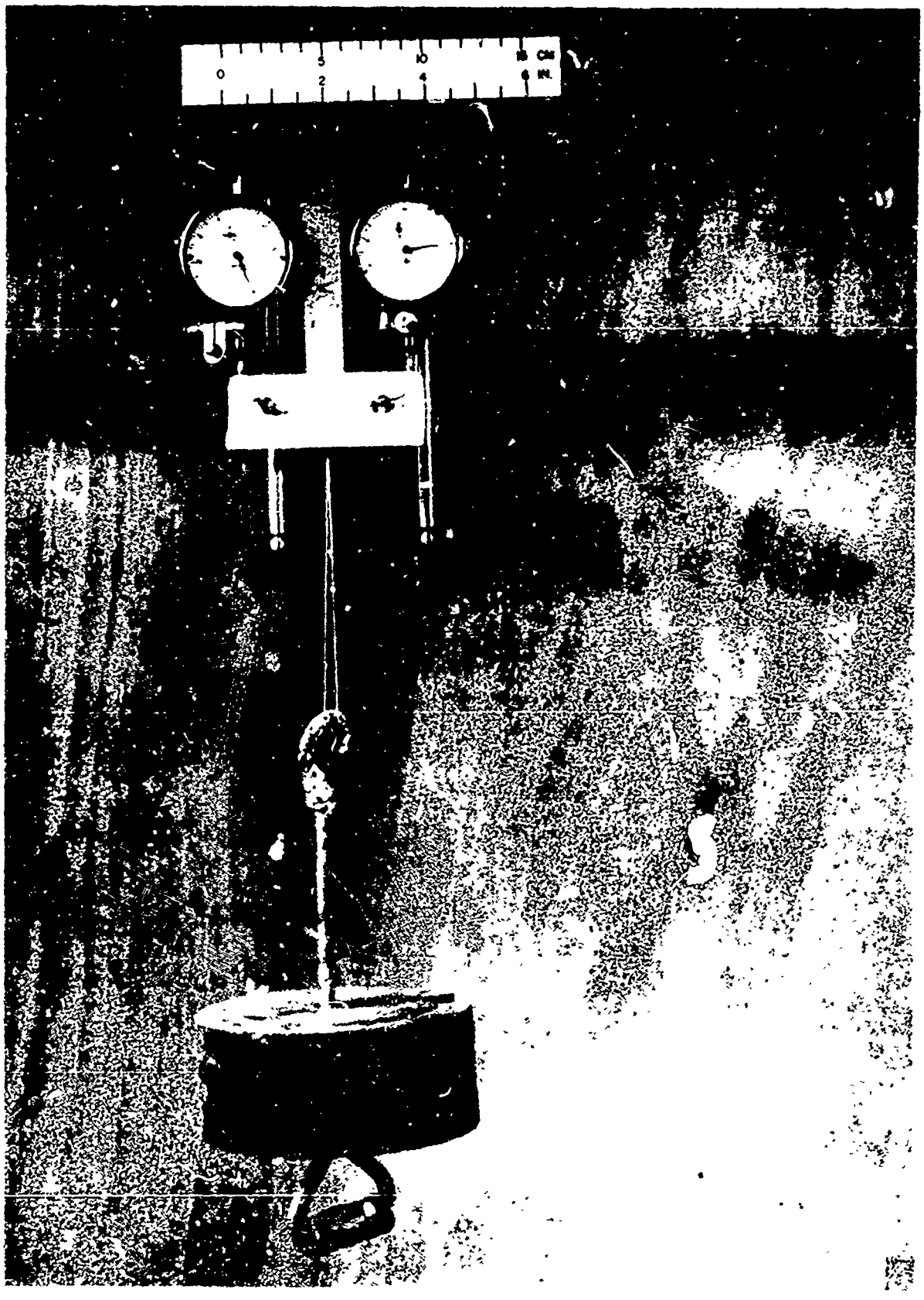

FIG. 12 SET-UP FOR MEASUREMENT OF AXIAL DEFLECTIONS OF THIN SPECIMENS UNDER STATIC LOAD

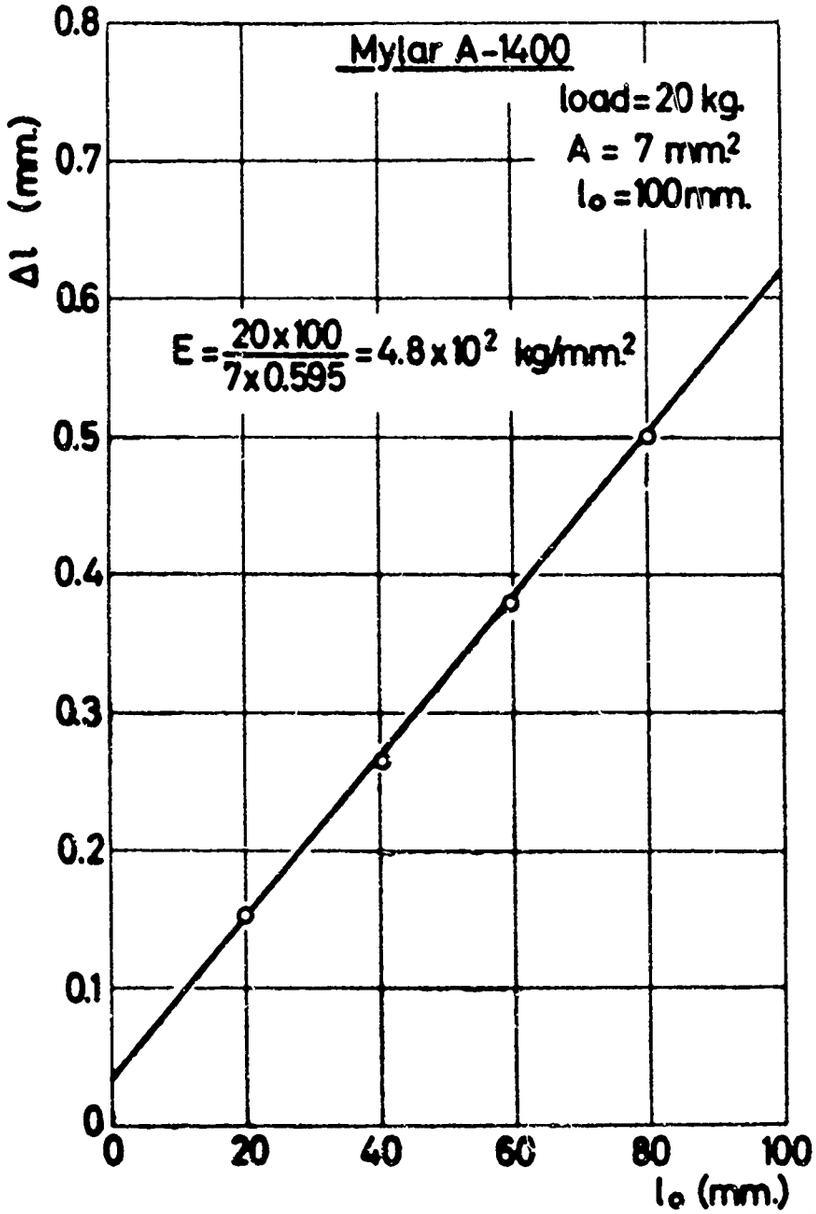

FIG. 13 TYPICAL PLOTS OF DEFLECTION VERSUS INITIAL GAGE LENGTH OF SAMPLES CUT FROM MYLAR A-1400 SHEETS (INSTRON)

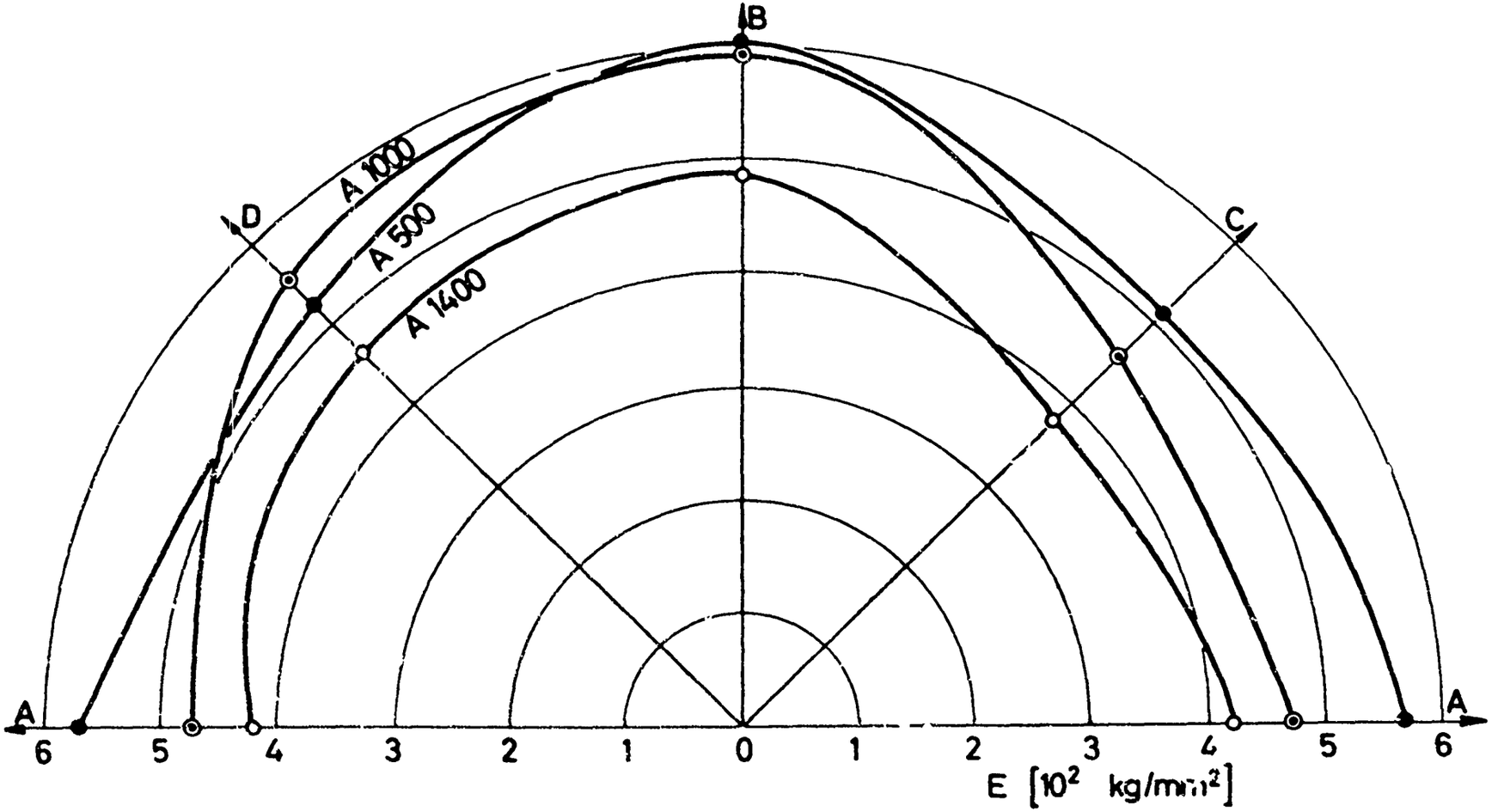

FIG. 14 VARIATION OF TENSILE YOUNG'S MODULUS OF MYLAR A SHEETS ALONG 4 DIFFERENT DIRECTIONS

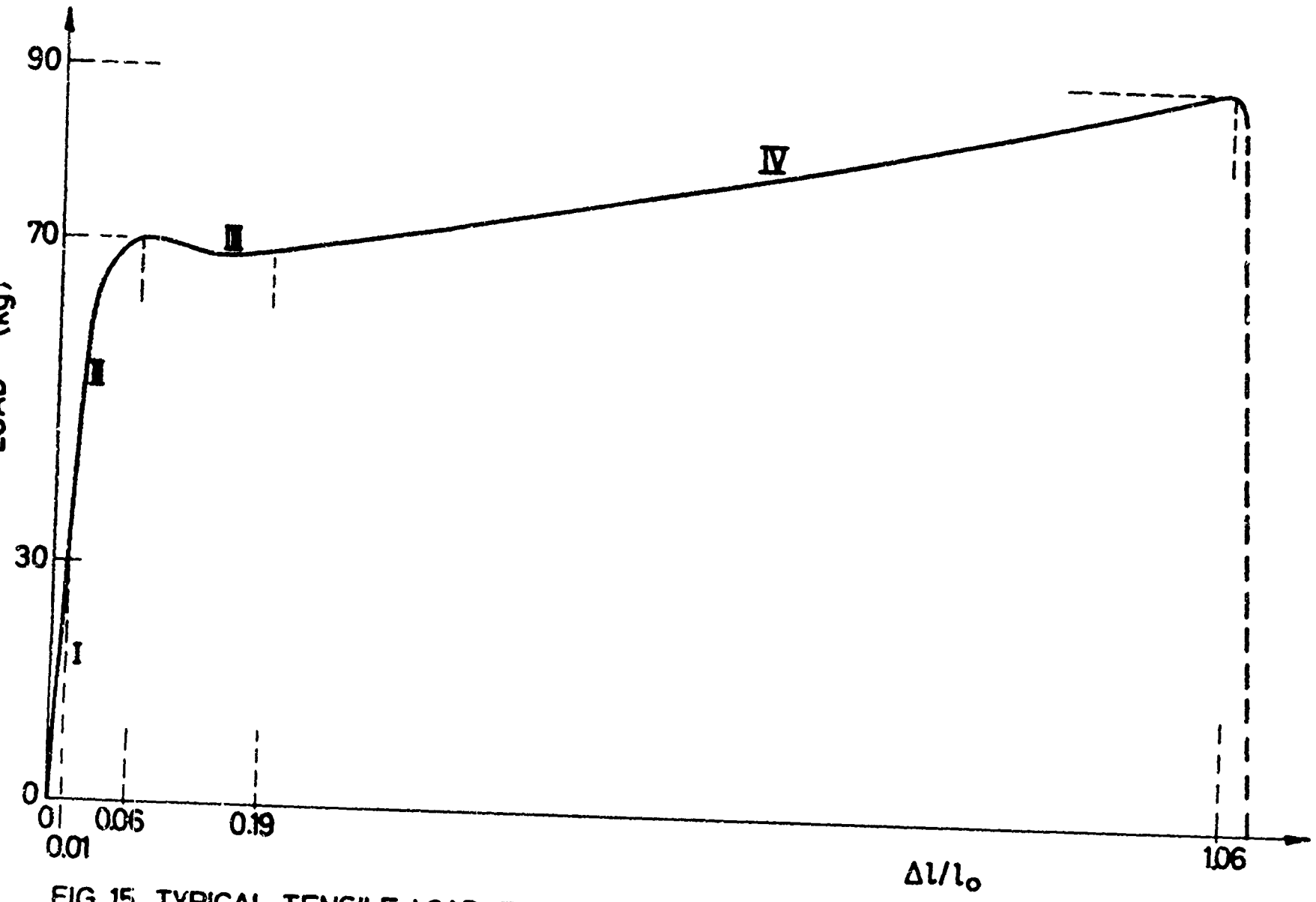

FIG. 15 TYPICAL TENSILE LOAD-ELONGATION CURVE FOR MYLAR A-1400 SAMPLE (RECORDED ON INSTRON)

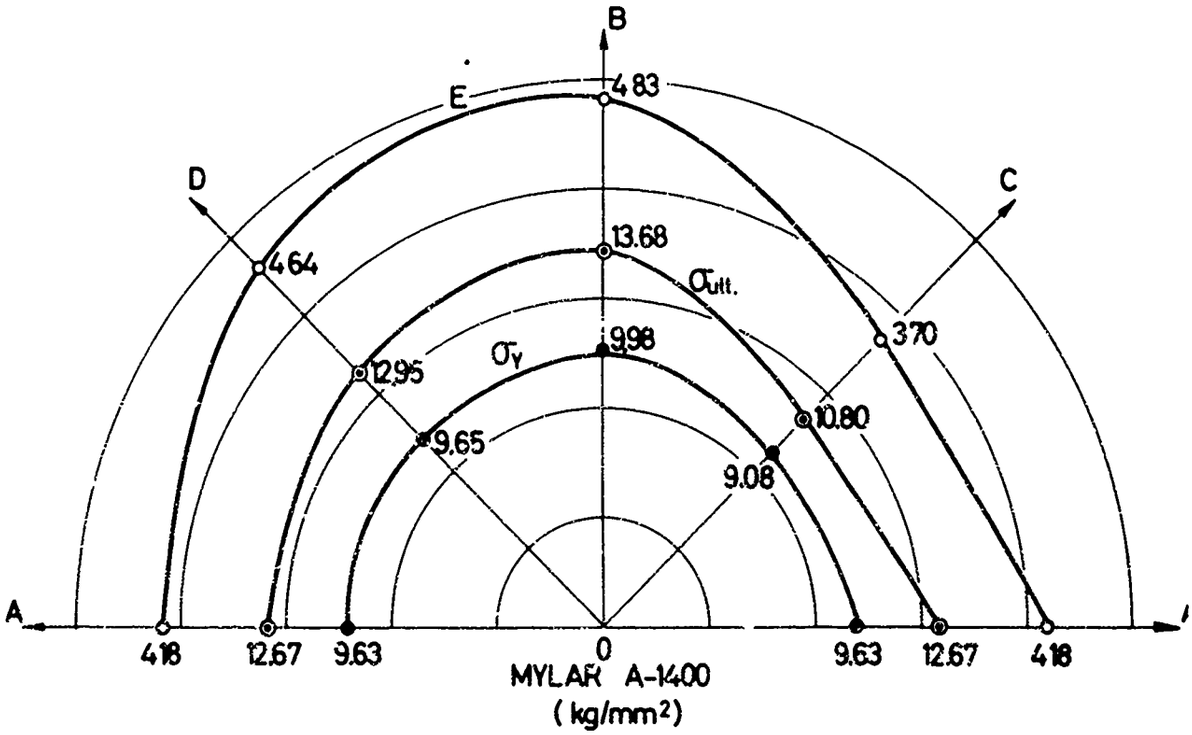

FIG. 16 VARIATION OF TENSILE YIELD AND ULTIMATE STRESSES OF MYLAR A-1400 SHEET ALONG 4 DIFFERENT DIRECTIONS

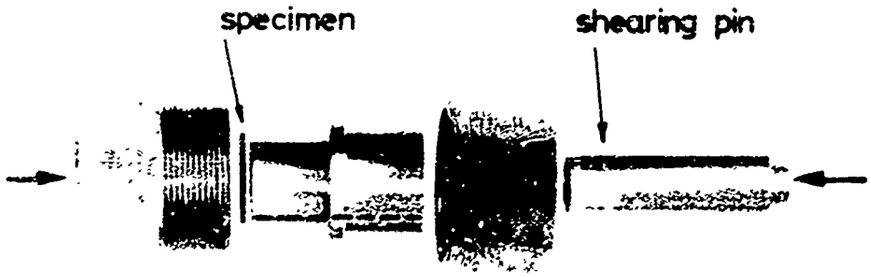

FIG. 17 SHEAR TEST OF A THIN CIRCULAR SAMPLE

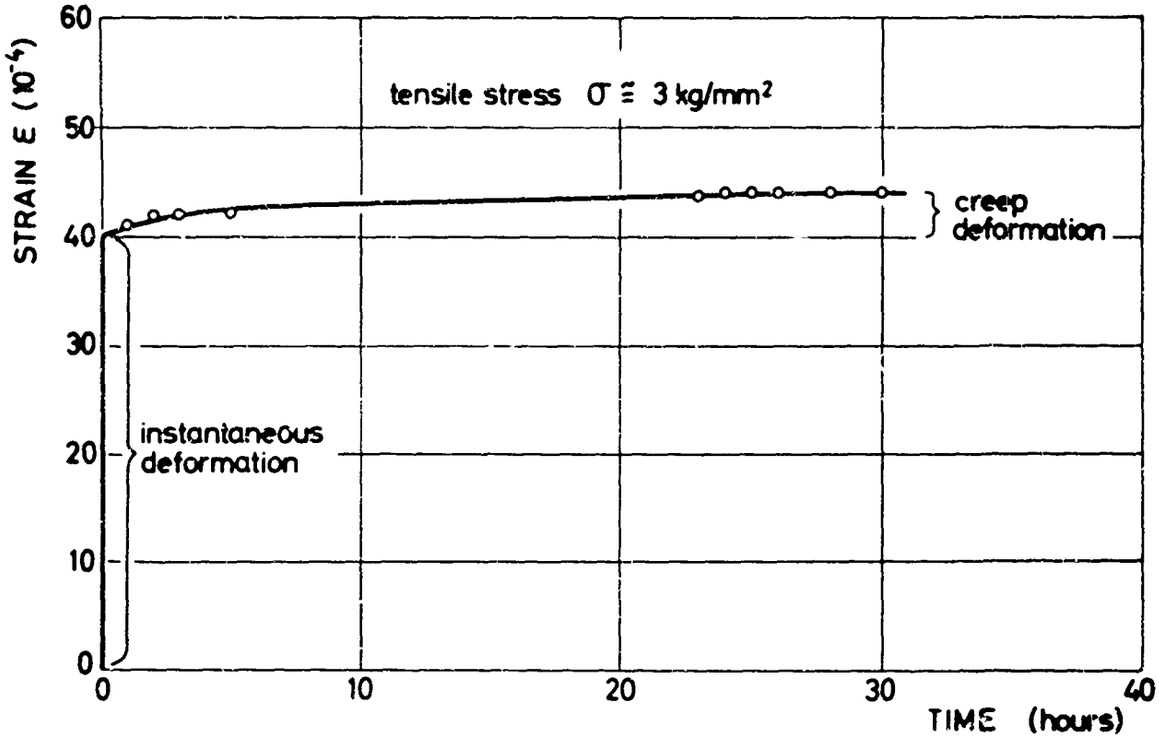

FIG. 18 TYPICAL TENSILE CREEP CURVE OF MYLAR A-1400 SAMPLE

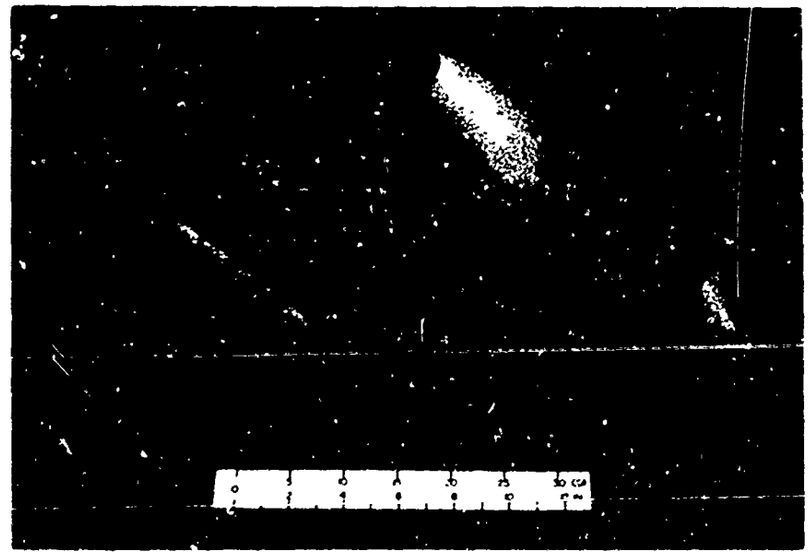

FIG. 19 MYLAR A-1400 IN CONICAL SHELLS REPRESENTING 3 TAPER RATIOS: ψ=0.5, 0.68 AND 0.80

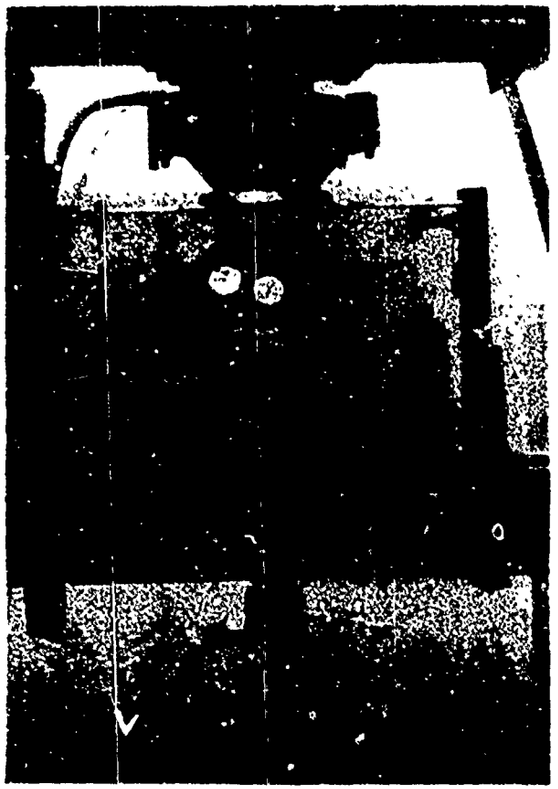

FIG. 20 LOADING APPARATUS FOR BUCKLING TESTS OF MYLAR CONICAL SHELLS

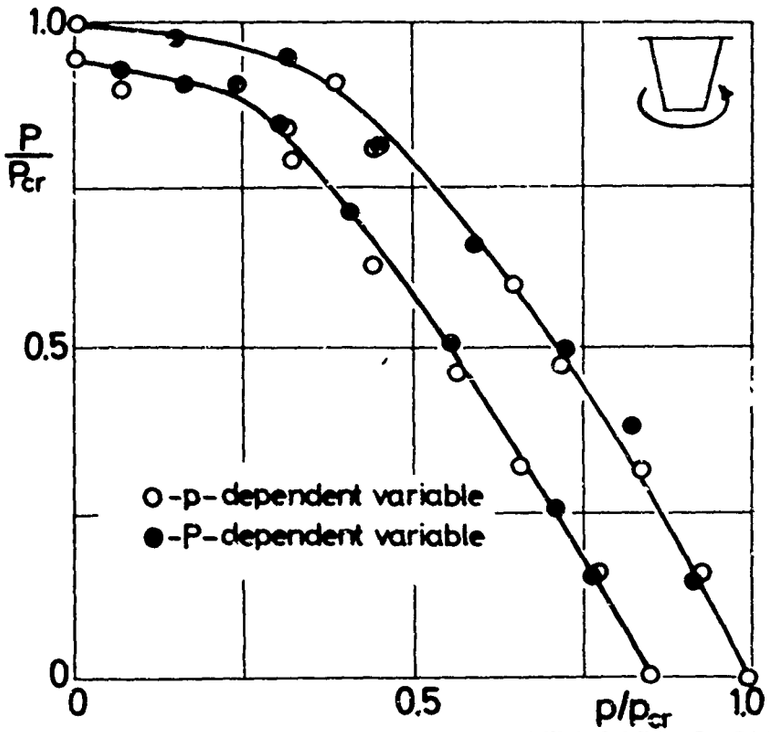

FIG. 21 INFLUENCE OF ORDER OF LOADING ON INTERACTION CURVES OF MYLAR SHELL $\psi = 0.80$

FIG. 22a TYPICAL BUCKLED MYLAR SHELLS
TORSION DOMINANT

FIG. 22b TYPICAL BUCKLED MYLAR SHELLS
AXIAL COMPRESSION DOMINANT

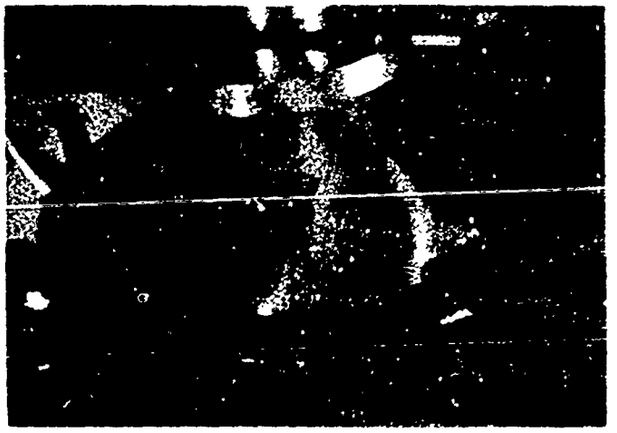

FIG. 22c TYPICAL BUCKLED MYLAR SHELLS
EXTERNAL PRESSURE DOMINANT

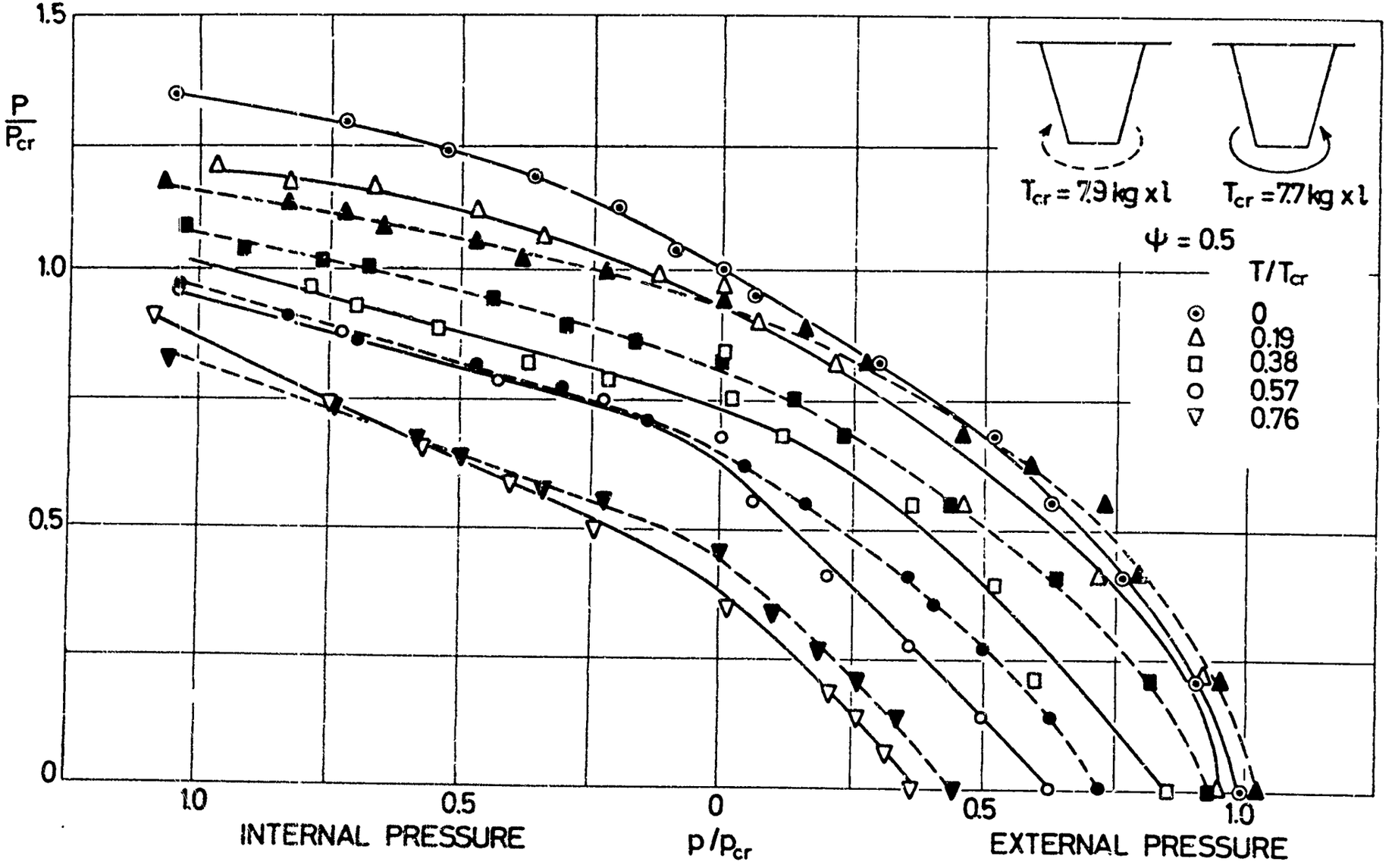

FIG. 23 TYPICAL INTERACTION CURVES OF MYLAR A SHELLS
$\Psi = 0.50$

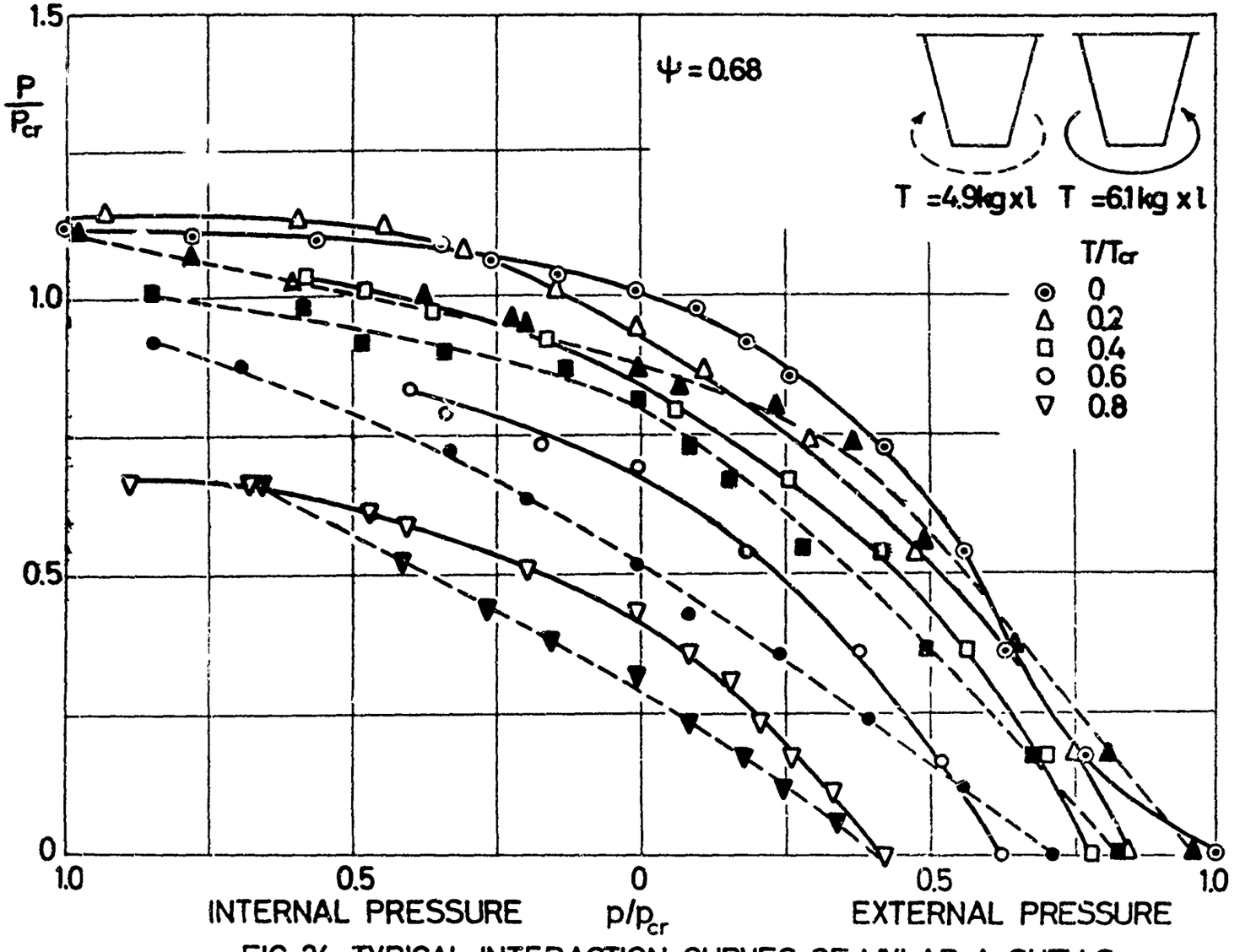

FIG. 24 TYPICAL INTERACTION CURVES OF MYLAR A SHELLS
$\Psi = 0.68$

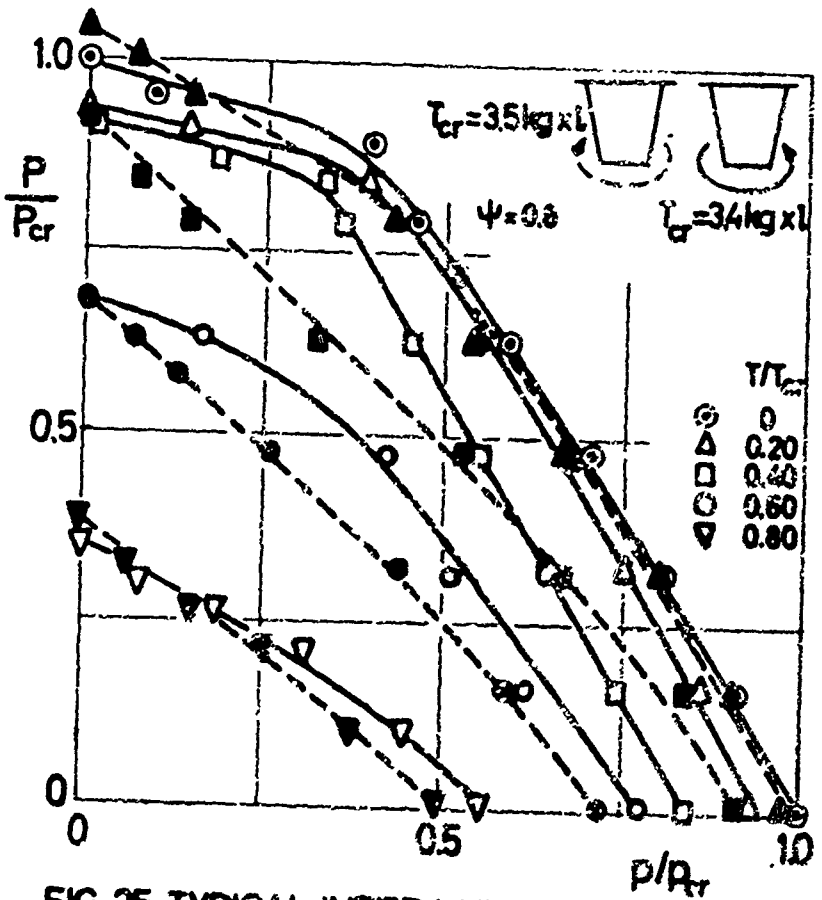

FIG. 25 TYPICAL INTERACTION CURVES OF MYLAR A SHELLS, $\psi = 0.80$

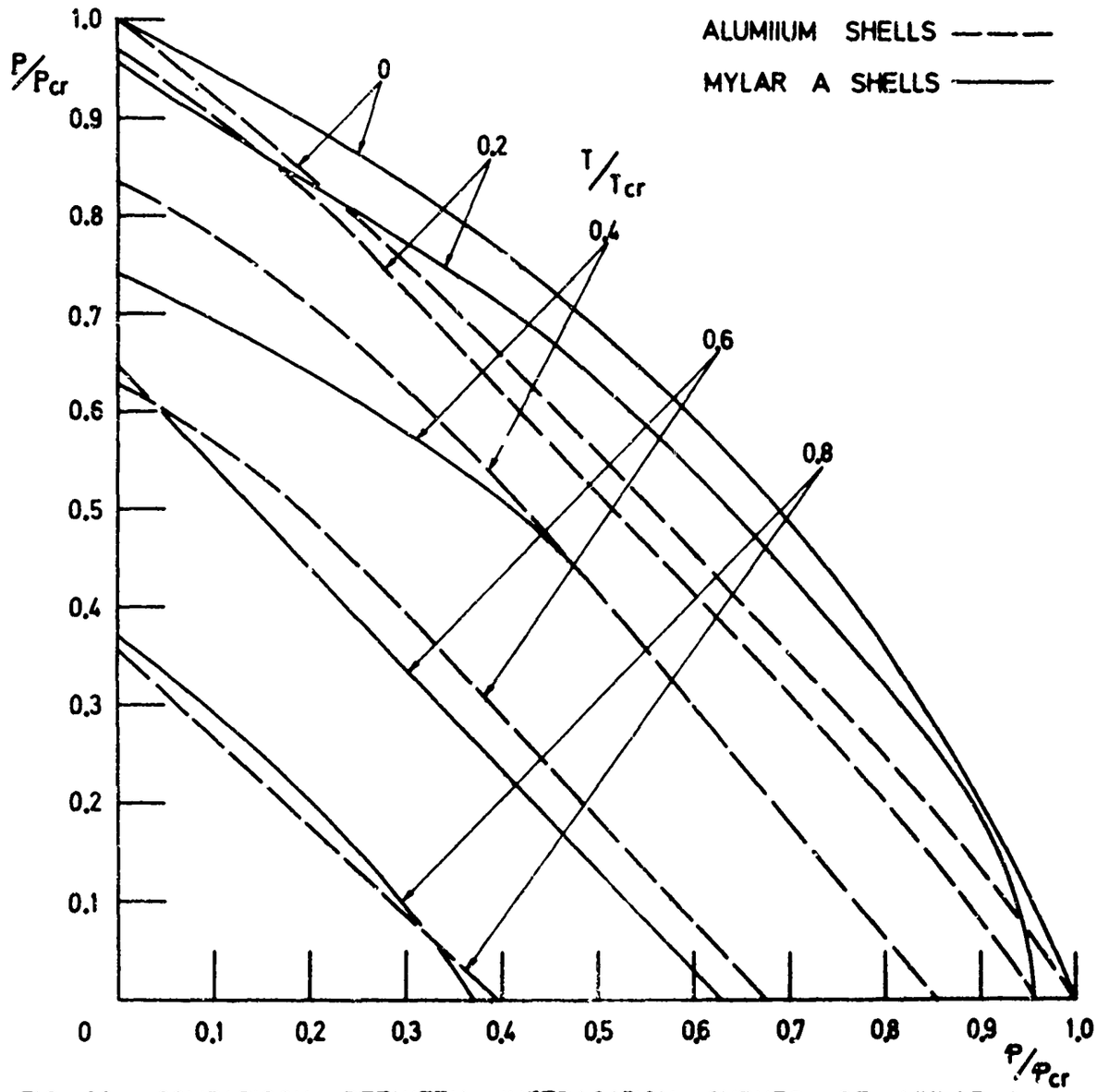

FIG. 26 COMPARISON BETWEEN INTERACATION CURVES OF MYLAR A AND ALUMINUM CONICAL SHELLS FOR $\psi = 0.500$

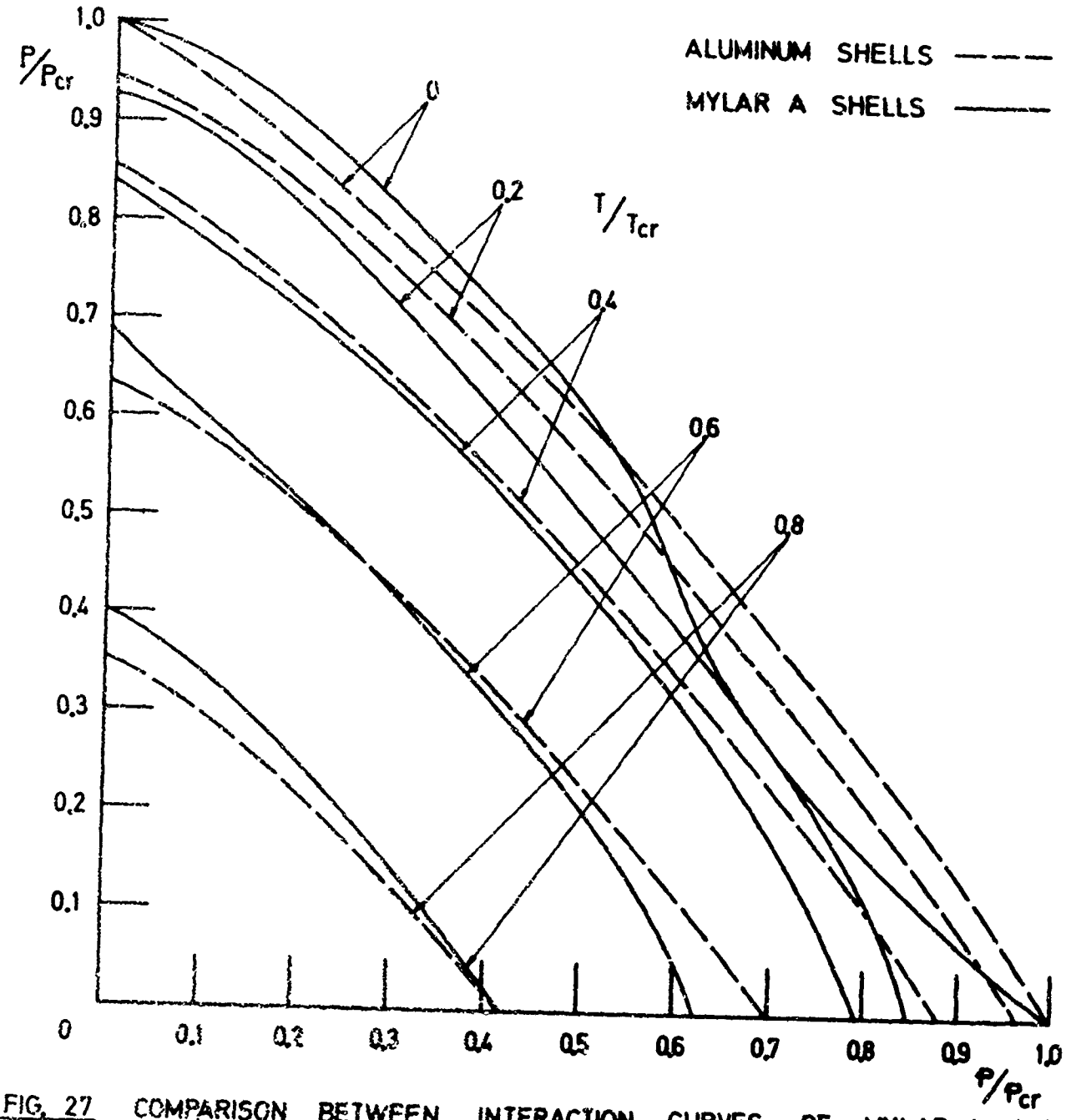

FIG. 27 COMPARISON BETWEEN INTERACTION CURVES OF MYLAR A AND ALUMINUM CONICAL SHELLS FOR $\psi = 0.678$

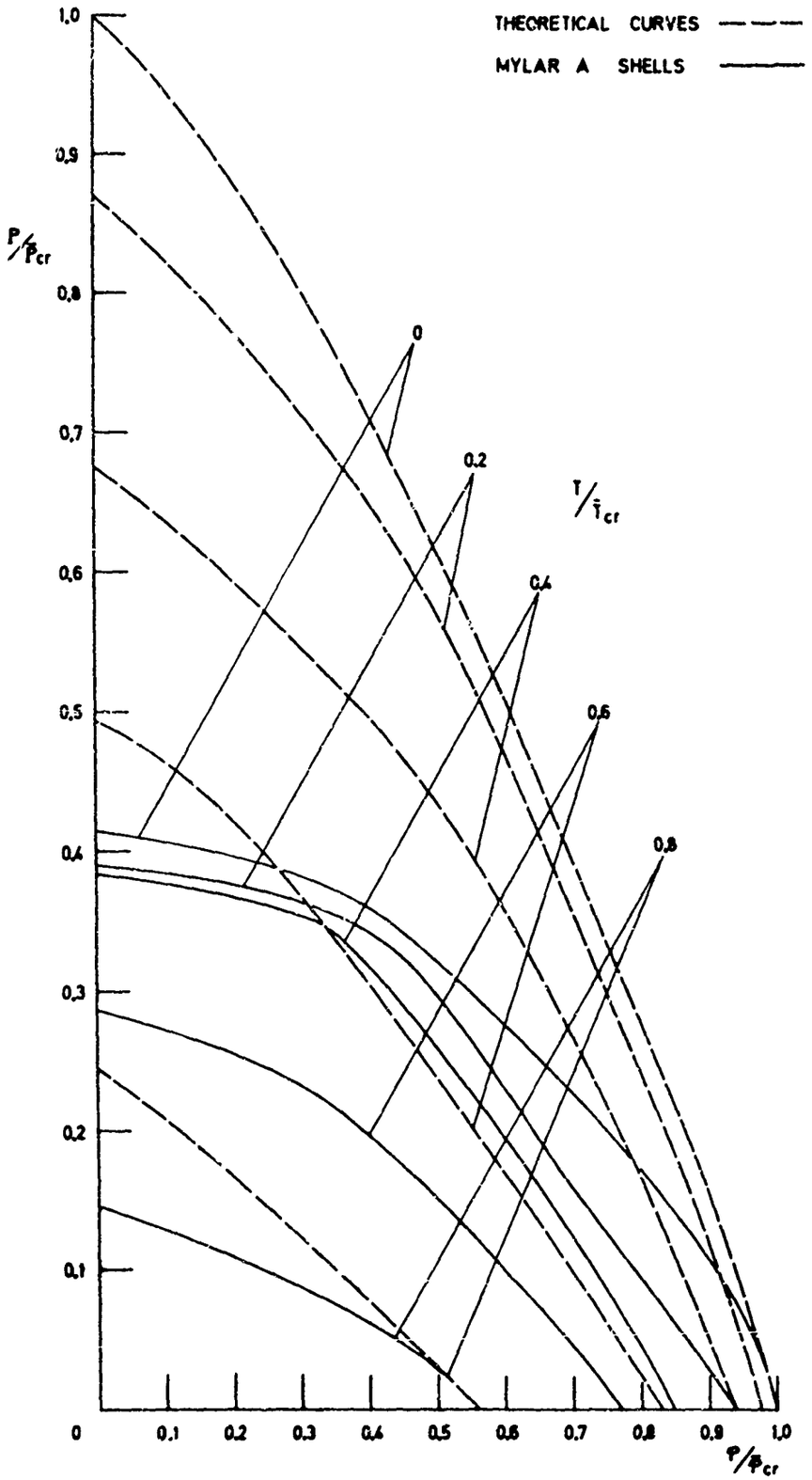

FIG. 28 COMPARISON BETWEEN EXPERIMENTAL INTERACTION CURVE OF MYLAR A SHELLS AND THEORETICAL RESULTS FOR $\psi = 0.800$

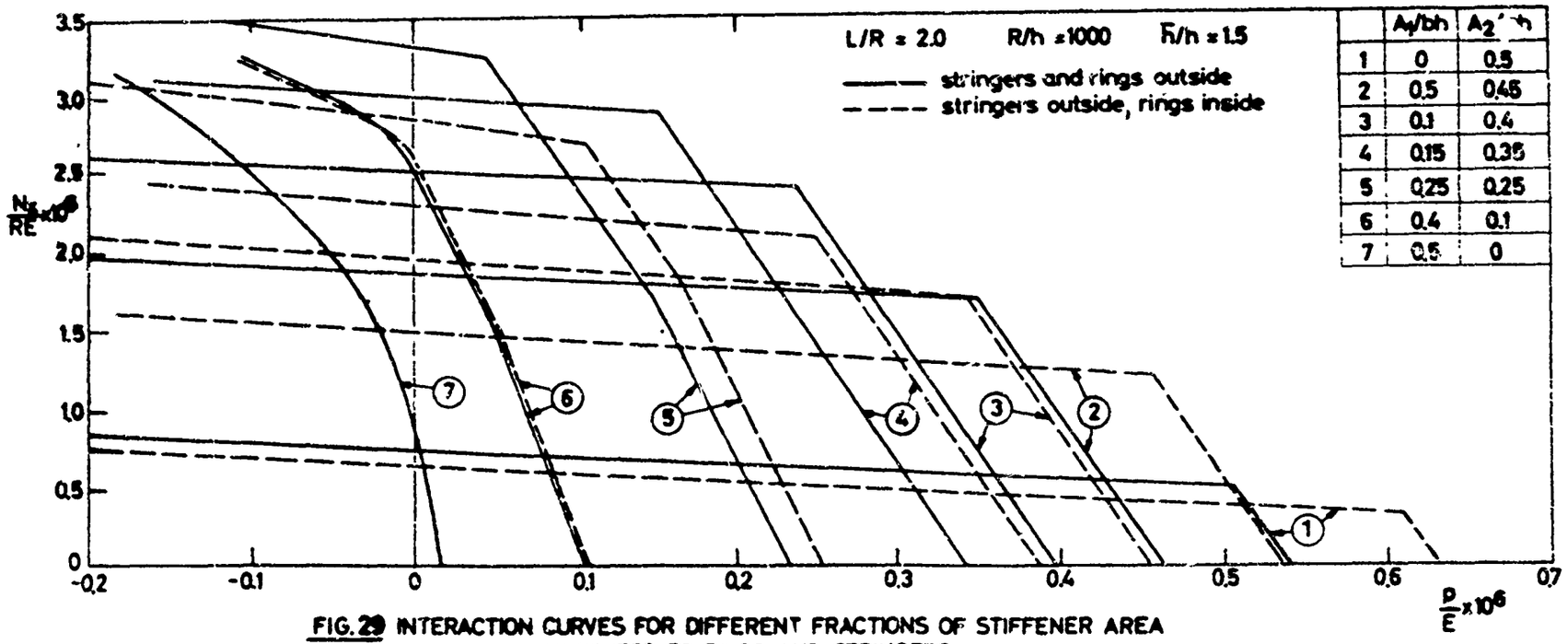

FIG. 29 INTERACTION CURVES FOR DIFFERENT FRACTIONS OF STIFFENER AREA ALLOCATED TO RINGS AND STRINGERS

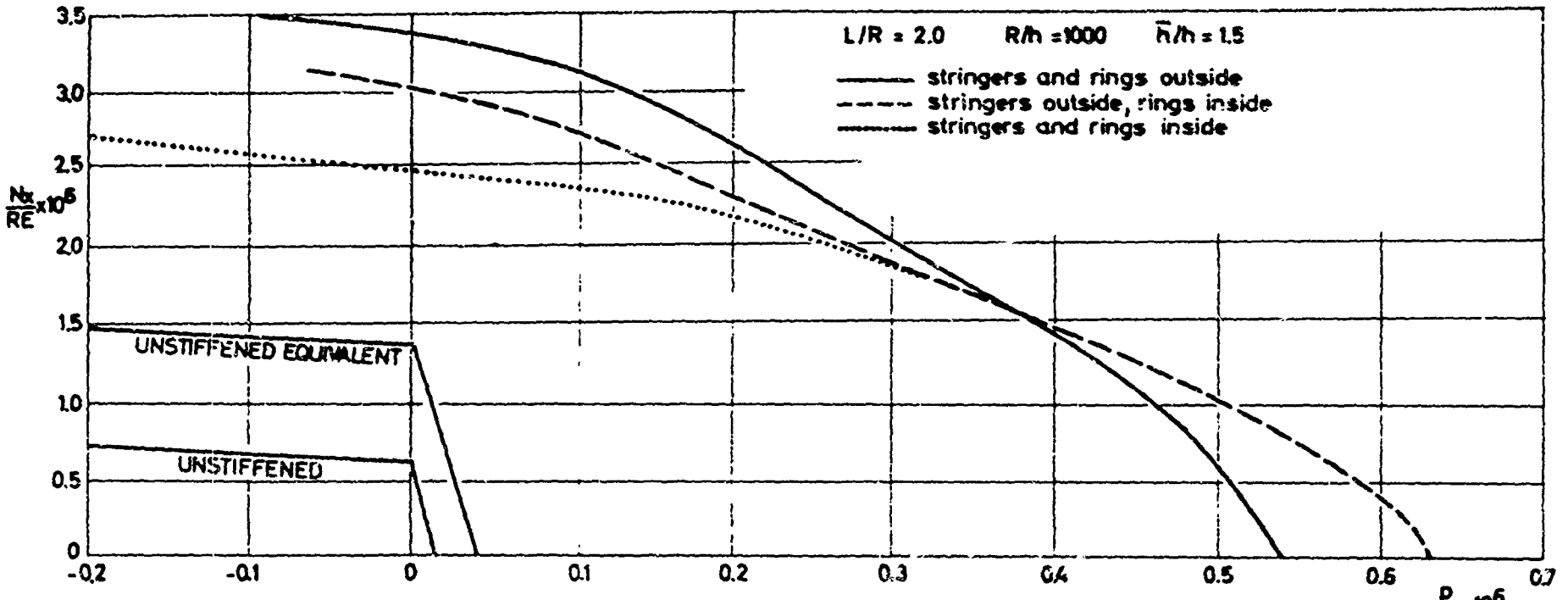

FIG. 30 INTERACTION CURVES FOR MOST EFFICIENT DISTRIBUTION OF STIFFENER MATERIAL

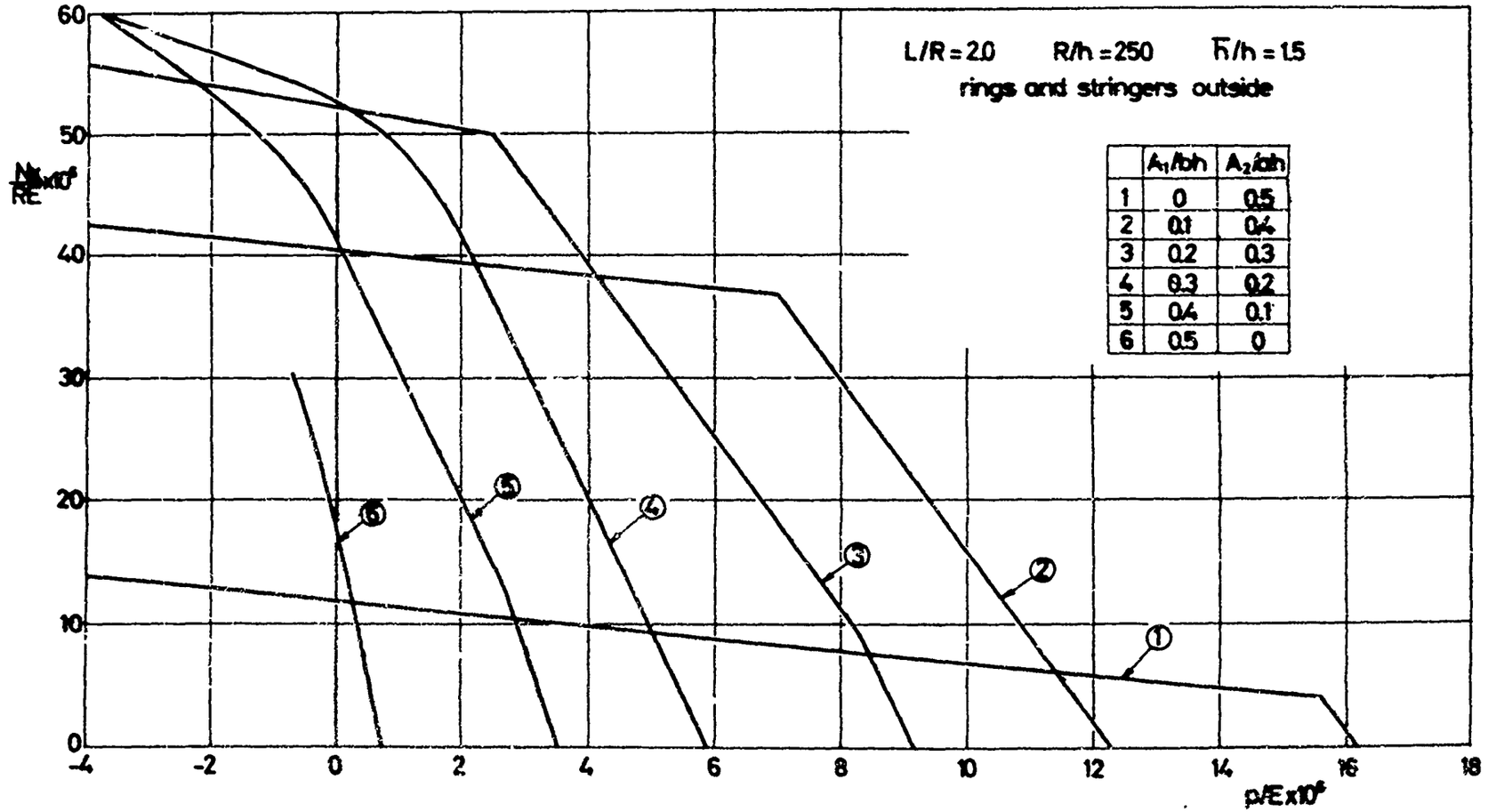

FIG. 31 INTERACTION CURVES FOR DIFFERENT FRACTIONS OF STIFFENER AREA ALLOCATED TO RINGS AND STRINGERS

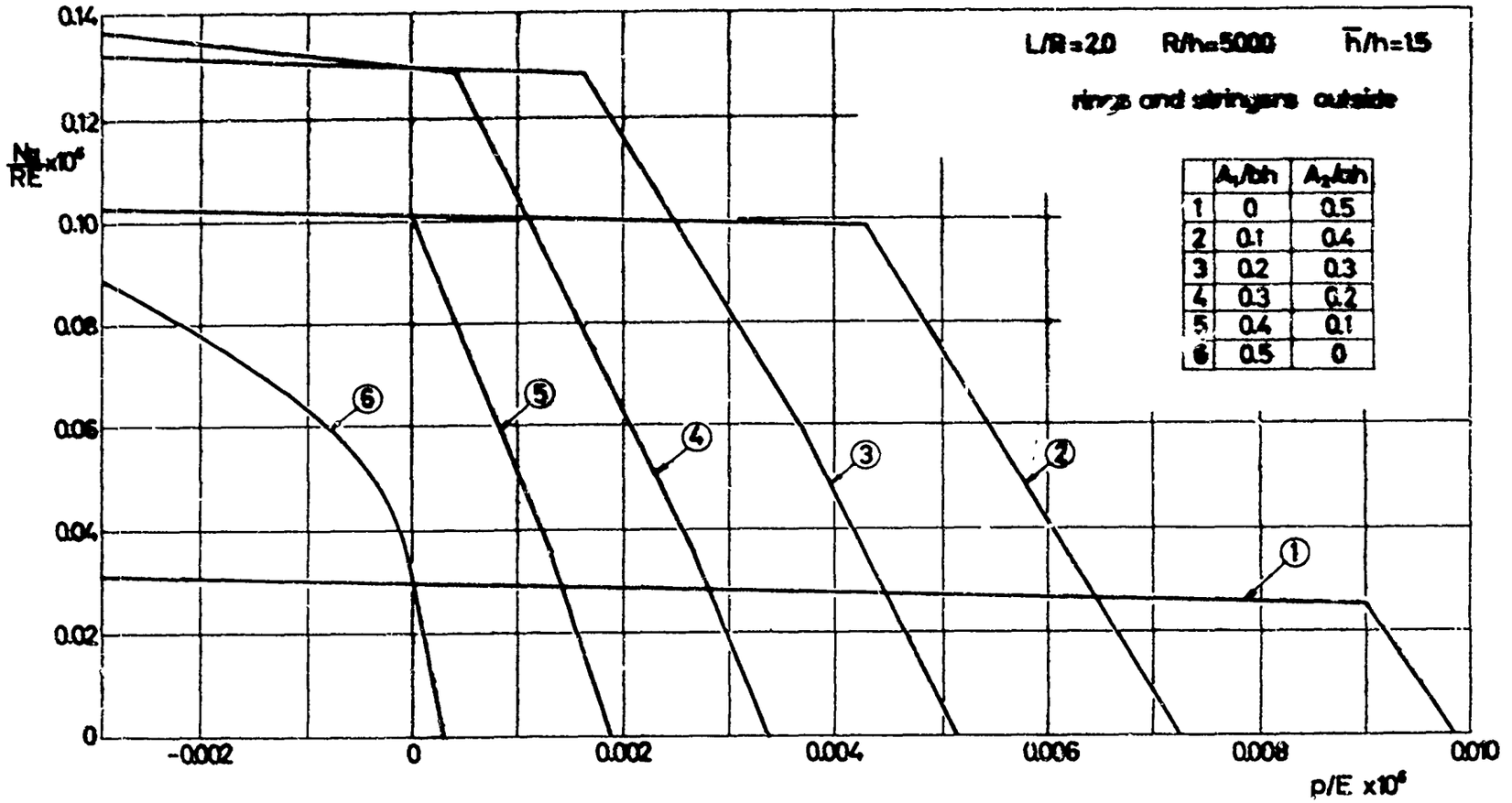

FIG. 32 INTERACTION CURVES FOR DIFFERENT FRACTIONS OF STIFFENER AREA ALLOCATED TO RINGS AND STRINGERS

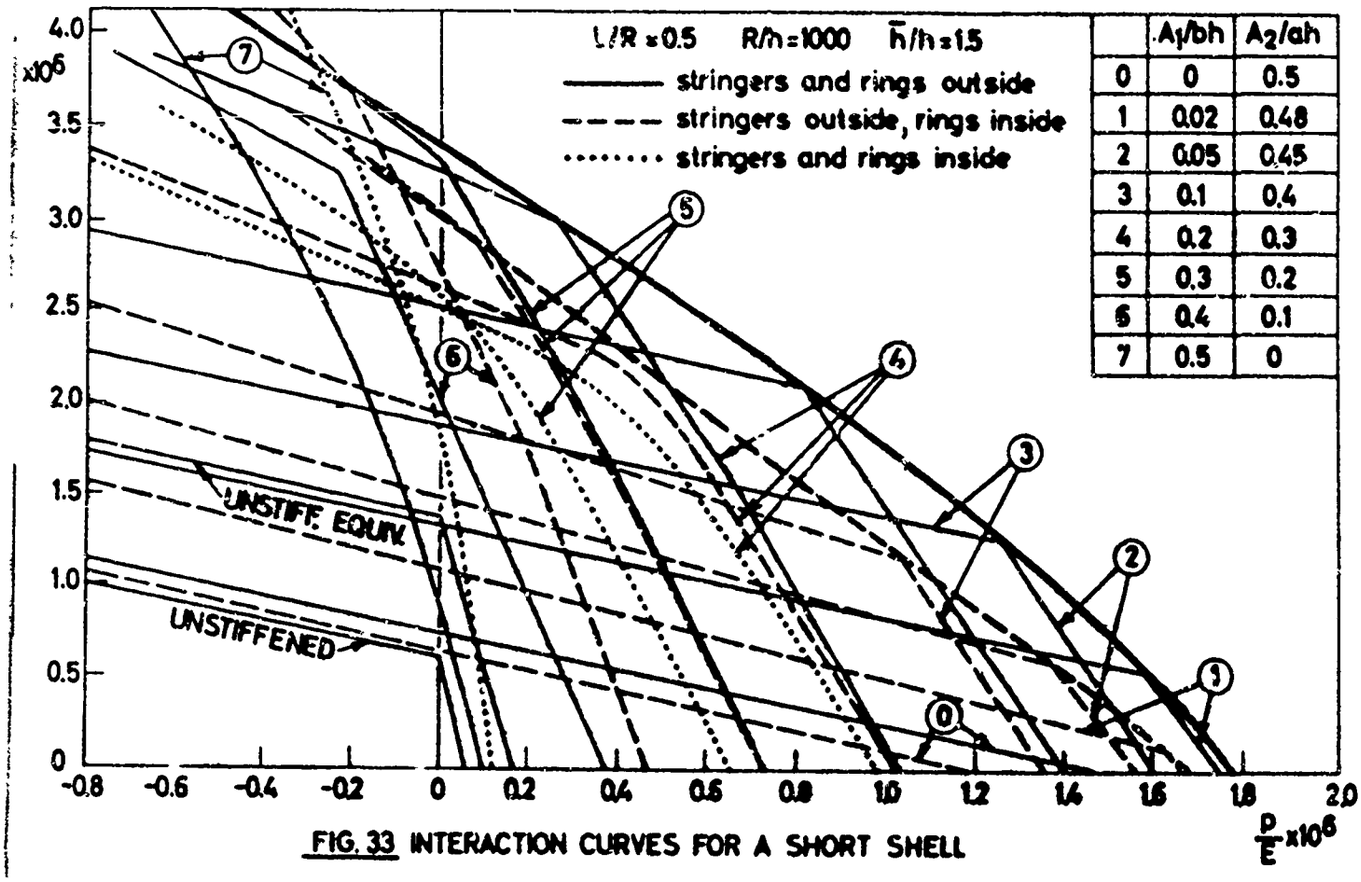

	A_1/bh	A_2/ah
0	0	0.5
1	0.02	0.48
2	0.05	0.45
3	0.1	0.4
4	0.2	0.3
5	0.3	0.2
6	0.4	0.1
7	0.5	0

FIG. 33 INTERACTION CURVES FOR A SHORT SHELL

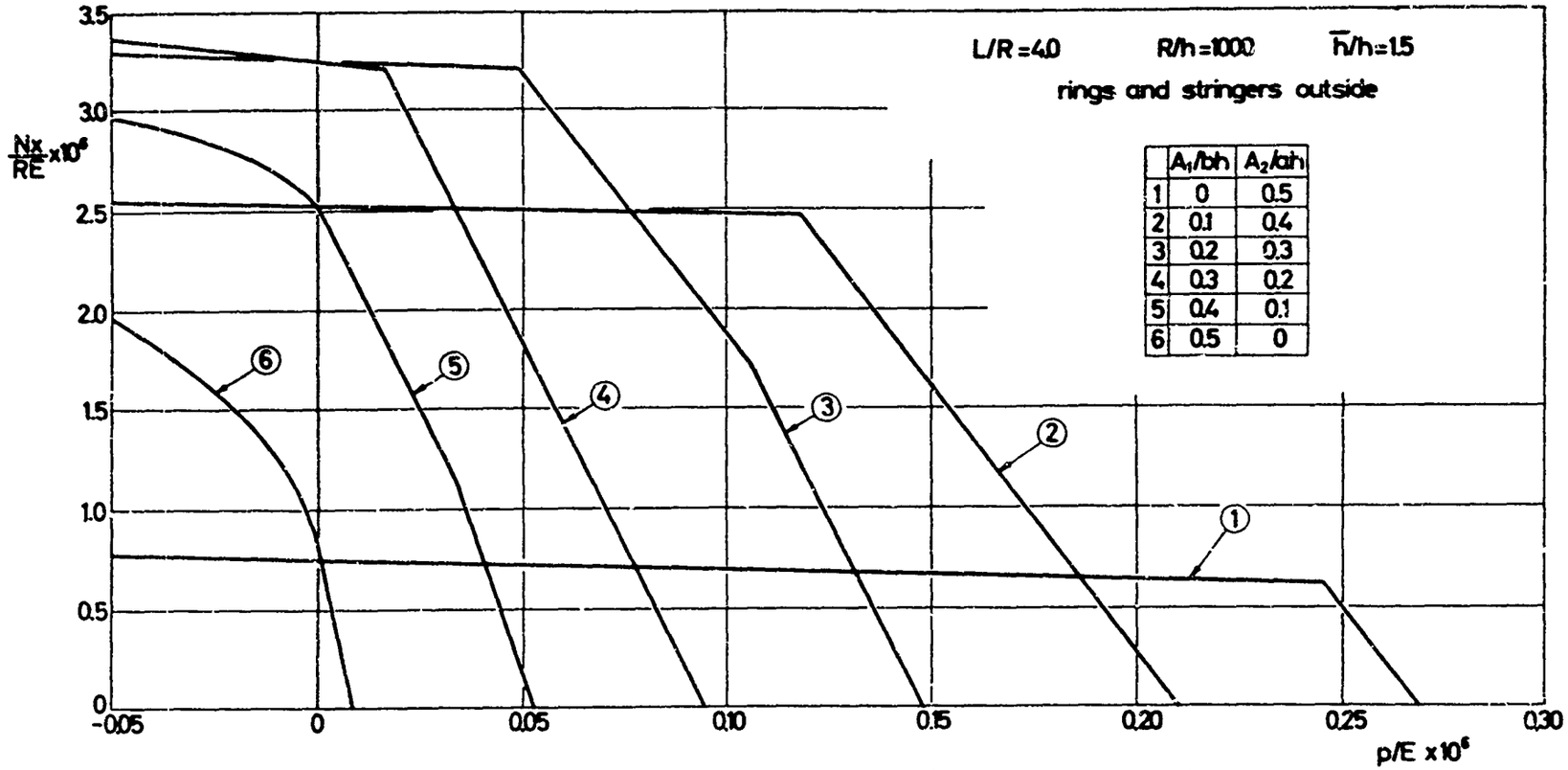

FIG. 34 INTERACTION CURVES FOR DIFFERENT FRACTIONS OF STIFFENER AREA ALLOCATED TO RINGS AND STRINGERS

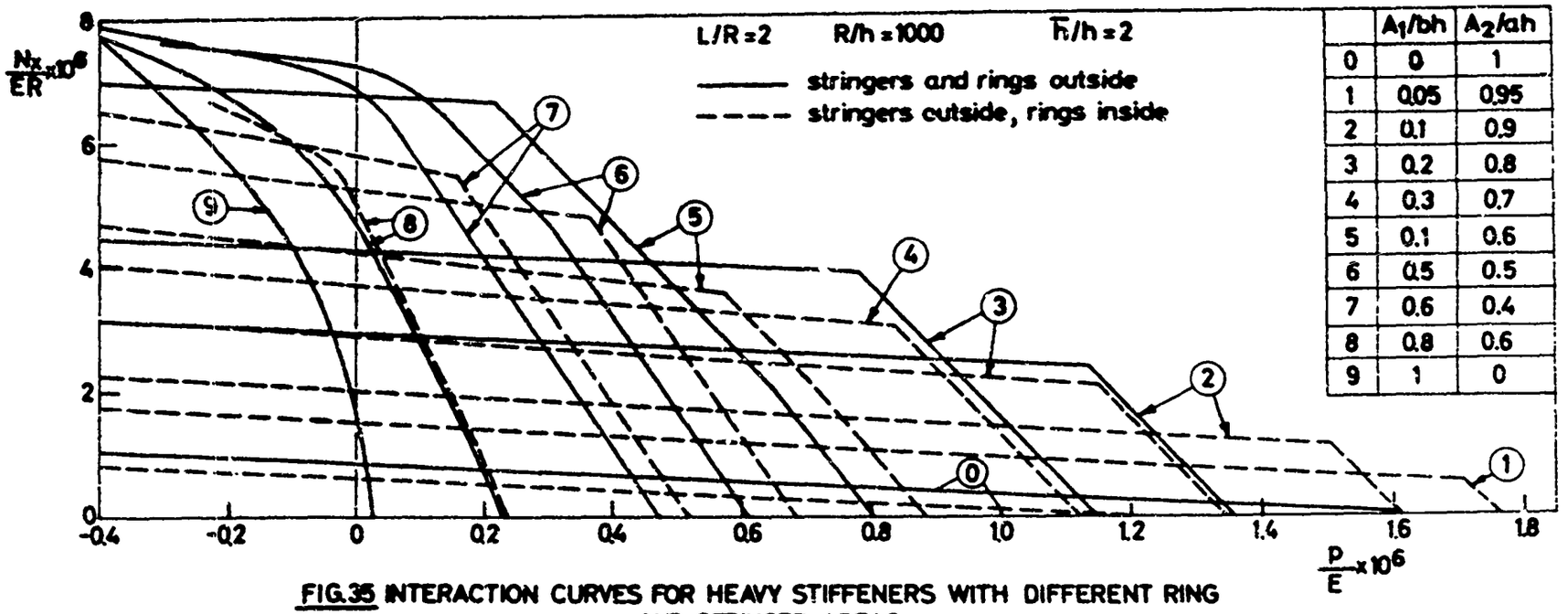

	A_1/bh	A_2/ah
0	0	1
1	0.05	0.95
2	0.1	0.9
3	0.2	0.8
4	0.3	0.7
5	0.1	0.6
6	0.5	0.5
7	0.6	0.4
8	0.8	0.6
9	1	0

FIG.35 INTERACTION CURVES FOR HEAVY STIFFENERS WITH DIFFERENT RING AND STRINGER AREAS

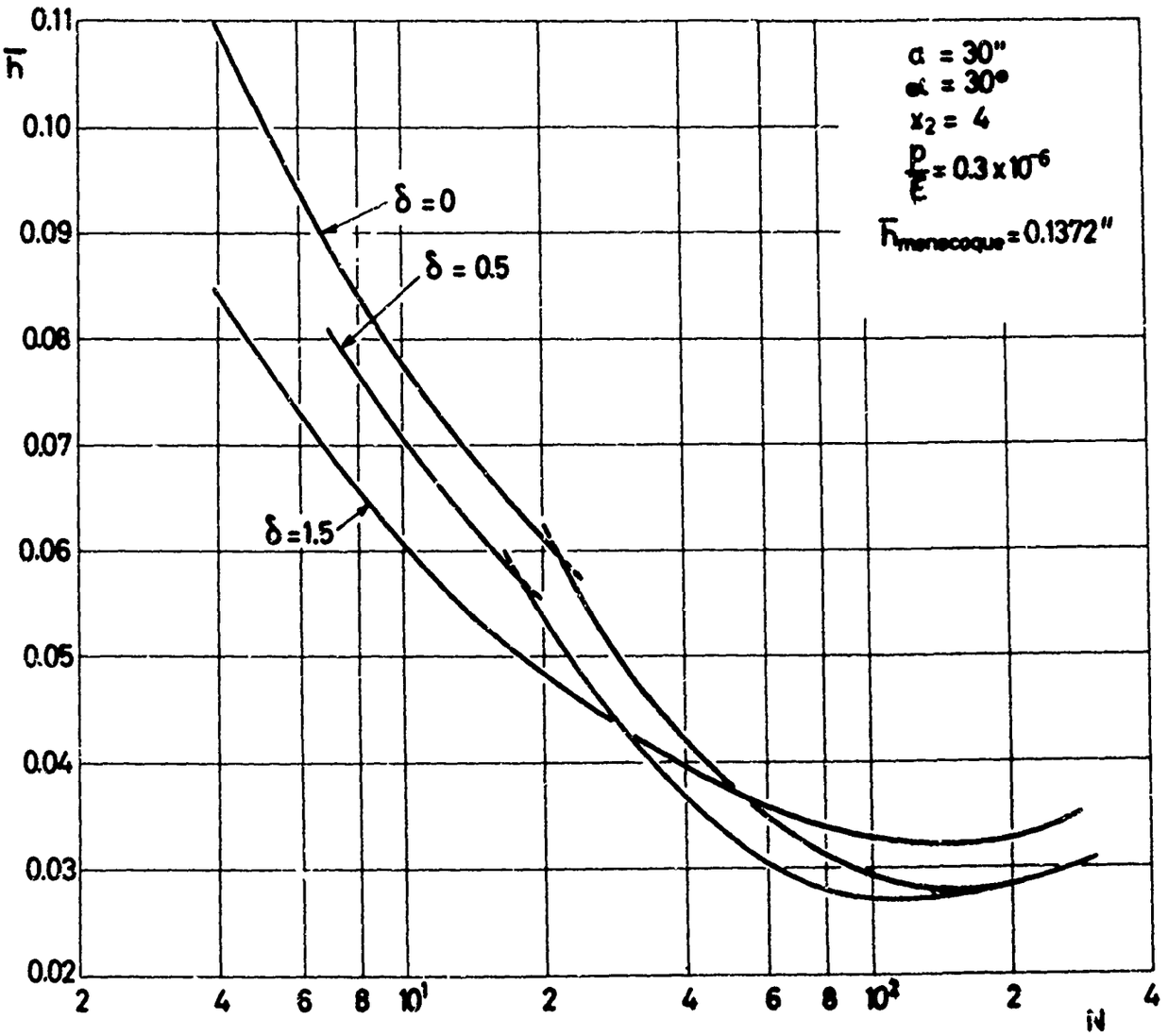

FIG. 36 OPTIMIZATION OF CONICAL SHELLS WITH NON-UNIFORMLY SPACED RINGS UNDER HYDROSTATIC PRESSURE

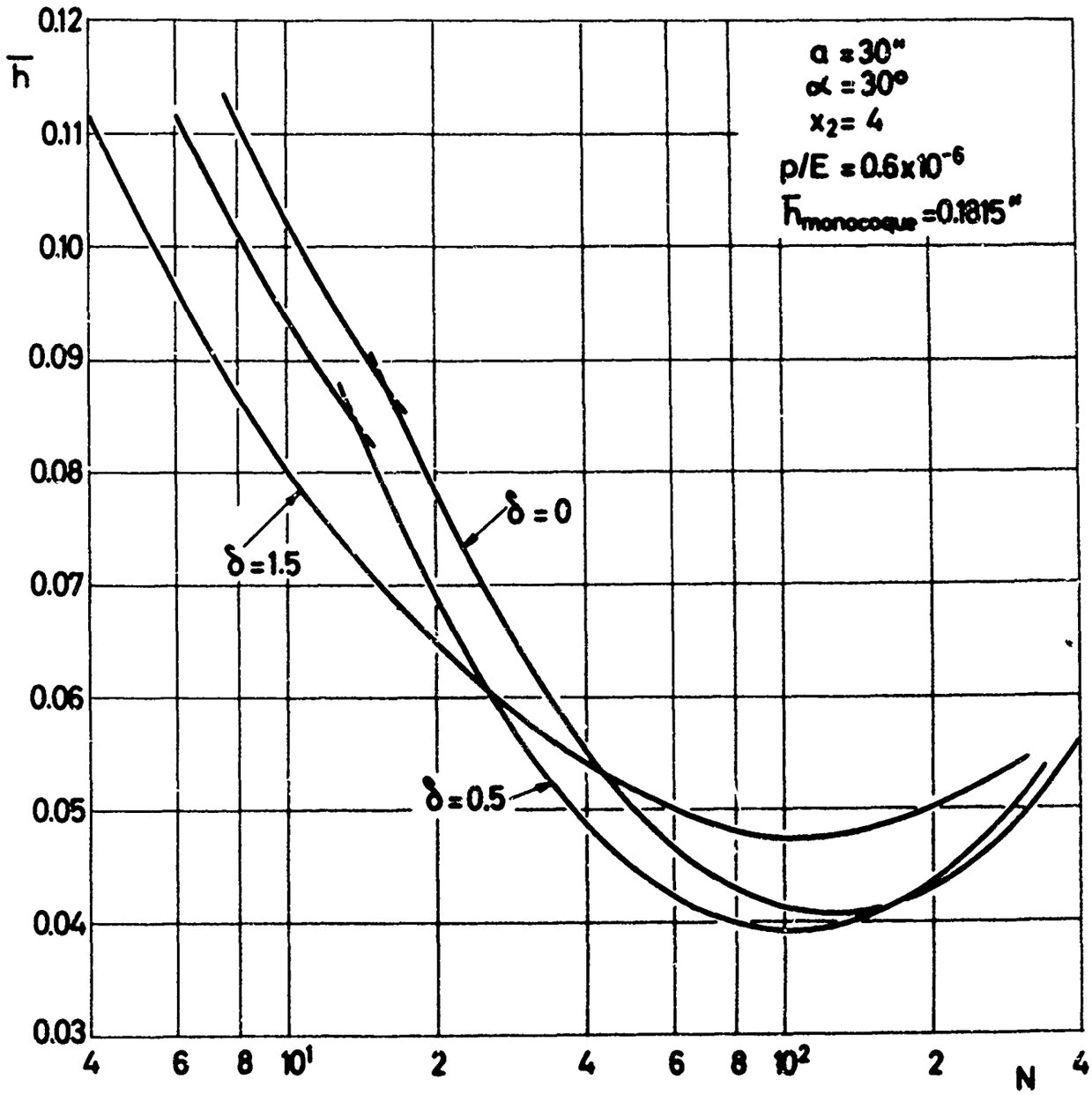

FIG. 37 OPTIMIZATION OF CONICAL SHELLS WITH NON-UNIFORMLY SPACED RINGS UNDER HYDROSTATIC PRESSURE

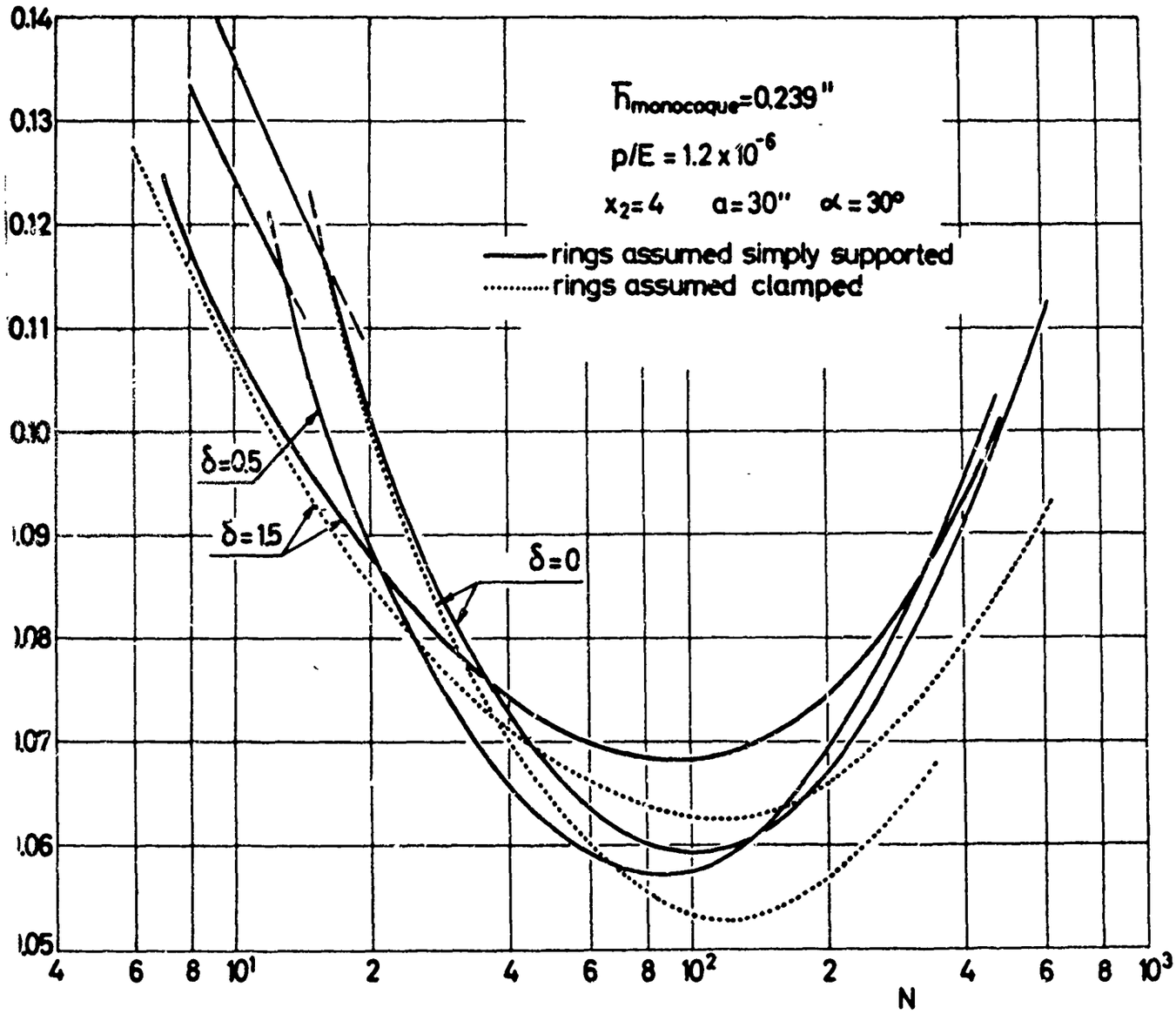

FIG. 38 OPTIMIZATION OF CONICAL SHELLS WITH NON-UNIFORMLY SPACED RINGS UNDER HYDROSTATIC PRESSURE

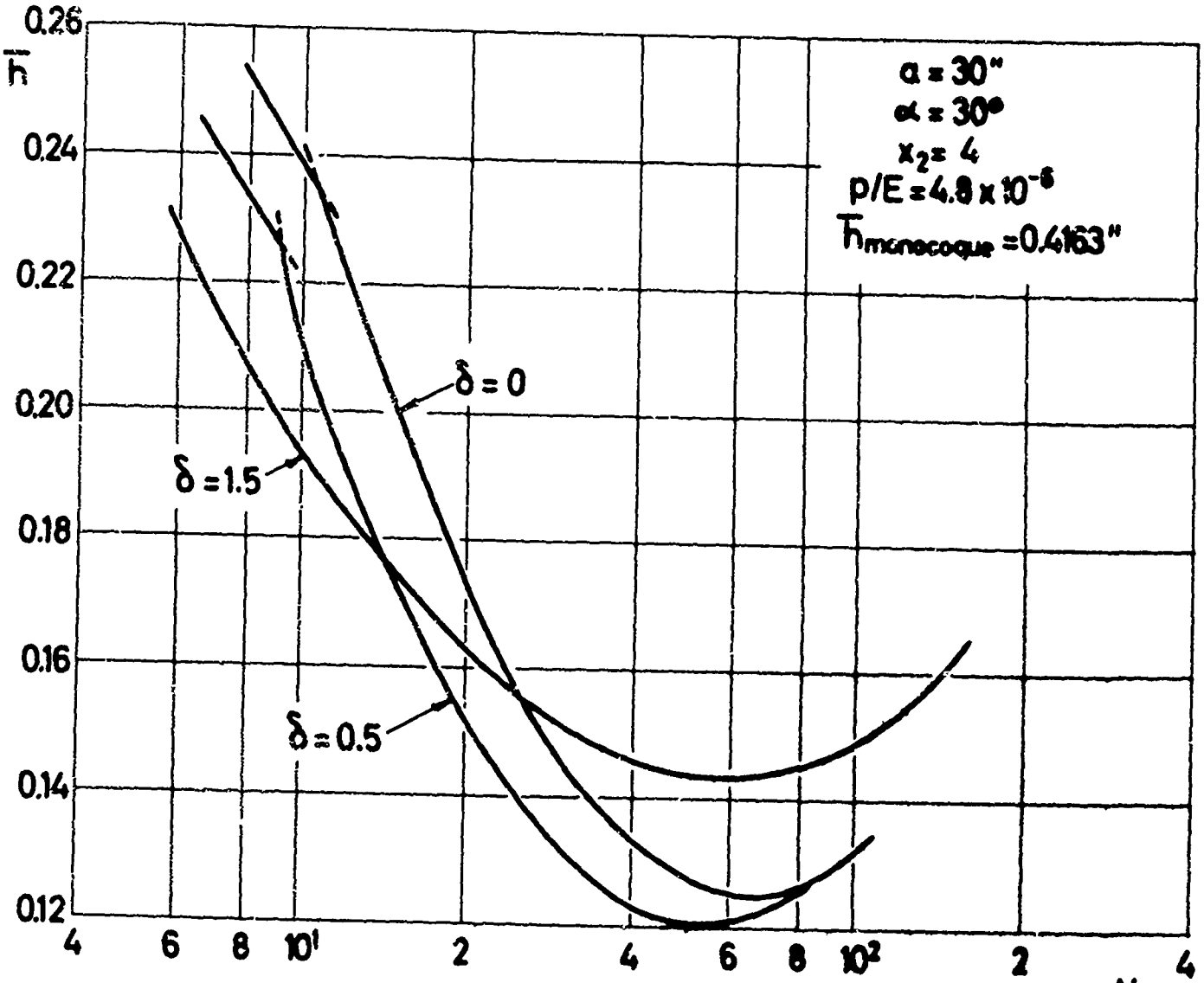

FIG. 39 OPTIMIZATION OF CONICAL SHELLS WITH NON-UNIFORMLY SPACED RINGS UNDER HYDROSTATIC PRESSURE

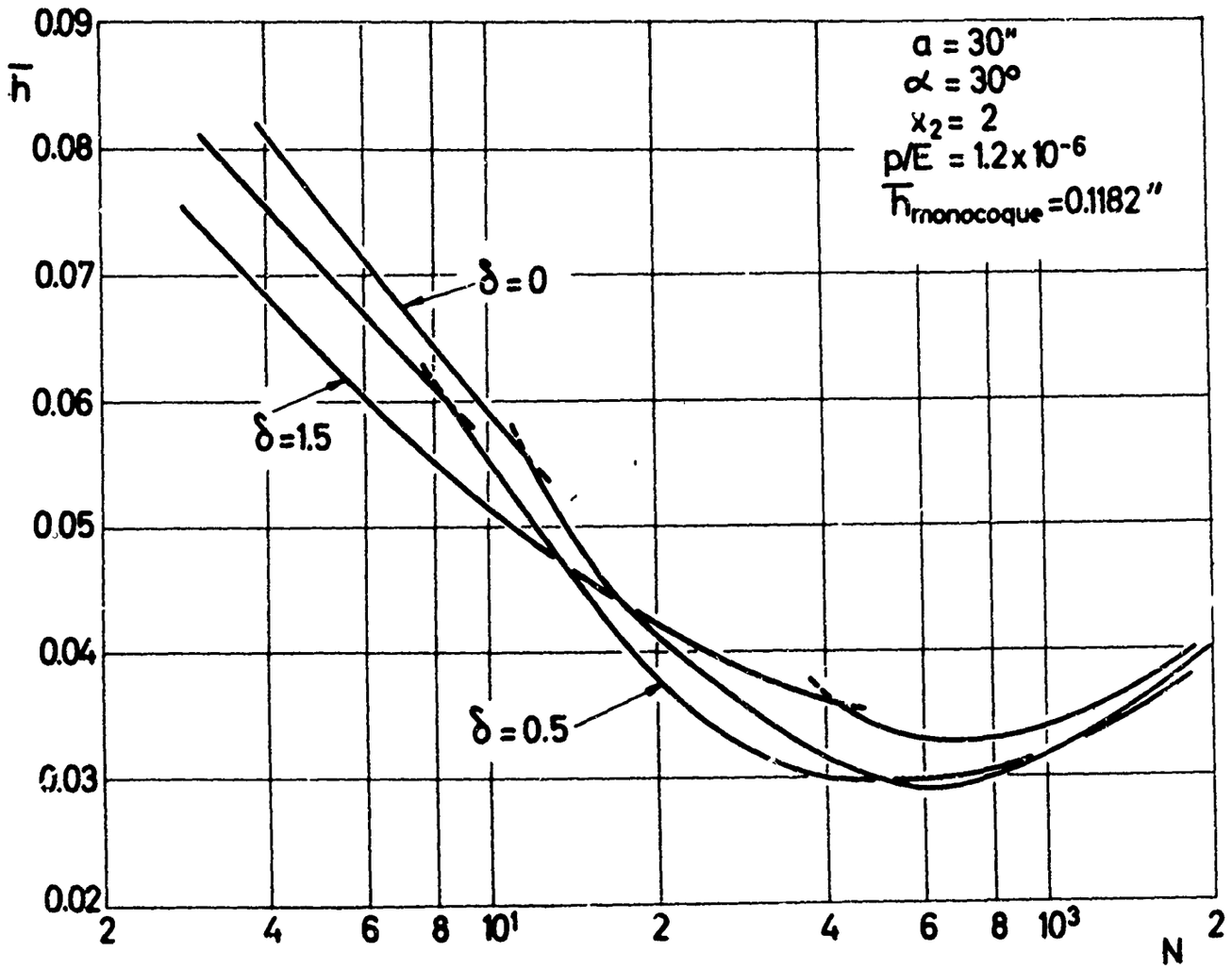

FIG. 40 OPTIMIZATION OF CONICAL SHELLS WITH NON UNIFORMLY SPACED RINGS UNDER HYDROSTATIC PRESSURE

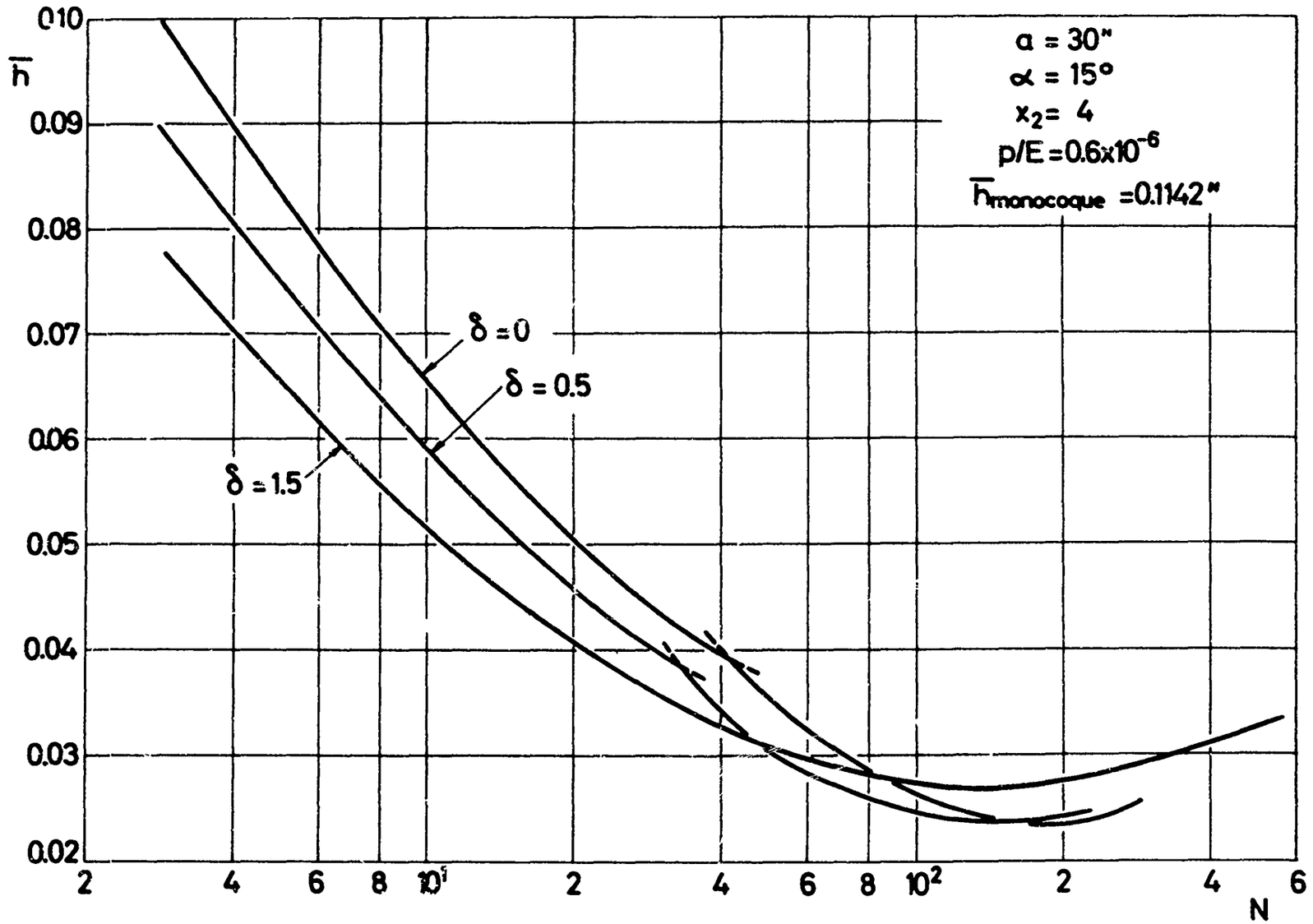

FIG. 41 OPTIMIZATION OF CONICAL SHELLS WITH NON-UNIFORMLY SPACED RINGS UNDER HYDROSTATIC PRESSURE

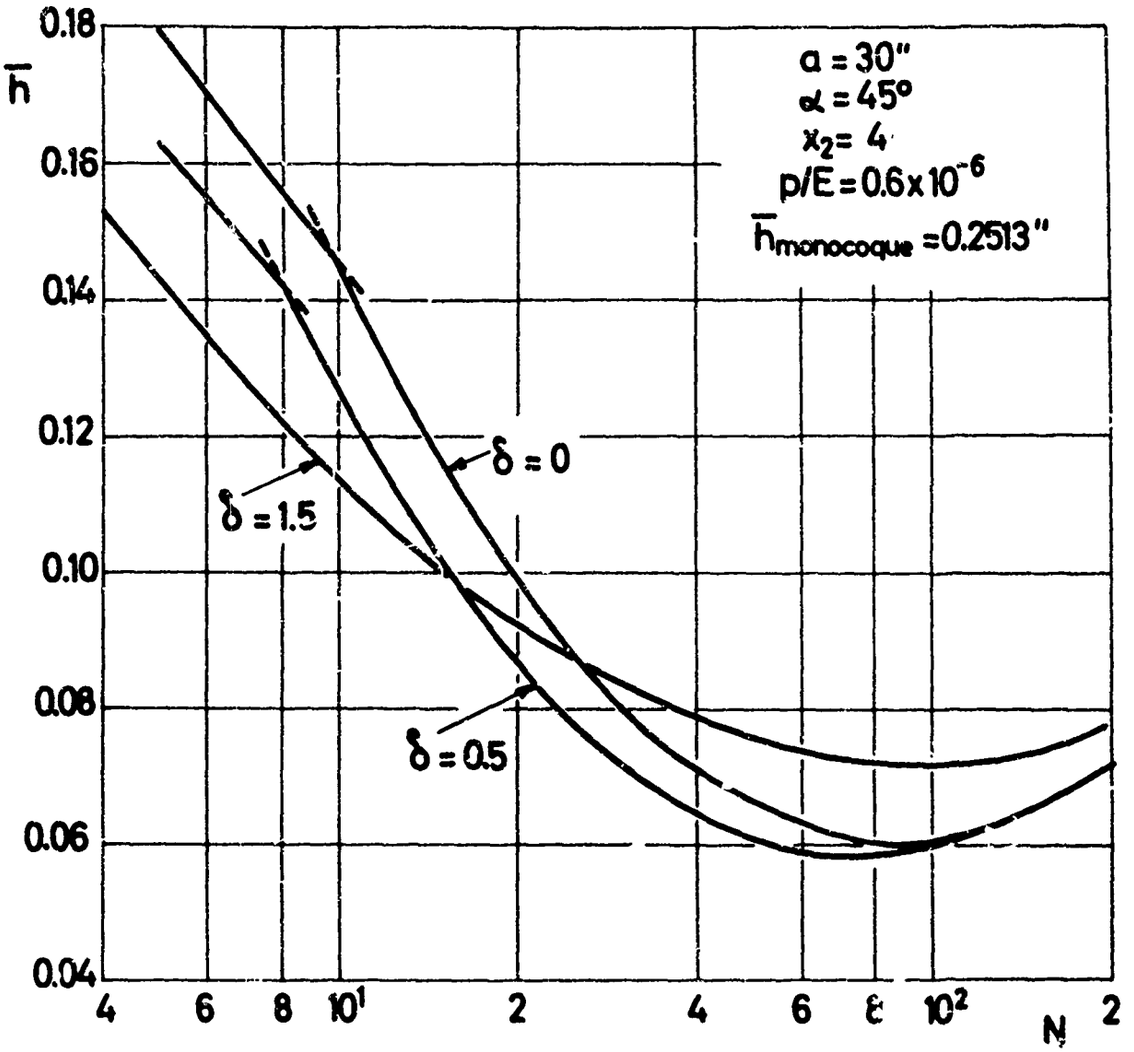

FIG. 42 OPTIMIZATION OF CONICAL SHELLS WITH NON-UNIFORMLY SPACED RINGS UNDER HYDROSTATIC PRESSURE

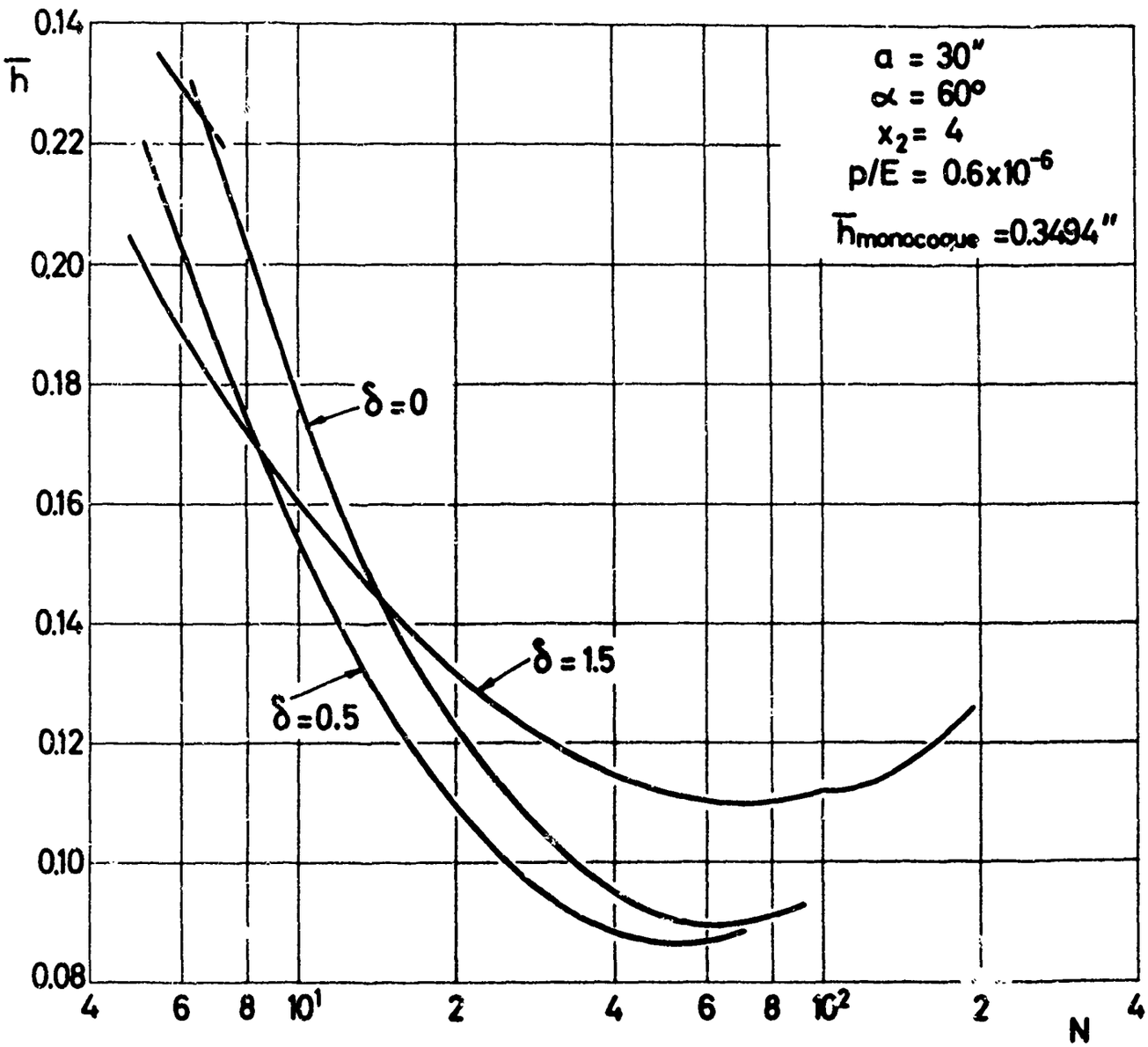

FIG. 43 OPTIMIZATION OF CONICAL SHELLS WITH NON-UNIFORMLY SPACED RINGS UNDER HYDROSTATIC PRESSURE

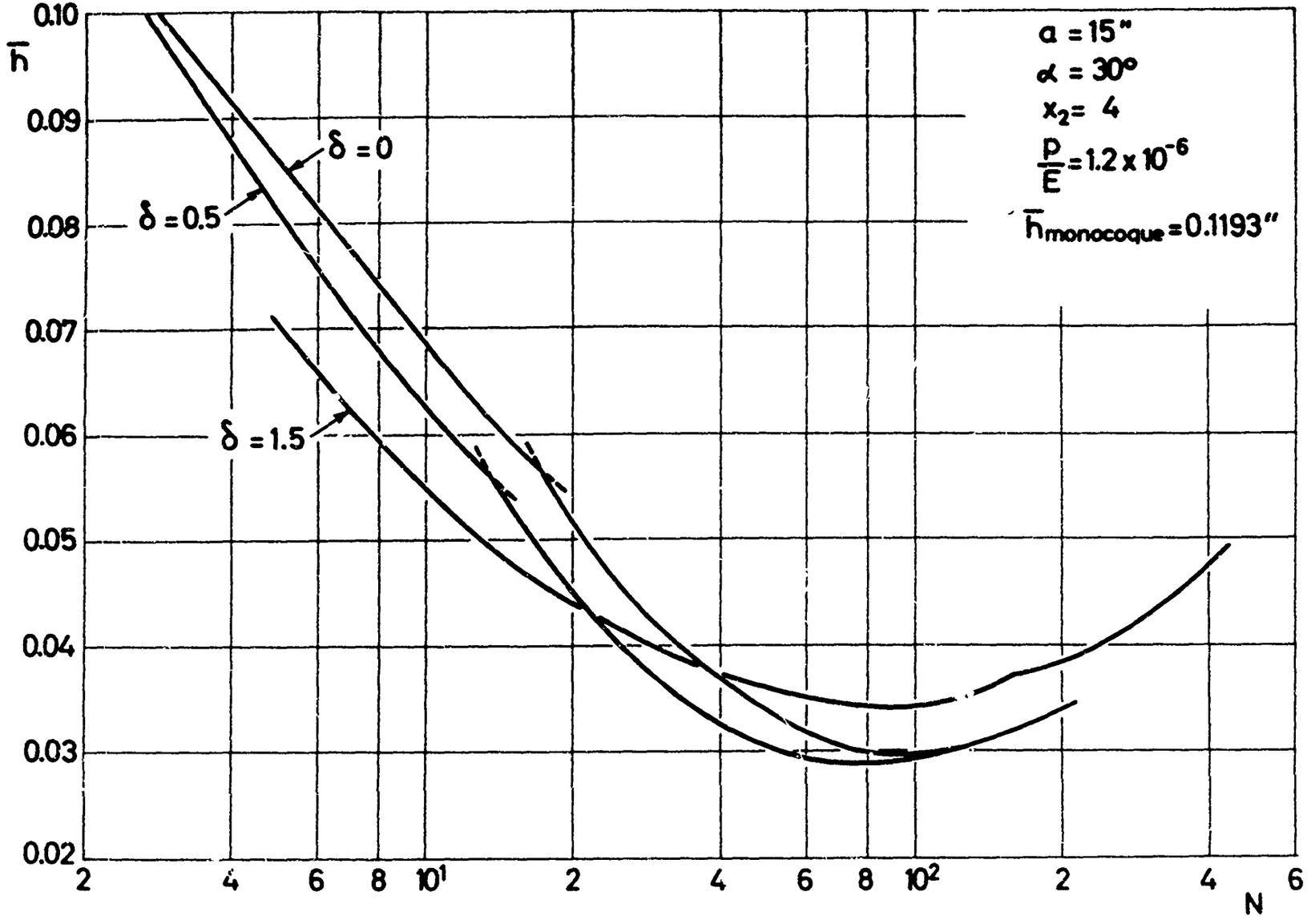

FIG. 4 OPTIMIZATION OF CONICAL SHELLS WITH NON-UNIFORMLY SPACED RINGS UNDER HYDROSTATIC PRESSURE

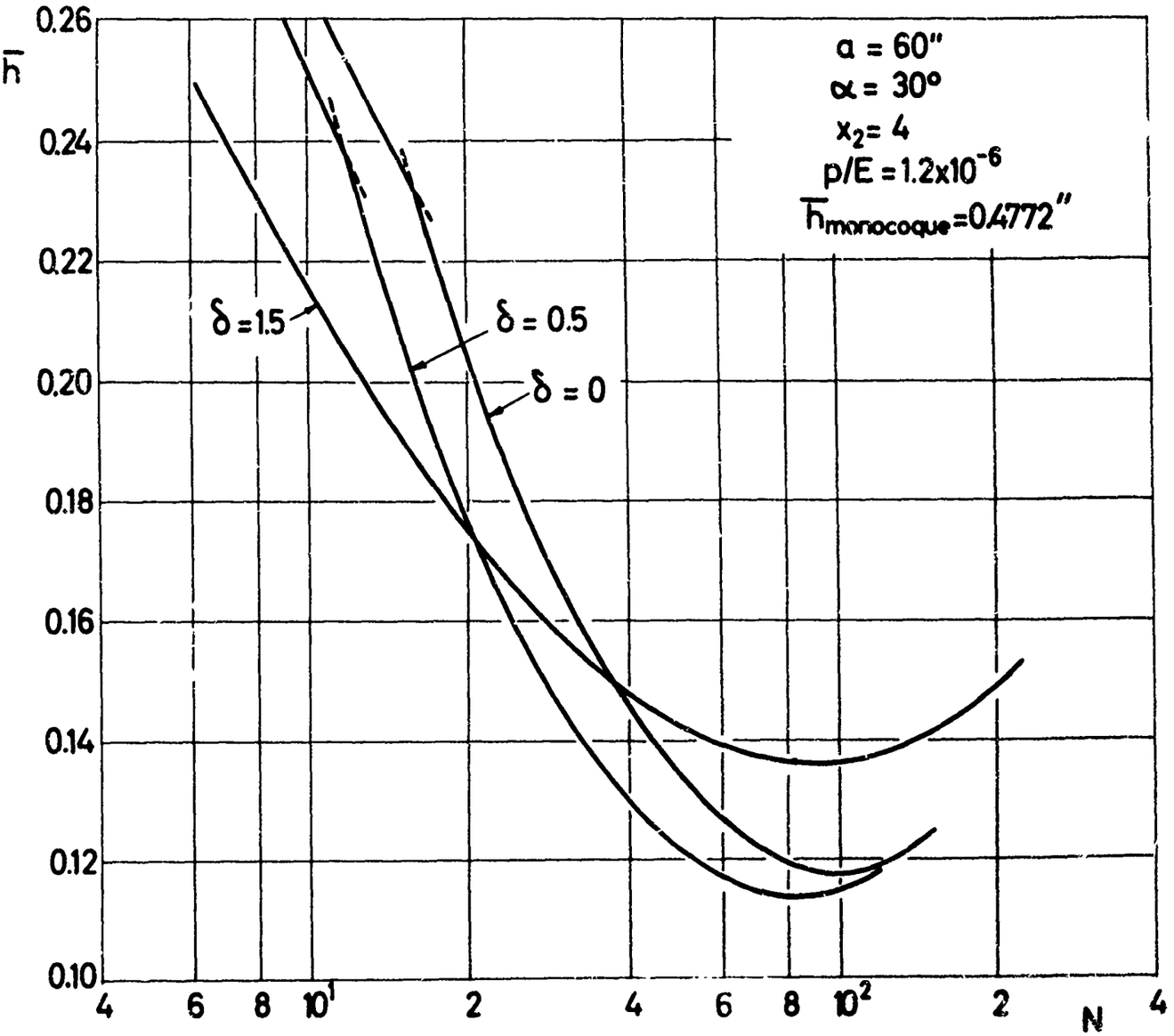

FIG. 45 OPTIMIZATION OF CONICAL SHELLS WITH NON-UNIFORMLY SPACED RINGS UNDER HYDROSTATIC PRESSURE

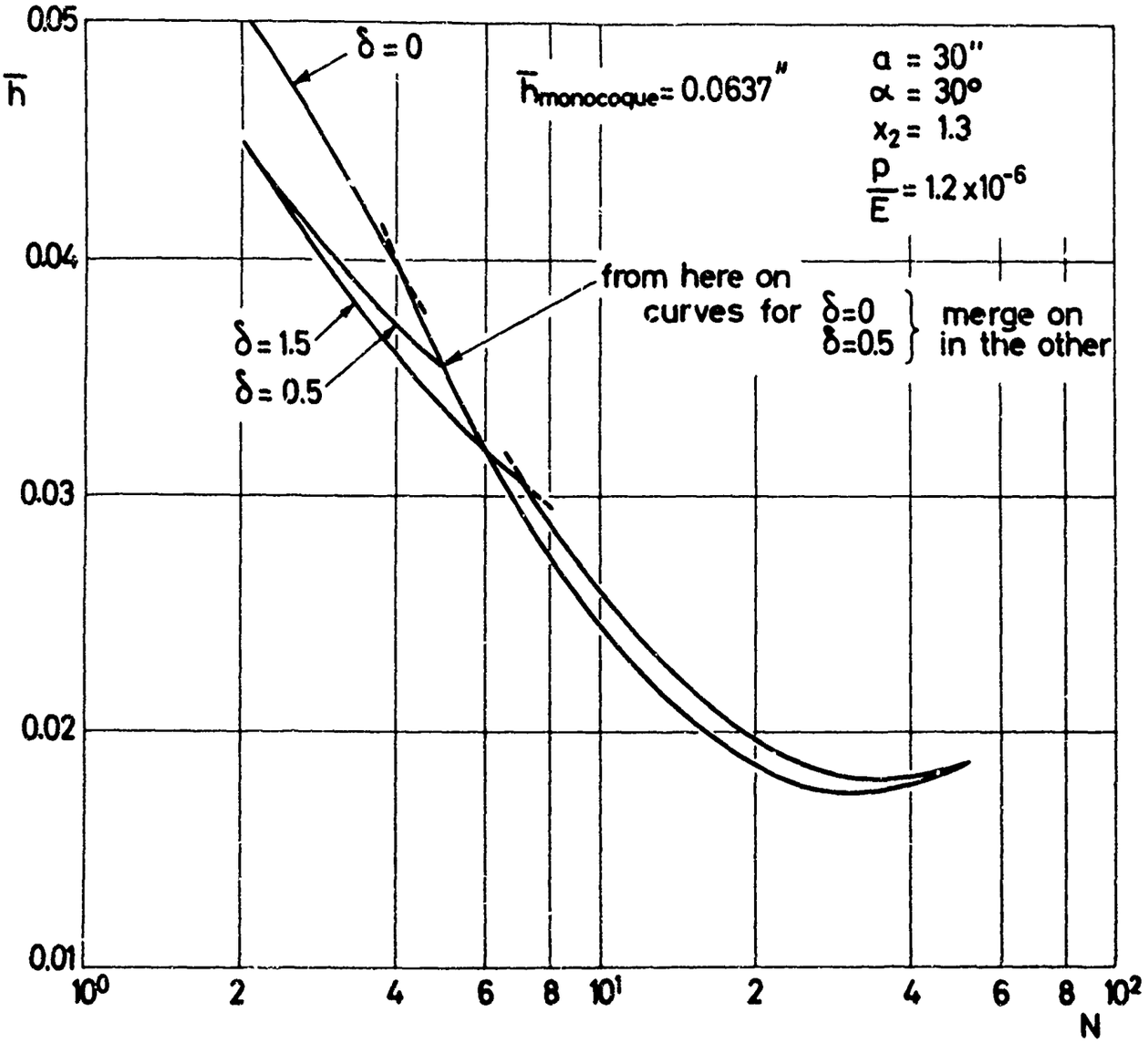

FIG. 46 OPTIMIZATION OF CONICAL SHELLS WITH NON-UNIFORMLY SPACED RINGS UNDER HYDROSTATIC PRESSURE

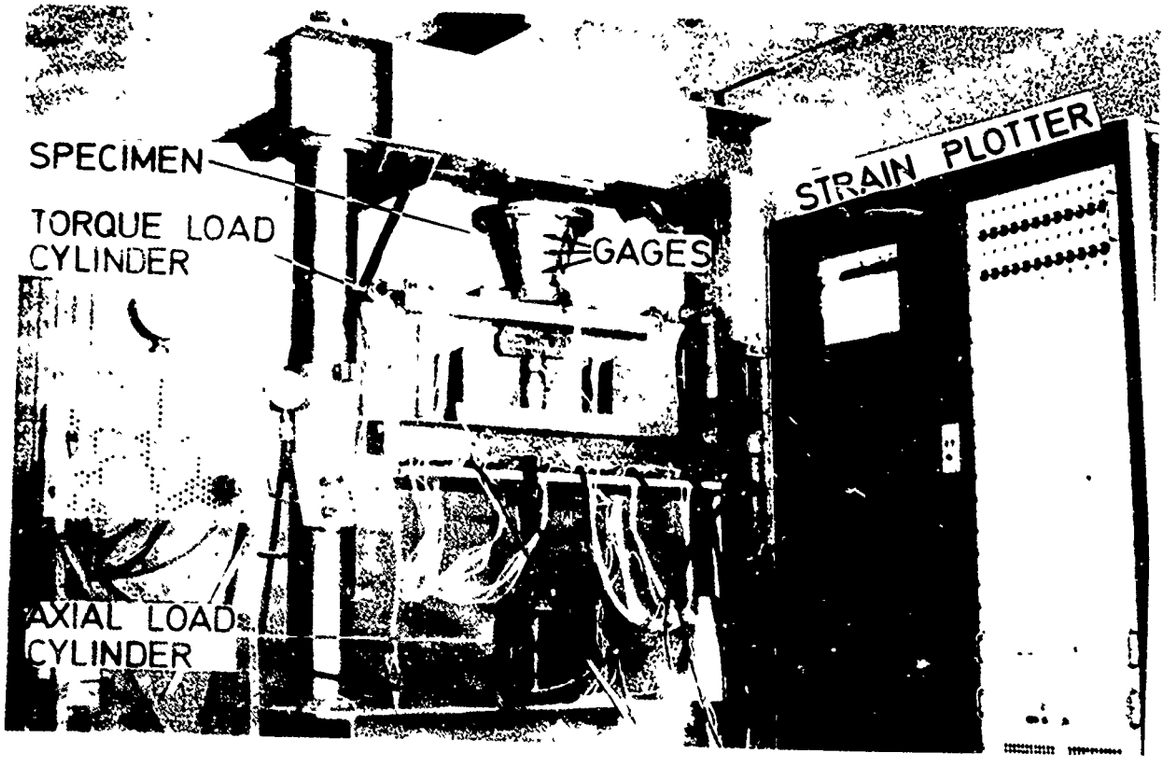

FIG. 47 TEST SET-UP FOR STIFFENED CONICAL SHELLS.

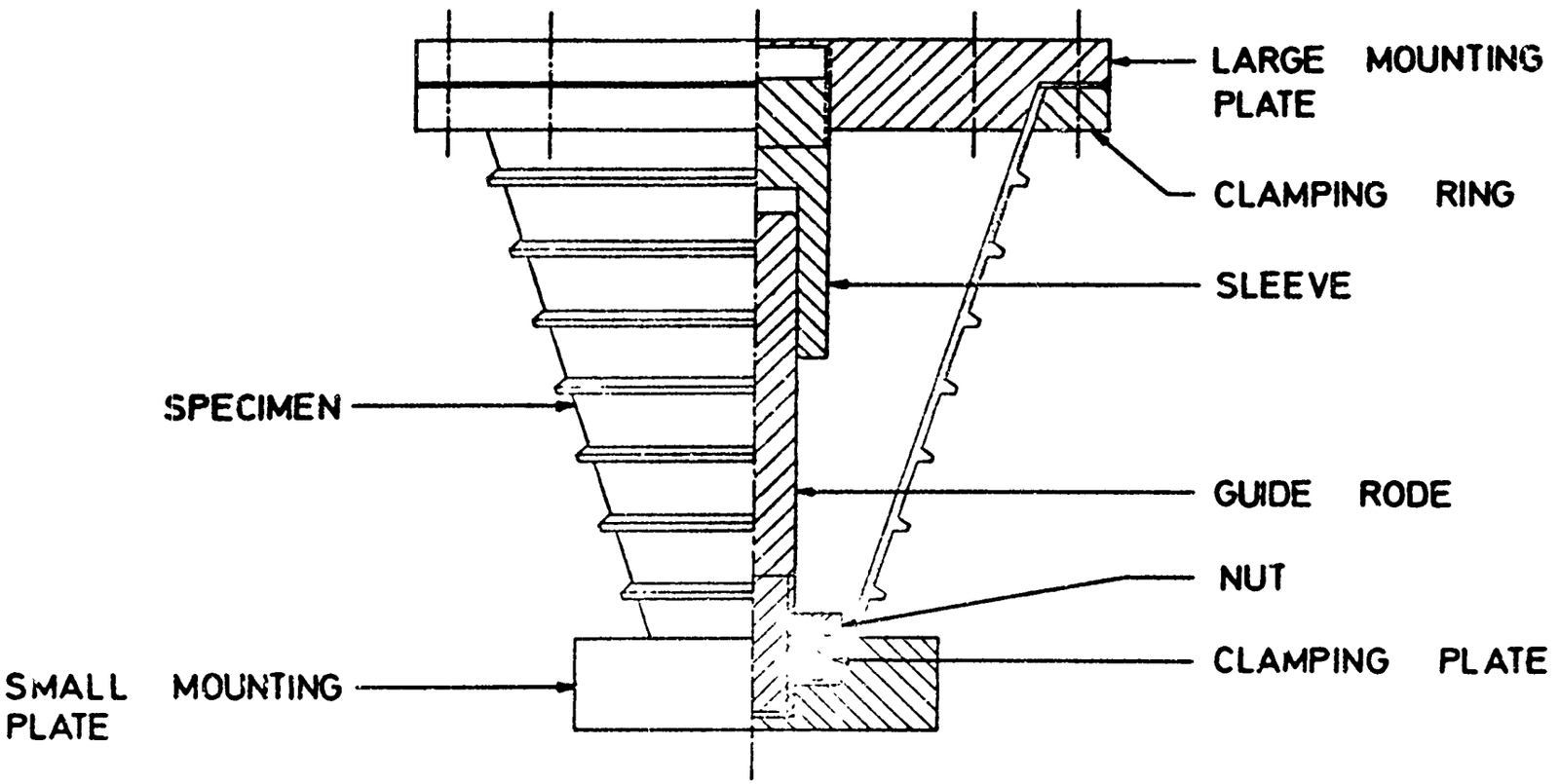

FIG. 48 END FITTING FOR STIFFENED CONICAL SHELLS.

FIG. 49 CLOSELY STIFFENED CONICAL SHELL (M3-3A) BUCKLED UNDER AXIAL COMPRESSION.

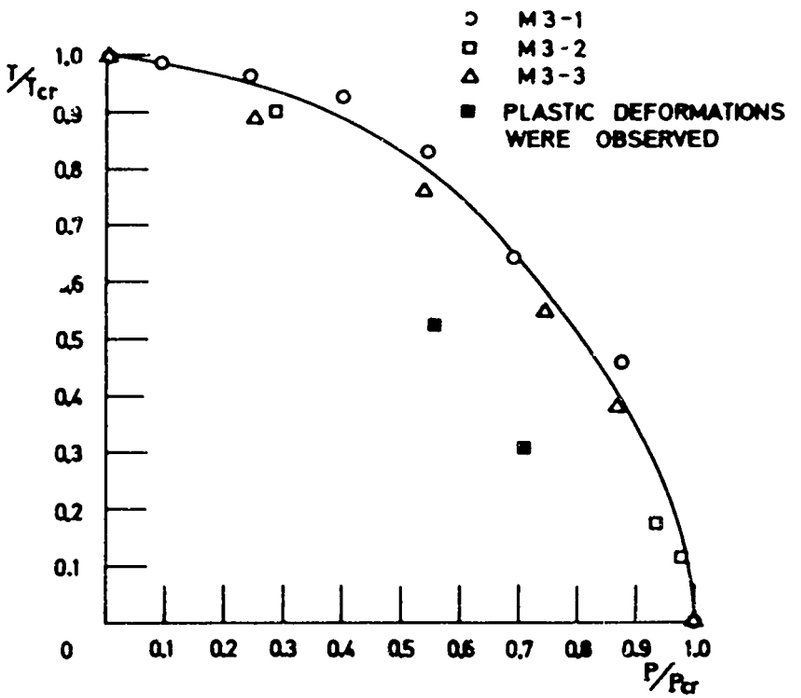

FIG. 50 EMPIRICAL INTERACTION CURVE FOR RING-STIFFENED CONICAL SHELLS

DOCUMENT CONTROL DATA - R & D

Security classification of title, body of abstract and indexing annotation must be entered when the overall report is classified

1. ORIGINATING ACTIVITY (Corporate author)

Technion - Israel Institute of Technology
Department of Aeronautical Engineering
Haifa, Israel

2a. REPORT SECURITY CLASSIFICATION

UNCLASSIFIED

2b. GROUP

3. REPORT TITLE

EXPERIMENTAL AND THEORETICAL STUDIES ON BUCKLING OF CONICAL AND CYLINDRICAL SHELLS UNDER COMBINED LOADING

4. DESCRIPTIVE NOTES (Type of report and inclusive dates)

Scientific [redacted] Final

5. AUTHOR(S) (First name, middle initial, last name)

Josef Singer
Avraham Berkovits
Tanchum Weller
Ori Ishai
Menahem Baruch
Ovadia Harari

6. REPORT DATE

June 1966

7a. TOTAL NO. OF PAGES

151

7b. NO. OF REFS

44

8a. CONTRACT OR GRANT NO.

AF-EOAR-63-58

b. PROJECT NO.

9782-01

c. 61445014

d. 681307

9a. ORIGINATOR'S REPORT NUMBER(S)

9b. OTHER REPORT NO(S) (Any other numbers that may be assigned this report)

AFOSR 66-2589

10. AVAILABILITY/LIMITATION NOTICES

1. Distribution of this document is unlimited

11. SUPPLEMENTARY NOTES

12. SPONSORING MILITARY ACTIVITY

AF Office of Scientific Research (SREM)
1400 Wilson Boulevard
Arlington, Virginia 22209

13. ABSTRACT

Results of an experimental program on the instability of unstiffened aluminum-alloy conical shells under combinations of 3 loadings, axial compression, torsion and external or internal pressure are presented and compared with linear theory. Improvements in experimental technique permitted many repeated buckling tests on the same metal specimen without noticeable damage and yielded reliable interaction curves. Some tests on Mylar conical shells under similar combined loading, are then discussed. Tests of the mechanical properties of Mylar A sheets revealed considerable anisotropy that casts some doubt on the reliability of results obtained with Mylar specimens. The general instability of stiffened cylindrical shells under combined axial compression and external or internal pressure is then discussed and design implications are considered. The variation of stiffener spacing in stiffened conical shells yields an improvement in structural efficiency. Optimization studies that investigate this improvement for ring stiffened cones in detail are presented. Results of a continuation of an experimental program on the general instability of ring-stiffened conical shells are presented. Tests on integrally machined steel specimens under torsion, axial compression and combined torsion and axial compression are discussed and compared with theory.

DD FORM 1473

Security Classification

14 KEY WORDS	LINK A		LINK B		LINK C	
	ROLE	WT	ROLE	WT	ROLE	WT
Axial Compression						
Torsion						
External Pressure						
Internal Pressure						
Mylar Conical Shells						
Stiffened Cylindrical Shells						
Stiffener Spacing						
Ring-Stiffened Conical Shells						

Security Classification